Noble Gas Solubility in Silicate Melts and its Geochemical Interpretation

Tomo SHIBATA

Department of Physics, Graduate School of Science,
Osaka University, Toyonaka, Osaka, 560 Japan

Ph. D Thesis

March, 1997

Abstract

New measurements of solubility of noble gases in binary silicate melts (Na_2O-SiO_2, CaO-SiO_2 and MgO-SiO_2) and ternary silicate melts (Na_2O-CaO-SiO_2 and CaO-MgO-SiO_2) at pressures of 1.10-1.99 kbars and temperatures of 1200-1600 °C are presented. The solubility is greater for lighter noble gases and is a strong function of melt composition; the solubility increases with SiO_2 content. There is also a linear correlation between the NBO/T (nonbridging oxygen per tetrahedrally coordinated cation) of the melt and the logarithm of noble gas solubility. This correlation is better than previously noted correlations between noble gas solubility and the physical parameters such as melt density, molar volume and ionic porosity. The obtained correlation provides a useful means of predicting how noble gas solubility varies with melt composition. Noble gas solubility is not governed by cations producing holes but is controlled by tetrahedral network structure, and could be defined by degree of polymerization in the silicate melt; it is higher with more polymerized melts. Specifically, the most important unit among network anionic structure units is three-dimensional unit. The equilibrium constants of Ar, Kr, and Xe in CaO-MgO-SiO_2 melt can be predicted by using both proportion of three-dimensional unit in the melt and equilibrium constants of three-dimensional unit estimated from Na_2O-SiO_2 and CaO-SiO_2 systems. There is also a correlation between noble gas solubility and NBO/T for a wide range of silicate melt compositions. However, the noble gas solubility in the melts falls off the linear correlation line, as the network forming cations except silicon atom in the melts increase. This deviation from the linear trend would be due to existence of network modifying cations accompanying with Al^{3+} in the network structure units, since most of the network forming cations are proposed to be aluminum.

Table of Contents

Abstract i

1. Introduction 1

1-1 General Introduction 1

1-2 Noble Gas Solution in Silicate Glass and Melt 2

1-3 Structure of Silicate Melts 8

1-3-1 Melts Versus Quenched Melts (Glasses) 8

1-3-2 Studies of Glass and Melt Structure 9

1-3-3 Structure of Silicate Melt 12

2. Experiment 15

2-1 Sample Preparation 15

2-2 Experiment of Noble Gas Solution in Silicate Melts 18

2-3 Noble Gas Analysis 21

3. Results 25

3-1 Equilibrium Condition 36

3-2 Noble Gas Solubility 41

4. Discussions 54

4-1 Thermodynamics 54

4-2 Melt Composition Dependence of Noble Gas Solubility 63

4-3 Relation between Melts Structure and Solubility 71
4-4 Application for Relation between Solubility and Structure to Natural Silicate Melts 79

Summary 86

Acknowledgments 88

References 89

Appendix A: Noble Gas Mass Spectrometry 97
Appendix B: Redlich-Kwong Equation 108
Appendix C: List of Publications 114

1. INTRODUCTION

1-1 General Introduction

Evolution of the Earth is one of the most intriguing problems in current Earth Science. Because of inert nature and its rarity in the Earth, noble gases serve as an excellent tracer in resolving the Earth evolution processes such as early differentiation of planetary bodies from the solar nebula, planetesimal impact melting, magma generation and its transportation, and mantle degassing and atmospheric evolution. One of the fundamental physical process controlling the noble gas behavior in the above processes is the noble gas solubility in silicate melt. For example, the variations of elemental abundance of noble gases in the mantle-derived magma are caused by the difference of the solubilities among individual species. Therefore, the noble gas solubility data are indispensable for further understanding of the Earth evolution problems. Many studies of the noble gas solubility in silicate glasses and melts have been carried out [e.g., *Doremus,* 1966; *Shackelford et al.*, 1972; *Shelby,* 1974, 1976; *Jambon et al.,* 1986; *Lux*, 1987; *Broadhurst et al.*, 1990, 1992; *Carroll and Stolper,* 1991, 1993; *Roselieb et al.,* 1992] in recent years. However, the process of noble gas solution in silicate glasses and melts has not yet been understood well. Therefore, I decided to pursuit this problem.

1-2 Noble Gas Solution in Silicate Glass and Melt

Behavior of noble gas dissolution in silicate glass and melt is very interesting. The dissolution in silicate glass and melt is strongly dependent on size of noble gas atom (See Figure 1-1). In general, dissolution is described by interaction between solute and solvent species which is usually related with electric property and atom size of both species. If solvents are benzene, carbon tetrachloride, liquid argon, pure water and seawater, noble gas solubility in those solvents is higher with increasing polarizability of noble gas atom [*Pierotti,* 1963; *Benson and Krause,* 1976] (See Figure 1-1a). However, noble gas solubility in silicate glass and melt shows different trend from that for above-mentioned solvents; the solubility is lower with increasing the polarizability of noble gas atom [*Lux,* 1987; *Hayatsu and Waboso,* 1985]. The solubility decreases as the noble gas atomic size becomes greater (See Figure 1-1b). From the previous work, noble gas dissolution in former solvents like benzene, water and so on is governed by polarizability of each noble gas atom, while the dissolution in silicate glasses and melts is controlled by size of each noble gas atom. The different behavior of noble gas dissolution among solvents would be due to the property of individual solvents. In silicate glass and melt silicon atom combines with a few oxygen atoms, and the combination of silicon and oxygen atoms forms random network structure [*Zachariasen,* 1932] (See Figure 1-2). It has been considered that the network structure in silicate melts leads to the dependence of noble gas dissolution on the atomic size of noble gas. Most studies on noble gas solubility in silicate glasses and melts have been carried out to understand the relationship between the noble gas solubility and the network structure [e.g., *Doremus,* 1966; *Shackelford et al.*, 1972; *Shelby,* 1974, 1976; *Lux,* 1987; *Carroll and Stolper,* 1991, 1993]. Two models have been proposed from these studies.

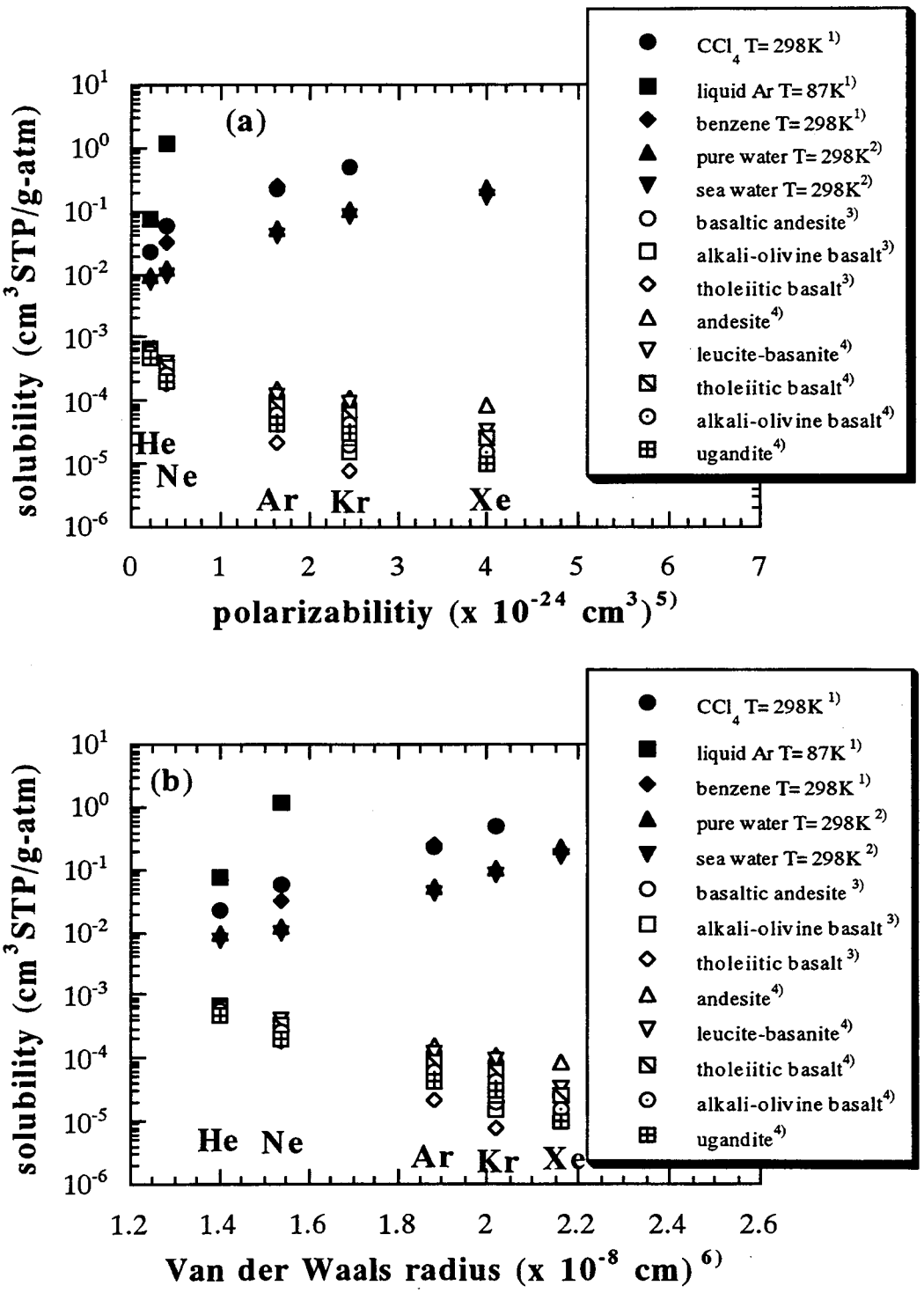

Figure 1-1. Noble gas solubility versus (a) polarizability and (b) Van der Waals radius. In the case of solvent as benzene, CCl_4, water and so on (closed symbols), noble gas solution is governed polarizability. In silicate melts (open symbols), noble gas solubility is dependent on atomic size of noble gas. (1) *Pierotti*, 1963; (2) *Benson and Krause,* 1976; (3) *Hayatsu and Waboso,* 1985; (4) *Lux,* 1987; (5) *Pierotti and Halsey,* 1959; (6) *Bondi,* 1964.

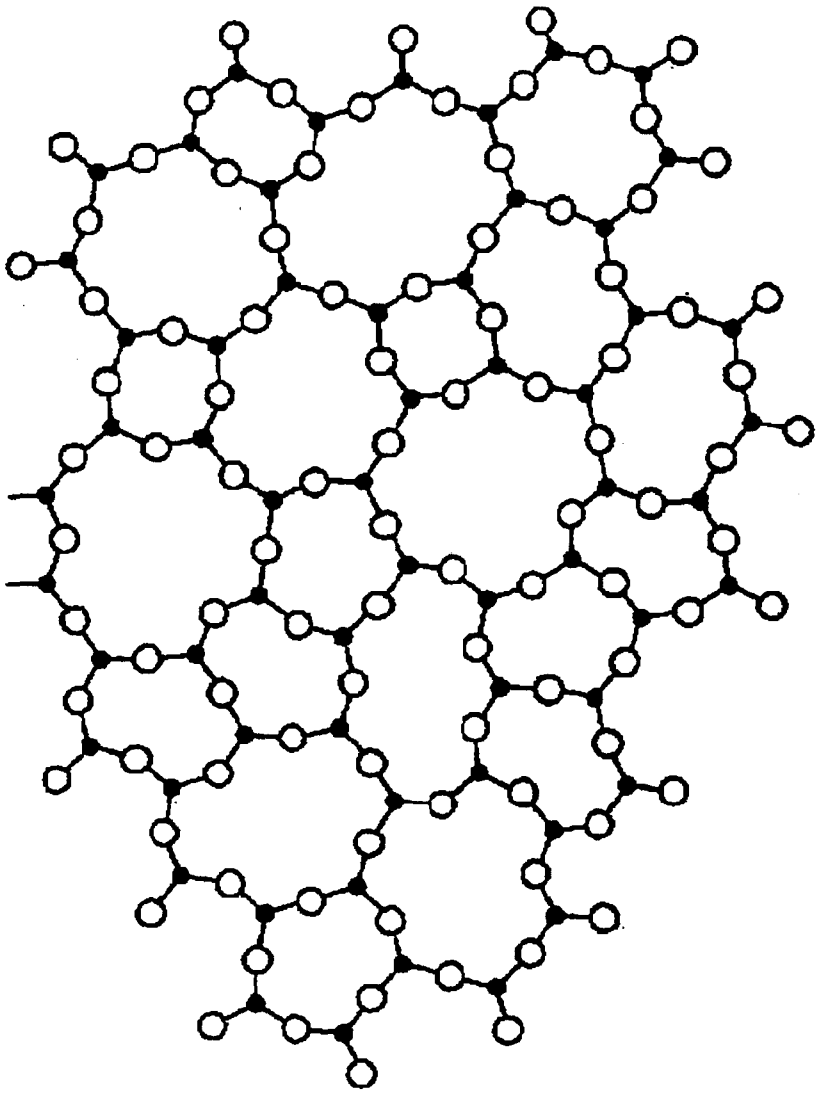

Figure 1-2. Zachariasen's schematic of an $AO_{3/2}$ glass in two dimensions. Open circle is oxygen, O, and closed circle is glass forming cations, A.

Doremus [1966] studied solubilities of He, Ne, H_2 and O_2 in fused silica, and proposed a "free-volume" model in which gas dissolves in an inert material that containing a certain amount of accessible free volume. Gas solubility is given as the ratio of gas concentration in the glass or melt to that in the gas phase. This ratio is constant with changing the partial pressure of the gas under the Henry's law, and changes with the temperature. However, there is small temperature variation of the ratio up to 1000°C. From this experimental result, the free volume should be constant with temperature and pressure as long as the glass structure was not appreciably affected by these variables.

The second model for gas solubility in glass is derived from statistical mechanics [*Shackelford et al.*, 1972]. They measured solubilities of He, Ne and H_2 in silica glass below glass transition zone, and assumed an equilibrium between the gas in the solution and the surrounding gas phase. The equilibrium constant is equal to the ratio of partition function for the dissolved gas atom to that for the gas atom within the gas phase. They estimated the bonding energies between dissolving gas species and surrounding species along with the vibrational frequencies for dissolved species. The bonding energies were of the order expected for Van der Waals bonding, and the vibrational frequencies showed the lower frequencies with heavier species. Although this is a more elegant model than the simple free-volume model by *Doremus* [1966], it is unclear whether the model is suitable for silicate melts containing many elements.

Carroll and Stolper [1991, 1993] have recently modified the free-volume model. They proposed that noble gases might dissolve in "holes" or "channels" in glass structure, and discussed their size distributions in silicate melt and glass in term of ionic porosity which is the difference between the bulk volume of a material and the calculated volume of constituent anion and cations. The ionic porosity is a kind of measure of integrated hole space in the melt and glass. They examined the relationship between the solubility and ionic porosity, and plotted

most published data of noble gas solubility in the simple and natural silicate melts versus ionic porosity, melt density and molar volume; latter two variables have been previously suggested as predictors of noble gas solubility [*Lux,* 1987; *White et al.,* 1989; *Broadhurst et al.,* 1990, 1992]. They concluded that ionic porosity was a better indicator of noble gas solubility than indicators such as molar volume or density for the simple and natural silicate melts (See Figure 1-3). However, this indicator was not useful for only CaO-MgO-Al_2O_3-SiO_2 (CMAS) melts, since the noble gas solubilities in these melts [*White et al.,* 1989; *Broadhurst et al.,* 1992] were lower than those expected from ionic porosity. *Lux* [1987] also indicated that noble gas solubilities in natural silicate melts decreased with increasing content of CaO or MgO.

Several previous studies have measured noble gas solubilities in silicate glasses and melts, and have shown that the solubilities are affected by melt composition; they are generally higher in more SiO_2 rich composition [e.g., *Shelby and Eagan,* 1976; *Hayatsu and Waboso,* 1985; *Lux,* 1987; *White et al.,* 1989]. As is mentioned above, noble gas solution in silicate melt is related with the structure and the composition of the silicate melt. There are many chemical components in natural silicate melts, which makes it complex and difficult to understand the process of noble gas solution. Therefore, I used three binary systems (Na_2O-SiO_2, CaO-SiO_2, MgO-SiO_2) and two ternary systems (Na_2O-CaO-SiO_2, CaO-MgO-SiO_2) as the solvent for noble gas solution. My objective is to understand the relationship between the noble gas solubility and the melt structure. The structures of some of these solvents have been well investigated [e.g., *Virgo et al., 1980*; *Mysen et al.,* 1980, 1982; *Furukawa et al.,* 1981], which aids us in the interpretation of the noble gas solubility data.

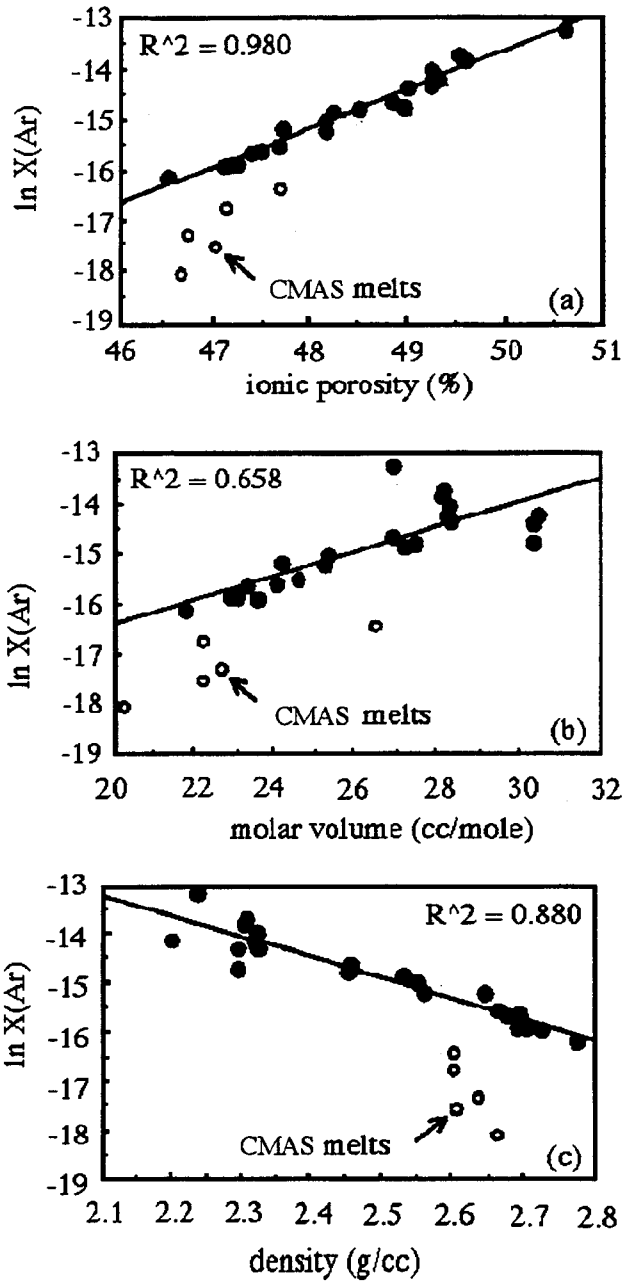

Figure 1-3. Comparisons of correlation between the natural logarithm of mole fraction dissolved Ar at 1 bar gas pressure and (a) ionic porosity, (b) molar volume, and (c) density [From *Carroll and Stolper,* 1993]. Results for simple CaO-MgO-Al_2O_3-SiO_2 (CMAS) melts, shown by open symbols, are excluded from the linear regressions shown by solid lines. Solid symbols show the simple and natural silicate melts except for CMAS melts.

1-3 Structure of Silicate Melts

Many studies for silicate melt structure have been carried out. An understanding of the structure of silicate melts provides basic information on physical and chemical properties of melt and melt-mineral systems. It has been shown that density, viscosity, and thermal expansivity of melts on binary metal oxides (MO or M_2O) and silica (SiO_2) systems are simple functions of the ratio of metal oxide to silica [*Bockris et al.,* 1955, 1956; *Bockris and Kojonen,* 1960]. In particular, the viscosity has been related directly to the anionic structure of the melt [*MacKenzie,* 1960]. The activation energies of viscous flow of more complex melts, involving Al^{3+}, have been used to deduce the structure of aluminosilicate melts [*Riebling,* 1964, 1966; *Shartsis,* 1952]. The pressure dependence of the viscosity of aluminosilicate melts with a three-dimensional network has been used to suggest structural changes with increasing pressure [*Kushiro,* 1976, 1978].

1-3-1. Melts Versus Quenched Melts (Glasses)

In the structural study of silicate melts, quenched melts (glasses) have been used. In order to relate the structure of quenched melts with that of molten silicates, it is necessary to confirm that the structural features under consideration are not significantly affected by quenching. *Riebling* [1968] and *Taylor et al.* [1980] found that the anionic units (silicate polymers) in melts with three-dimensional network structure, such as the melt of $NaAlSi_3O_8$ composition, remain the same when the melt is quenched to glass. Direct experimental proof for structural similarity between melts and glasses on Na_2O-SiO_2 system was provided by *Sweet and White* [1969]. In these studies, infrared and Raman

spectra of melts of Na_2SiO_3, $Na_2Si_2O_5$, and $Na_2Si_3O_7$ compositions were comparable to the spectra of quenched melts. Thermochemical data on 1 atm glasses by *Navrotsky et al.* [1980] indicated that the heat capacity associated with the glass transition was so small that the essential structural features of melts in the system $NaAlSi_3O_8$-$CaAl_2Si_2O_8$-$CaMgSi_2O_6$ at 1 atm were not changed by rapid quenching (several hundred degrees Celsius per second). Therefore, it was concluded that the average structure in silicate melts was virtually the same before and after the quenching.

1-3-2. Studies of Glass and Melt Structure

One of the first theories of silicate glass structure is attributed to *Frankenheim* [1835] who postulated that the glasses are made up of very small crystals which are referred to as crystallites. He speculated that there is a size distribution of crystallites with the smaller ones melting earlier than the larger ones. This speculation can explain the "lubricating" glass which flow at lower temperatures than the melting point. This theory was thought to explain the well-known phenomenon known as glass softening. A similar crystallite structure theory was proposed by *Lebedev* [1921] to explain relatively sharp changes in the properties of silicate glass at temperatures near the $\alpha \leftrightarrow ß$ transition of quartz. *Randall et al.* [1930] carried out one of the first X-ray scattering studies on silicate glasses of geochemical relevance, including the compositions SiO_2, $CaSiO_3$, $NaAlSi_3O_8$ and $KAlSi_3O_8$. They noticed gross similarities between the positions of scattering maxima of each glass and those of the corresponding crystal. On the basis of those observations, they concluded that each of these glasses consisted of very small crystallites (10 to 100 Å in diameter) with an atomic arrangement like the crystal of the same composition. Additional support for the crystallite model was provide by *Valenkov and Porai-Koshits* [1936] who

proposed a revised estimate of crystallite dimension of 7.5 to 25 Å on the basis of X-ray scattering measurements on silicate glass.

Zachariasen [1932, 1935] and *Warren* [1933] proposed a very different model for silicate glass and melt structure which disputed the idea of crystallites. This was the random network model where silicate tetrahedra are linked through corners, that is bridging oxygens, but display no structural ordering similar to crystals of the same composition at distances beyond about 8 Å. *Zachariasen* [1932] envisioned the model that cations such as Na, K and Ca are fitting into the voids created by a random network of corner-linked SiO_4 and AlO_4 tetrahedra and are serving to balance valences. *Zachariasen* [1935] pointed out that a continuous random network was not necessary for glass formation in multi-component silicate systems.

The random network model proposed by *Zachariasen* [1932, 1935] and *Warren* [1933] has also indicated the concept of network forming and network modifying cation. Network formers are those cations that form polyhedra (typically oxygen tetrahedra or triangles) which link through corners to form a three-dimensional network, whereas network modifiers tend to cause depolymerization of these networks. The basis for this concept was provided by *Goldschmidt* [1926] who first suggested that elements with the radius of 0.2 to 0.4 of oxygen atom readily formed glasses. *Zachariasen* [1935] extended Goldschmidt's idea to a set of rules for glass formation. Zachariasen's rules are closely related to Pauling's rules for stable ionic crystals [*Pauling*, 1929] and can be stated as follows for A_mO_n composition [*Rawson*, 1967]:

1. No oxygen atom may be linked to more than two atom A.
2. The number of oxygen atoms surrounding atom A must be small.
3. The oxygen polyhedra share corners with each other, not edges or faces.
4. At least three corners of each oxygen polyhedron must be shared.

On the basis of the rules, the idea of random network is embodied in Figure 1-2. In Figure 1-2, geometric regularity can be avoided without destroying the coordination polyhedra of oxygen about the cation by having A-O-A bond angles, distributed in a random way. This feature ensures that the correlation between the positions of atomic centers will become vanishingly small at distance greater than several O-O bond lengths.

Dietzel [1942] classified forming oxides as those with high field strength. *Sun* [1947] also classified cations as network-forming, intermediate, and network-modifying ones according to high-bonding energy (See Table 1-1).

Table 1-1. Classification of cations in silicate and germanate glasses among three groups.

Cation	valence	CN(1)	BE(2) kJ/mol
network forming cations			
B	3	3	497
B	3	4	372
Si	4	4	443
Ge	3	4	451
P	5	4	464
As	5	4	364
intermediate cations			
Al	3	4	334
Al	3	6	222
Ti	4	6	305
Zn	2	2	301
Zn	2	4	151
Pb	2	2	180
Pb	2	6	163
Be	2	4	263
Cd	2	2	251
network modifying cations			
Sc	3	6	251
La	3	7	242
Y	3	8	209
Sn	4	6	192
Ba	2	8	138

Ca	2	8	134
Sr	2	8	134
Mg	2	6	155
Li	1	4	151
Na	1	6	84
K	1	9	54
Rb	2	10	50
Cs	1	12	42

(1): coordination number
(2): bonding energy

1-3-3. Structure of Silicate Melt

The polymeric nature of liquid and glassy silicates has been recognized and accepted. The concept of silicate as an inorganic polymer is an implicit assumption in the random network model of *Zachariasen* [1932, 1935] which indicates a three-dimensional polymer formed by silicon atoms combining oxygen atoms. In the application of polymer theory to silicate melts [*Masson*, 1965] it is assumed that the simplest species of discrete silicate ion is the orthosilicate ion SiO^{4-}, which is regarded as the monomer. These ions can undergo self-condensation with elimination of free oxygen ion to yield the more polymeric units as dimers, chains, sheets and three-dimensional network structures. However, the polymer theory does not lead to distinction of silicate melts where a fixed number of anionic units coexists [*Masson*, 1977] and does not take into account the effect of metal cations that control the types of anionic structure in silicate melts [*DentGlasser*, 1979]. *Mysen et al.* [1980] noted that polymer models were not likely to give an adequate description of the melt structure, as the primary experimental supporting data by chromatography of trimethylsilyl (TMS) derivatives had been found to be unreliable [*Kuroda and Kato,* 1979]. Instead of TMS derivatives, vibrational spectroscopic methods were pioneered by *Brawer* [1975] and *Brawer and White* [1975, 1977] to study silicate melts. On the

basis of their Raman spectroscopic studies of alkali metal-silica melts, *Brawer and White* [1975] concluded that in the compositional range with NBO/Si (nonbridging oxygen per silicon) less than that of metasilicate the predominant anionic structural units were monomers, chains and sheets. These ideas were formalized and developed further by *Virgo et al.* [1980] and *Mysen et al.* [1980]. Similar data were obtained by *Verweij* [1979] and *Furukawa et al.* [1978]. They concluded that a very limited number of anionic structural units occurred in silicate melts. These units are three-dimensional network structures (SiO_2 units), sheets ($Si_2O_5^{2-}$ units), chains ($Si_2O_6^{4-}$ units), dimers ($Si_2O_7^{6-}$ units) and monomers (SiO_4^{4-} units) (See Figure 1-4).

Objective of this study is to understand the relationship between the noble gas solubility and the melt structure. The structures of some of these solvents have been well investigated [e.g., *Virgo et al.,* 1980; *Mysen et al.,* 1980, 1982; *Furukawa et al.,* 1981], which aids us to interpret the noble gas solubility data. On the basis of many previous data of silicate melt structure and my experimental data of noble gas solubility, I discuss the relationship between noble gas solubility and the melt structure.

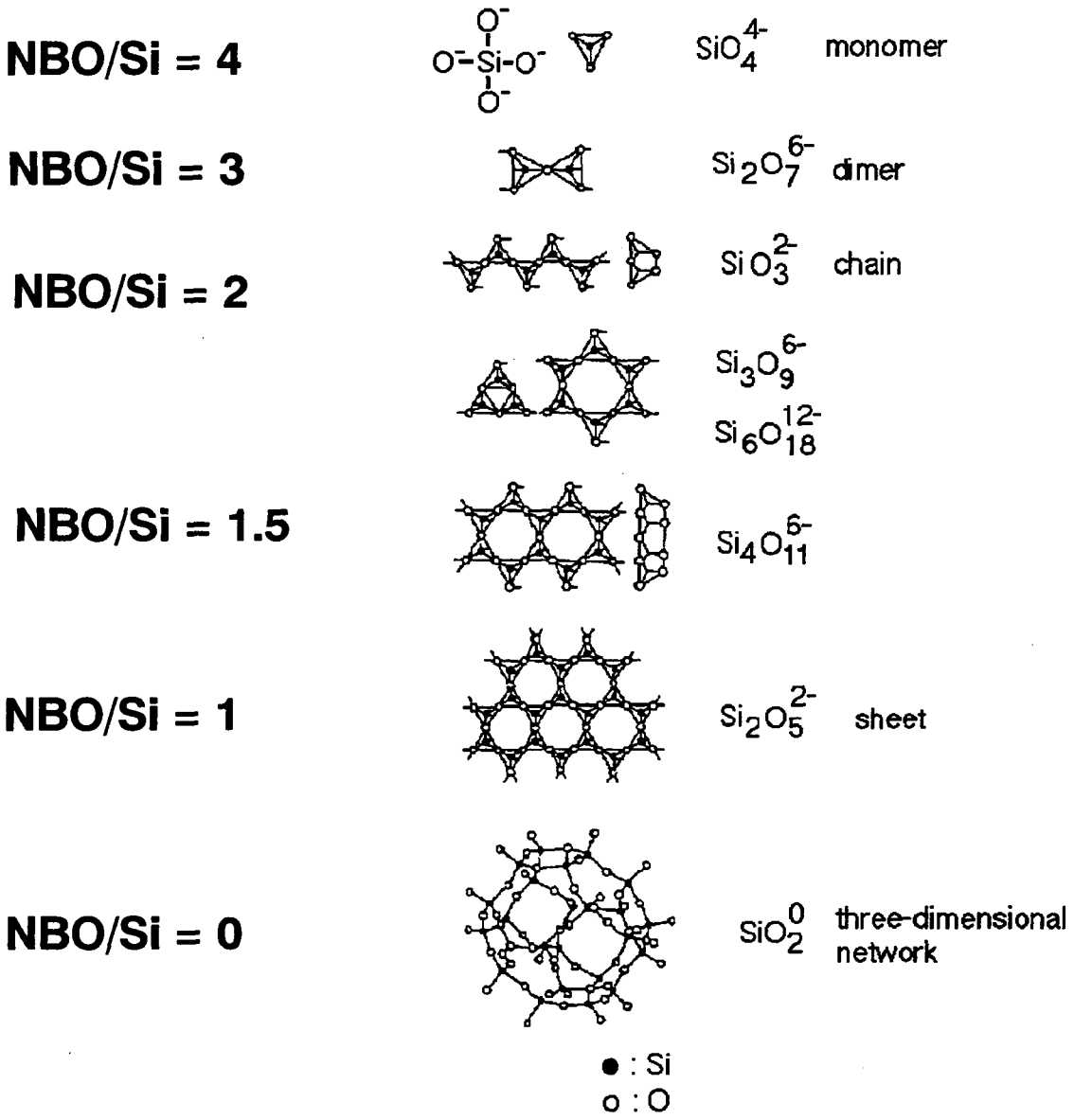

Figure 1-4. In silicate glass and melt, there are the limited anionic structure units; monomer, dimer, chain, sheet and three-dimensional units. Open circle is oxygen and closed circle is silicon. As NBO/Si decreases, the structure units become more polymerization.

2. EXPERIMENT

2-1 Sample Preparation

Three kinds of binary systems (Na_2O-SiO_2, CaO-SiO_2, MgO-SiO_2) and two kinds of ternary systems (Na_2O-CaO-SiO_2, CaO-MgO-SiO_2) were prepared from reagent powders as solvents for noble gas solution. Network structure of some of prepared systems has been well investigated [e.g., *Virgo et al.,* 1980; *Mysen et al.,* 1980, 1982; *Furukawa et al.,* 1981].

Binary Systems

Three sodium silicate glasses (NS1, NS2 and NS3) and three calcium silicate glasses (CS1, CS2 and CS3) were prepared from mixing reagent powders of SiO_2, Na_2CO_3, and $CaCO_3$. One magnesium silicate (MS1) glass was prepared from reagent powder of SiO_2 and forsterite powder made by *Morioka* [1980]. Magnesium silicate glass could be made more easily from forsterite than from MgO, because SiO_2 would be more reactive with forsterite than with reagent powder of MgO. Each glass was mixed in a mortar for one hour. Three SiO_2-Na_2CO_3 mixtures and three SiO_2-$CaCO_3$ mixtures were wrapped in platinum sheets or loaded into platinum baskets, respectively. The SiO_2-Na_2CO_3 mixtures were melted, and decarbonated at 1250°C for one hour in air, and the SiO_2-

$CaCO_3$ mixtures were also heated up from 700°C to 1500°C for 6 hours, melted at 1500°C for 12 hours, and decarbonated in air. The melted mixtures were quenched to form glasses. In order to make magnesium silicate glass, the SiO_2-forsterite mixture was heated at 1600°C for one hour, and melted in air. The melted mixture was quenched by dropping in water.

Ternary Systems

Ternary system glasses were prepared by mixing two binary system glasses described above. Three sodium-calcium silicate glasses (NCS1, NCS2 and NCS3) and three calcium-magnesium silicate glasses (CMS1, CMS2 and CMS3) were mixed by sodium silicate glass (NS2) and calcium silicate glass (CS2), and calcium silicate glass (CS2) and magnesium silicate glass (MS1), respectively. Each of six mixtures was ground into pieces in a mortar for one hour, heated at 1400°C for the NS2-CS2 mixtures and at 1600°C for the CS2-MS1 mixtures, and quenched to glasses, respectively.

Whether the quenched samples were perfectly converted into glasses or not, it caused no serious problem because the samples were again melted at the experiments of noble gas solution. In order to confirm whether the compositions of the samples change during experiments of noble gas solution, the compositions of NS1 sample before and after the dissolution experiments were analyzed by electron microprobe (JEOL JXA-733). NS1 sample has the highest concentration of Na_2O among the samples used in this study. Na is one of highly volatile elements, and is most likely to be lost among the constituent elements. Nine points were analyzed in individual samples before and after the solution experiments. The conditions of the analyses are following: 15 kV for the acceleration voltage, 1.2×10^{-8} A for the beam current, and 50 μm for the beam size. Since the analyzed compositions were practically the same before and after the experiments of noble gas solution, it was not considered that Na is lost from

the samples during the experiments of noble gas solution. Consequently, the compositions did not differ before and after the dissolution experiments and, therefore, compositions only after the experiments were analyzed for the other samples. Results of the composition analyses are listed in Table 2-1.

Table 2-1a. Composition of binary sodium silicate (Na_2O-SiO_2) system (wt%).

Sample	NS1	NS2	NS3
Na_2O	35.67 ±0.23	30.85 ±0.21	23.69 ±0.08
SiO_2	65.12 ±3.23	70.81 ±2.05	76.79 ±0.52
MgO	0.02 ±0.01	0.00 ±0.00	0.03 ±0.00
Total	100.81	101.66	100.51

Analyzed with electron microprobe (JEOL JXA-733) at Osaka University. Eighteen points were analyzed in NS1 sample, and nine points were analyzed in NS2 and NS3 samples. Errors are the reproducibility of the composition analyses for each sample, and show 1 σ.

Table 2-1b. Composition of ternary sodium calcium silicate (Na_2O-CaO-SiO_2) system (wt%).

Sample	NCS1	NCS2	NCS3
Na_2O	19.20 ±0.30	13.82 ±2.58	10.60 ±0.24
SiO_2	69.44 ±0.42	62.35 ±0.32	55.53 ±0.29
CaO	9.13 ±0.13	19.08 ±0.47	30.01 ±0.30
Total	97.77	95.25	96.14

Analyzed with electron microprobe (JEOL-8800) at Tokyo Institute of Technology. Three points were analyzed in individual samples. Errors are the reproducibility of the composition analyses for each sample, and show 1 σ.

Table 2-1c. Composition of CaO-MgO-SiO_2 system (wt%).

Sample	CMS1	CMS2	CMS3
Na_2O	0.08 ±0.01	0.07 ±0.03	0.07 ±0.01
MgO	8.34 ±0.11	16.98 ±0.23	26.35 ±0.26

Al_2O_3	0.82 ±0.06	0.77 ±0.03	0.75 ±0.01
SiO_2	52.50 ±0.10	54.19 ±0.89	57.69 ±0.21
K_2O	0.09 ±0.02	0.09 ±0.01	0.09 ±0.01
CaO	35.83 ±0.12	25.02 ±0.26	13.64 ±0.20
Cr_2O_3	0.01 ±0.01	0.01 ±0.01	0.02 ±0.03
FeO	0.04 ±0.01	0.04 ±0.01	0.03 ±0.03
Total	97.71	97.17	98.64

Analyzed with electron microprobe (JEOL-8800) at Tokyo Institute of Technology. Three points were analyzed in individual samples. Errors are the reproducibility of the composition analyses for each sample, and show 1 σ.

Table 2-1d. Composition of binary calcium silicate and magnesium silicate (CaO-SiO_2 and MgO-SiO_2) system (wt%).

Sample	CS1	CS2	CS3	MS1
Na_2O	0.03	0.04	0.09	0.11
MgO	0.05	0.07	0.03	39.37
Al_2O_3	0.54	0.84	0.88	0.52
SiO_2	48.11	56.71	66.84	53.36
CaO	51.38	41.57	30.69	0.10
FeO	0.04	0.04	0.00	0.00
Total	100.15	99.27	98.53	93.46

Analyzed with electron microprobe (JEOL-8800) at Tokyo Institute of Technology. Since one point was analyzed in individual samples, errors can not be calculated.

2-2 Experiment of Noble Gas Solution in Silicate Melts

An internally heated gas-medium high pressure apparatus with quenching device (KOBELCO SMC-2000) was employed for the experiment of noble gas solution in silicate melts. The apparatus vessel is shown in Figure 2-1. Noble gas mixture, whose volume ratio was listed in Table 2-2 and isotope compositions

were the same as those of atmosphere, was used as pressure medium in the apparatus. The noble gas mixture was prepared and analyzed by Takachiho Trading Co., Ltd.

All prepared glasses were ground to produce grains with their sizes 500-1000 μm. Approximately 10-50 mg of these glass grains were introduced into each platinum capsule (2 or 3 mm in diameter and 10-15 mm in length). One end of the platinum capsule was welded, but the other end was only loosely pinched, so that noble gas mixture could be freely exchanged between the inside of the capsule and noble gas atmosphere outside. These capsules were loaded into a molybdenum basket, and the basket was hung by a molybdenum wire on the position **A** in the internally heated pressure apparatus vessel (See Figure 2-1). The melts in unsealed platinum capsules were exposed to a pressurized noble gas mixture under conditions listed in Table 2-3. The required temperatures in the dissolution experiments were at least above the melting points under an atmospheric pressure for all the samples which were known: NS1, $T_m \approx 870°C$; NS2, $T_m \approx 850°C$; NS3, $T_m \approx 880°C$; NCS1, $T_m \approx 950°C$; NCS2, $T_m \approx 1100°C$; NCS3, $T_m \approx 1250°C$; CS1, $T_m \approx 1550°C$; CS2, $T_m \approx 1550°C$; CS3, $T_m \approx 1550°C$; CMS1, $T_m \approx 1400°C$; CMS2, $T_m \approx 1430°C$; CMS3, $T_m \approx 1450°C$; MS1, $T_m \approx 1550°C$. The pressure was controlled to ± 2 bars and the temperature to ± 2 °C. The experiments were terminated by quenching the silicate melts. The sample quenching is performed by cutting the wire hanging the basket by an electric current, so that the basket drops from **A** to **B**. The temperature of site **B** was constantly less than 150 °C during experiments and quench rate of the samples was over 200 °C/sec. All the quenched glasses were transparent, indicating that all the samples were completely melted under experiments of noble gas solution.

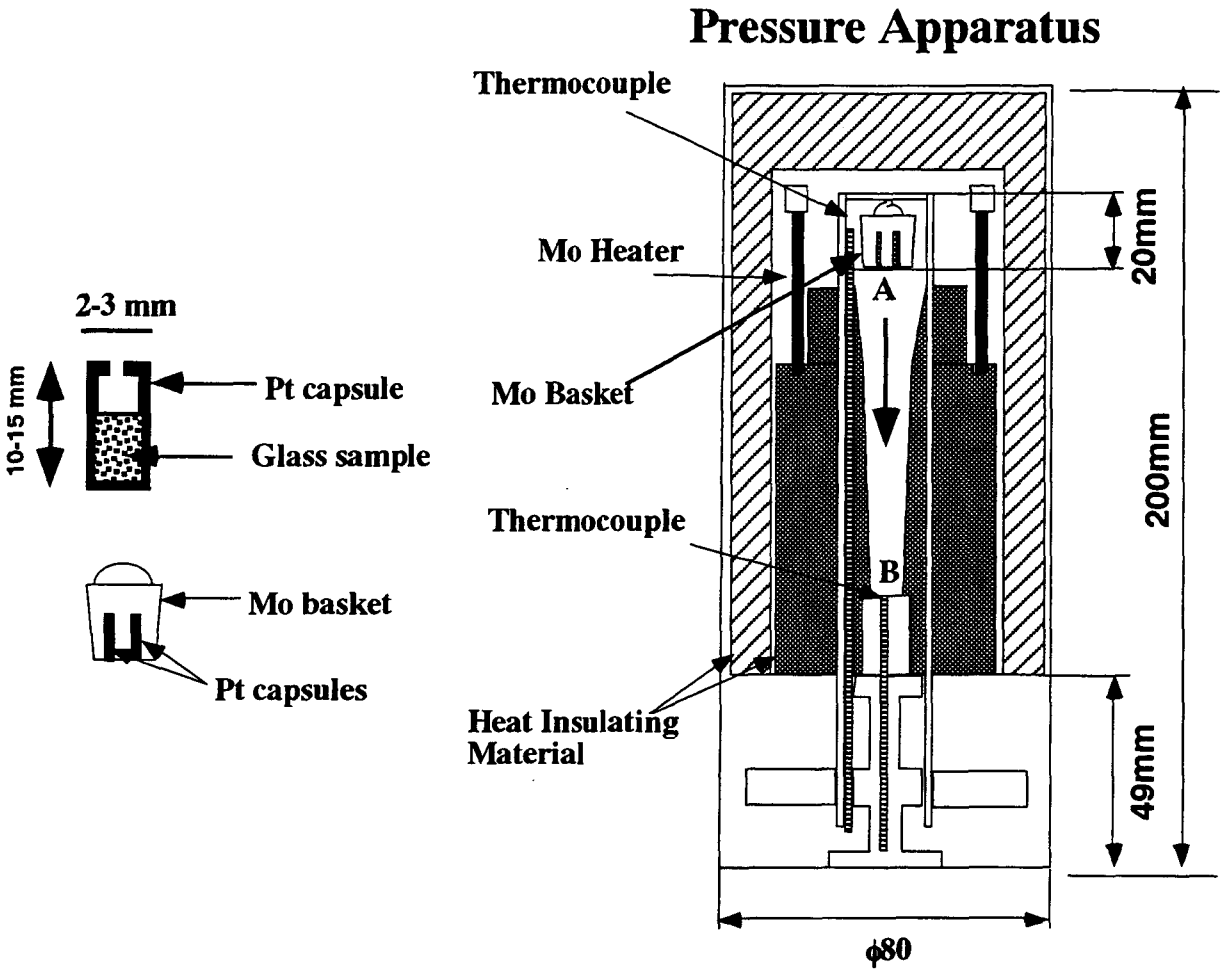

Figure 2-1. The appearance of an internally heated gas-medium high pressure apparatus with quenching device (KOBELCO SMC-2000). Noble gas mixture was used as pressure medium in this apparatus. About 10-50 mg of glass samples were load into Pt capsules, respectively. One end of the Pt capsule was welded, but the other end was only loosely pinched, so that noble gas mixture could be freely exchanged between the inside of the capsule and noble gas atmosphere outside. These capsules were loaded into a molybdenum basket, and the basket was hung by a molybdenum wire on position **A** in the internally heated pressure apparatus. All the melts in unsealed Pt capsules were exposed to a pressurized noble gas mixture. The samples were quenched by dropping the basket from **A** to **B**. The temperature of site **B** was constantly less than 150 °C during experiments and quench rate of the samples is over 200 °C/sec.

No bubble larger than 1 μm could be detected under an optical microscope. Detailed properties of this apparatus are described by *Takahashi and Tomiya* [1992], and the experimental methods are similar to those we used previously [*Shibata et al.,* 1994].

Table 2-2. Volume ratio of noble gas mixture in each run of experiments of noble gas solution in silicate melts. The isotope compositions were the same as those of atmosphere.

run #	G156	G205-G212	G212-G215
He	0.509	0.501	0.506
Ne	1.03	0.0944	0.0931
Ar	98.3	99.3	99.3
Kr	0.102	0.0998	0.100
Xe	0.0104	0.0103	0.0108

Analyzed with gas chromatograph at Takachiho Trading Co., Ltd.

Table 2-3. Conditions of experiments of noble gas solution in silicate melts.

run #	P (kbar)	Temp. (°C)	time duration (hours)	sample
G156	1.10	1600	2.0	CS1, CS2, CS3, and MS1
G205	1.89	1200	13.0	NS1, NS2, NS3, NCS1, and NCS2
G206	1.93	1200	3.0	NS1, NS2, NS3, NCS1, and NCS2
G209	1.97	1300	14.5	NS1, NS2, NS3, NCS1, and NCS2
G211	1.88	1400	12.0	NS1, NS2, NS3, NCS1, NCS2 and NCS3
G212	1.99	1500	5.5	CMS1, CMS2 and CMS3
G215	1.95	1600	5.0	CMS1, CMS2 and CMS3

The temperatures are above the melting points under an atmospheric pressure for all the samples.

2-3 Noble Gas Analysis

A quadrupole mass spectrometer (BALZERS QMG 421) and a sector type mass spectrometer (150 mm radius with both incident and exit angles of 55°) were used for the quantitative noble gas analysis. Calcium silicate system and magnesium silicate system were analyzed by a quadrupole mass spectrometer, and the other silicate systems were by a sector type mass spectrometer. Each mass spectrometer is connected with individual high vacuum lines for gas extraction. The gas extraction line with sector type mass spectrometer is kept in vacuum lower than that with quadrupole mass spectrometer. Although the former line consists very simple sections, it is good enough to measure noble gas in silicate glasses of this study. Some of the important experimental details are outlined here and in the Appendix A. These apparatuses were set up in Planetary Science laboratory at Osaka University.

Individual quenched glasses were separated into several fractions and the amounts of noble gases in two or three fractions for the individual glasses were measured. In order to confirm whether there were bubbles and voids in the silicate glass or not, the glasses were crushed in a high vacuum gas extraction line and extracted gases were analyzed before the glasses were analyzed by fusion. Each fraction of all the glasses was wrapped in clean aluminum foil, put into a crushing apparatus in a high vacuum gas extraction line, and preheated to 150 °C for at least 7 hours to remove adsorbing atmospheric gases. The glass fraction was slowly crushed by the crushing apparatus that consisted of three parts made of stainless steel as shown in Figure 2-1: a piston rod (10 mm in diameter and 30 mm in length) with a disk (10 mm in thickness and 25 mm in diameter), a cylinder (10 mm in inner diameter, 25 mm in outer diameter and 25 mm in length) and a disk (10 mm in thickness and 25 mm in diameter). The crushing apparatus was loaded in a metal valve that was connected with the high vacuum gas extraction line and was tightened by 300 kgf•cm. The amounts of noble gases extracted from the sample were measured. Very small amounts of noble gases

were extracted during the crushing experiments from almost all the glasses. This indicated that there were few bubbles in the glasses. Therefore, the subsequent fractions of the glasses without prior crushing were analyzed by fusion extraction. However, a large amount of noble gases was extracted from only one glass (CS3) during the crushing experiment, indicating the presence of bubbles. Therefore, all three fractions for this sample were crushed to eliminate gas in occluded bubbles, and the crushed fractions were used for the noble gas analyses. The gases extracted during the crushing measurement are not counted as gases dissolving in the specimens.

The crushed and non-crushed glass samples were loaded into glass "Christmas tree" holder connected to the furnace. The samples were baked at 150 °C for at least 7 hours to remove adsorbing atmospheric gases. After baking, the tantalum crucible and molybdenum liner were heated by electric resistance furnace and degassed. Following measurement of blanks, a sample was dropped into the crucible with magnets and iron piece. The sample in the crucible was heated to required temperature for 20 minutes. The temperatures where gases were extracted from samples are higher than melting point under an atmospheric pressure of each sample: 1250 °C for NS1, NS2, NS3, NCS1 and NCS2 systems; 1400 °C for NCS3 system; 1500 °C for CMS1, CMS2 and CMS3 systems; 1630 °C for CS1, CS2, CS3 and MS1 systems. Individually experimental details for all the silicate glasses were also described in Appendix A.

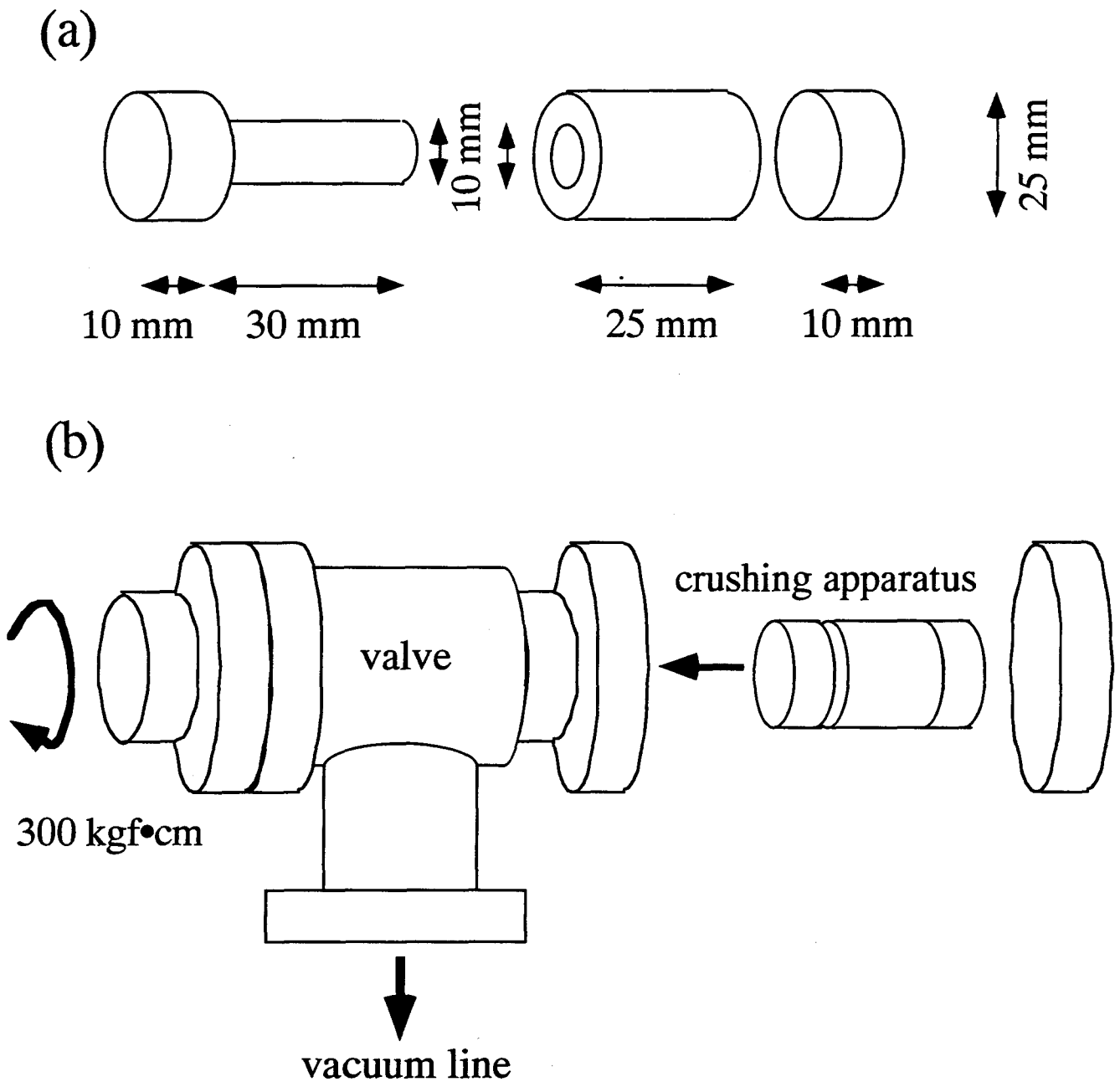

Figure 2-2. Crushing apparatus for gas extraction (a). The crushing vessel was loaded in a metal valve connected to a vacuum line (b). Each glass fraction was crushed in the crushing apparatus attached to the valve. The valve was tightened by 300 kgf•cm.

3. RESULTS

Analyzed samples are listed in Table 2-3 with synthesized conditions of samples. For all the samples, I measured concentrations of helium, neon, argon, krypton and xenon. Results of the concentration measurements are listed in Table 3-1. Although it is not confirmed whether noble gas solubility obeys Henry's law in this work, the noble gas solubility has been proved to obey Henry's law under the pressure of 20 kbars [*White et al.,* 1989; *Montana et al.,* 1993]. Therefore, it would not be serious problem to suppose that the noble gas solubility obeys Henry's law. If the noble gas solubility obeys Henry's law, the noble gas solubility can be approximated by Henry's law; i.e., $f_i = X_i H_i$, where f_i is the fugacity of gas phase "i", X_i is the equilibrium concentration of gas "i" in the solution (here reported in units of cm^3STP/g), and H_i is the Henry's law constant of gas "i". The fugacities during the dissolution experiments are calculated from a Redlich-Kwong equation of state [*Ferry and Baumgartner,* 1987]. Details of the Redlich-Kwong equation are described in Appendix B. The calculated fugacities are listed in Table 3-2. Henry's law constants for all melts are calculated from the fugacities and listed in Table 3-3.

Table 3-1a. Measured noble gas isotopic concentrations in Na_2O-SiO_2 system (cm^3STP/g)

sample run#	temp. (°C)	pressure (kbars)	time (hours)	weight (mg)	^4He	^{20}Ne	^{22}Ne	^{40}Ar cm^3STP/g^*	^{84}Kr	^{132}Xe
NS1										
G205 #1[a]	1200	1.89	13.0	1.49	4.66(-4)	1.17(-6)	3.86(-7)	7.95(-5)	2.43(-8)	5.57(-10)
G205 #1[b]	1200	1.89	13.0	1.49	3.38(-3)	1.10(-3)	1.06(-4)	2.33(-1)	7.12(-5)	1.79(-6)
G205 #1[c]	1200	1.89	13.0	1.49	4.01(-6)	1.39(-7)	1.26(-6)	5.05(-5)	1.67(-8)	4.54(-8)
G205 #2	1200	1.89	13.0	1.98	3.98(-3)	-	1.49(-4)	2.09(-1)	6.12(-5)	1.73(-6)
G206 #1	1200	1.93	3.0	1.96	4.86(-3)	1.04(-3)	1.02(-4)	2.34(-1)	7.33(-5)	1.69(-6)
G209 #1	1300	1.97	14.5	1.93	4.22(-3)	1.12(-3)	1.10(-4)	2.92(-1)	9.56(-5)	2.47(-6)
G209 #2	1300	1.97	14.5	1.20	6.03(-3)	-	1.62(-4)	2.09(-1)	6.11(-5)	1.97(-6)
G209 #3	1300	1.97	14.5	0.98	5.47(-3)	-	1.66(-4)	1.91(-1)	5.06(-5)	1.75(-6)
G211 #1	1400	1.88	12.0	1.41	9.65(-3)	1.63(-3)	1.63(-4)	2.80(-1)	6.23(-5)	6.25(-7)
G211 #2	1400	1.88	12.0	1.14	4.95(-3)	-	1.65(-4)	2.41(-1)	6.87(-5)	2.14(-6)
G211 #3	1400	1.88	12.0	1.05	4.50(-3)	-	1.59(-4)	2.29(-1)	7.11(-5)	8.69(-7)
NS2										
G205 #1[a]	1200	1.89	13.0	2.12	4.70(-3)	1.03(-5)	1.18(-6)	3.18(-4)	8.90(-8)	1.27(-9)
G205 #1[b]	1200	1.89	13.0	2.12	3.11(-4)	1.31(-3)	1.19(-4)	3.29(-1)	1.10(-4)	2.20(-6)
G205 #1[c]	1200	1.89	13.0	2.12	1.49(-5)	2.75(-8)	7.58(-7)	2.90(-4)	4.20(-7)	7.68(-8)
G205 #2	1200	1.89	13.0	1.49	7.79(-3)	-	1.58(-4)	2.22(-1)	4.24(-5)	3.57(-7)

G206 #1	1200	1.93	3.0	1.48	5.38(-3)	1.23(-3)	1.31(-4)	1.21(-1)	2.03(-5)	1.59(-7)
G209 #1	1300	1.97	14.5	0.80	5.78(-3)	1.50(-3)	1.68(-4)	3.90(-1)	1.22(-4)	2.68(-6)
G209 #3	1300	1.97	14.5	1.12	8.18(-3)	-	1.88(-4)	4.20(-1)	1.24(-4)	2.93(-6)
G211 #1	1400	1.88	12.0	1.09	7.72(-3)	1.86(-3)	1.84(-4)	4.33(-1)	1.55(-4)	5.39(-6)
G211 #2	1400	1.88	12.0	1.65	8.24(-3)	-	1.74(-4)	3.41(-1)	1.24(-4)	4.88(-6)
G211 #3	1400	1.88	12.0	1.15	9.25(-3)	-	1.95(-4)	3.25(-1)	1.17(-4)	4.64(-6)
NS3										
G205 #1	1200	1.89	13.0	0.98	9.73(-4)	-	2.03(-4)	4.14(-1)	1.43(-4)	3.98(-6)
G205 #2[a]	1200	1.89	13.0	1.64	1.93(-3)	6.28(-6)	6.66(-7)	2.18(-4)	4.97(-8)	6.79(-10)
G205 #2[b]	1200	1.89	13.0	1.64	6.98(-5)	1.61(-3)	1.51(-4)	3.94(-1)	6.66(-5)	6.28(-7)
G205 #2[c]	1200	1.89	13.0	1.64	3.88(-6)	5.79(-6)	3.51(-8)	5.47(-3)	2.32(-6)	1.08(-7)
G205 #3	1200	1.89	13.0	0.60	3.13(-3)	-	1.76(-4)	3.90(-1)	9.58(-5)	1.14(-6)
G206 #1	1200	1.93	3.0	1.79	3.51(-3)	1.74(-3)	1.71(-4)	2.41(-1)	4.61(-5)	2.13(-6)
G209 #1	1300	1.97	14.5	1.67	5.72(-3)	2.05(-3)	1.88(-4)	5.47(-1)	1.84(-4)	6.25(-6)
G209 #2	1300	1.97	14.5	1.92	4.13(-3)	-	2.10(-4)	5.47(-1)	1.84(-4)	2.77(-6)
G209 #3	1300	1.97	14.5	1.38	3.65(-3)	-	2.50(-4)	5.39(-1)	1.89(-4)	3.99(-6)
G211 #1	1400	1.88	12.0	2.22	8.06(-3)	2.22(-3)	1.94(-4)	5.66(-1)	1.97(-4)	6.25(-6)
G211 #2	1400	1.88	12.0	1.34	4.28(-3)	-	2.41(-4)	5.61(-1)	2.04(-4)	5.82(-6)
G211 #3	1400	1.88	12.0	2.03	2.99(-3)	-	2.08(-4)	5.54(-1)	1.99(-4)	5.59(-6)

All gases were extracted by fusion at 1250°C.

*: The numerical value in the parentheses is exponent factor.

[a]: These values were estimated from released gases by crushing the samples (300 kgf•cm) in a high vacuum line.

[b]: These gases were extracted by fusion at 1250°C after crushing extraction.

[c]: In order to confirm whether all gases were extracted from samples with a single fusion at 1250°C or not, the samples were again heated to 1250°C, and the gases were subsequently analyzed and amounts of the gases were close to those of hot blank. It is concluded that all gases were extracted from samples with a single fusion at 1250°C.

Hot Blanks at 1250°C (cm^3STP) ^{4}He: (3.1-52) $x10^{-9}$; ^{20}Ne: (2.1-190) $x10^{-10}$; ^{22}Ne: (1.5-34) $x10^{-9}$; ^{40}Ar: (7.5-230) $x10^{-8}$; ^{84}Kr: (1.8-4200) $x10^{-11}$; ^{132}Xe: (4.7-1300) $x10^{-11}$.

Table 3-1b. Measured noble gas isotopic concentrations in Na_2O-CaO-SiO_2 system (cm^3STP/g)

sample run#	temp. (°C)	pressure (kbars)	time (hours)	weight (mg)	^{4}He	^{20}Ne	^{22}Ne	^{40}Ar	^{84}Kr	^{132}Xe
								cm^3STP/g*		
NCS1										
G205 #1	1200	1.89	13.0	1.20	4.34(-3)	-	8.56(-5)	2.17(-1)	7.32(-5)	2.04(-6)
G205 #3	1200	1.89	13.0	1.30	6.50(-3)	-	9.11(-5)	1.92(-1)	6.38(-5)	1.62(-6)
G206 #1	1200	1.93	3.0	1.85	7.78(-3)	1.01(-3)	9.96(-5)	2.06(-1)	5.43(-5)	1.05(-6)
G209 #2	1300	1.97	14.5	1.45	7.78(-3)	-	1.48(-4)	2.48(-1)	8.17(-5)	1.59(-6)
G209 #3	1300	1.97	14.5	1.05	6.50(-3)	-	9.26(-5)	1.87(-1)	6.52(-5)	1.46(-6)
G211 #1	1400	1.88	12.0	2.00	6.01(-3)	1.31(-3)	1.25(-4)	3.01(-1)	1.01(-4)	2.66(-6)

G211 #3	1400	1.88	12.0	1.73	6.32(-3)	-	1.48(-4)	2.93(-1)	1.01(-4)	2.64(-6)
NCS2										
G205 #1	1200	1.89	13.0	0.73	5.07(-3)	-	7.62(-5)	1.48(-1)	4.76(-5)	9.03(-7)
G205 #2[a]	1200	1.89	13.0	1.42	2.55(-4)	6.38(-7)	5.54(-7)	3.54(-5)	1.38(-8)	5.35(-11)
G205 #2[b]	1200	1.89	13.0	1.42	3.12(-3)	7.14(-4)	6.20(-5)	1.32(-1)	3.81(-5)	5.84(-7)
G205 #2[c]	1200	1.89	13.0	1.42	4.14(-6)	1.45(-6)	1.07(-6)	1.34(-3)	6.28(-7)	1.18(-7)
G205 #3	1200	1.89	13.0	0.89	5.74(-3)	-	7.02(-5)	1.19(-1)	2.82(-5)	3.82(-7)
G206 #1	1200	1.93	3.0	1.15	5.39(-3)	6.95(-4)	6.44(-5)	9.44(-2)	2.17(-5)	3.26(-7)
G209 #1	1300	1.97	14.5	0.91	1.90(-3)	7.14(-4)	6.06(-5)	1.62(-1)	5.27(-5)	1.24(-6)
G209 #4	1300	1.97	14.5	1.76	7.80(-3)	-	8.15(-5)	1.75(-1)	5.61(-5)	1.11(-6)
G209 #6	1300	1.97	14.5	1.82	4.50(-3)	-	1.24(-4)	1.57(-1)	5.17(-5)	1.39(-6)
G211 #3	1400	1.88	12.0	2.31	6.42(-3)	1.00(-3)	9.69(-5)	2.10(-1)	7.03(-5)	1.74(-6)
G211 #4	1400	1.88	12.0	1.65	8.06(-3)	-	8.00(-5)	1.79(-1)	5.83(-5)	1.10(-6)
G211 #5	1400	1.88	12.0	2.24	7.44(-3)	-	1.11(-4)	1.83(-1)	6.14(-5)	1.51(-6)
NCS3										
G211 #1	1400	1.88	12.0	0.99	4.90(-3)	-	5.40(-5)	1.02(-1)	3.17(-5)	5.71(-7)
G211 #1[c]	1400	1.88	12.0	0.99	1.90(-4)	-	4.73(-6)	1.24(-4)	8.56(-8)	2.92(-7)
G211 #2	1400	1.88	12.0	0.95	5.03(-3)	-	5.23(-5)	9.83(-2)	3.02(-5)	6.97(-7)
G211 #3[a]	1400	1.88	12.0	1.02	8.01(-6)	1.60(-7)	4.90(-7)	1.89(-5)	3.47(-10)	1.44(-10)
G211 #3[b]	1400	1.88	12.0	1.02	1.87(-3)	2.55(-4)	2.45(-5)	5.67(-2)	1.82(-5)	6.40(-7)

Gases in NCS1 and NCS2 glasses and in NCS3 glass were extracted by fusion at 1250°C and 1400°C.

*: The numerical value in the parentheses is exponent factor.

[a]: These values were estimated from released gases by crushing the samples (300 kgf•cm) in a high vacuum line.

[b]: These gases were extracted by fusion at 1250°C (or 1400°C) after crushing extraction.

[c]: In order to confirm whether all gases were extracted from samples with a single fusion at 1250°C (or 1400°C) or not, the samples were again heated to 1250°C (or 1400°C), and the gases were subsequently analyzed and amounts of the gases were close to those of hot blank. It is concluded that all gases were extracted from samples with a single fusion at 1250°C (or 1400°C).

Hot Blanks at 1250°C (cm^3STP) ^{4}He: (3.1-38) x10^{-9}; ^{20}Ne: (8.6-190) x10^{-10}; ^{22}Ne: (1.5-9.9) x10^{-9}; ^{40}Ar: (0.87-230) x10^{-7}; ^{84}Kr: (1.1-130) x10^{-10}; ^{132}Xe: (1.7-130) x10^{-10}.

Hot Blanks at 1400°C (cm^3STP) ^{4}He: (2.2-47) x10^{-8}; ^{20}Ne: (8.6-9.0) x10^{-8}; ^{22}Ne: (2.7-8.3) x10^{-9}; ^{40}Ar: (1.1-17) x10^{-7}; ^{84}Kr: (6.0-97) x10^{-11}; ^{132}Xe: (1.3-18) x10^{-10}.

Table 3-1c. Measured noble gas isotopic concentrations in CaO-MgO-SiO_2 system (cm^3STP/g)

sample run#	temp. (°C)	pressure (kbars)	time (hours)	weight (mg)	^{4}He	^{20}Ne	^{22}Ne	^{40}Ar	^{84}Kr	^{132}Xe
								cm^3STP/g*		
CMS1										
G212 #2[a]	1500	1.99	5.5	1.47	1.54(-5)	2.75(-6)	7.59(-7)	1.62(-3)	9.74(-7)	5.50(-8)
G212 #2[b]	1500	1.99	5.5	1.47	2.29(-3)	2.45(-4)	1.96(-5)	4.01(-2)	1.37(-5)	5.67(-7)
G212 #3	1500	1.99	5.5	0.87	1.73(-3)	-	2.75(-5)	4.01(-2)	1.18(-5)	4.94(-7)
G212 #4	1500	1.99	5.5	2.00	2.97(-3)	-	2.67(-5)	3.86(-2)	1.17(-5)	5.12(-7)
G215 #1	1600	1.95	5.0	1.83	2.36(-3)	-	2.67(-5)	4.34(-2)	1.29(-5)	3.65(-7)
G215 #2	1600	1.95	5.0	2.05	3.19(-3)	-	3.10(-5)	4.71(-2)	1.35(-5)	2.06(-7)

G215 #3	1600	1.95	5.0	1.92	2.95(-3)	2.83(-4)	2.48(-5)	4.56(-2)	1.44(-5)	2.90(-7)
CMS2										
G212 #3[a]	1500	1.99	5.5	2.16	1.78(-6)	8.94(-8)	2.76(-7)	1.47(-5)	1.54(-9)	3.27(-10)
G212 #3[b]	1500	1.99	5.5	2.16	3.07(-3)	2.67(-4)	2.26(-5)	4.05(-2)	1.31(-5)	2.99(-7)
G212 #4	1500	1.99	5.5	2.90	3.28(-3)	-	2.55(-5)	4.37(-2)	1.35(-5)	4.10(-7)
G212 #4[c]	1500	1.99	5.5	2.90	4.23(-6)	-	1.11(-6)	1.19(-4)	7.74(-8)	9.25(-8)
G212 #5	1500	1.99	5.5	2.59	2.79(-3)	-	2.46(-5)	4.23(-2)	1.29(-5)	3.48(-7)
CMS3										
G212 #1	1500	1.99	5.5	1.30	2.66(-3)	-	3.94(-5)	5.20(-2)	1.59(-5)	4.97(-7)
G212 #2[a]	1500	1.99	5.5	2.10	1.49(-6)	3.29(-8)	2.83(-7)	1.61(-5)	8.40(-9)	2.05(-10)
G212 #2[b]	1500	1.99	5.5	2.10	2.41(-3)	2.42(-4)	2.04(-5)	3.91(-2)	1.24(-5)	2.53(-7)
G212 #3	1500	1.99	5.5	1.58	2.77(-3)	-	3.82(-5)	5.21(-2)	1.60(-5)	4.55(-7)
G215 #1	1600	1.95	5.0	1.72	3.53(-3)	-	3.38(-5)	6.18(-2)	1.93(-5)	4.29(-7)
G215 #2	1600	1.95	5.0	2.28	3.48(-3)	-	3.34(-5)	5.97(-2)	2.00(-5)	3.47(-7)

All gases were extracted by fusion at 1500°C.

*: The numerical value in the parentheses is exponent factor.

[a]: These values were estimated from released gases by crushing the samples (300 kgf•cm) in a high vacuum line.

[b]: These gases were extracted by fusion at 1500°C after crushing extraction.

[c]: In order to confirm whether all gases were extracted from samples with a single fusion at 1500°C or not, the samples were again heated to 1500°C, and the gases were subsequently analyzed and amounts of the gases were close to those of hot blank. It is concluded that all gases were extracted from samples with a single fusion at 1500°C.

Hot Blanks at 1500°C (cm^3STP) ^{4}He: (2.2-47) $x10^{-8}$; ^{20}Ne: (8.6-9.0) $x10^{-8}$; ^{22}Ne: (2.7-8.3) $x10^{-9}$; ^{40}Ar: (1.1-17) $x10^{-7}$; ^{84}Kr: (6.0-97) $x10^{-11}$; ^{132}Xe: (1.3-18) $x10^{-10}$.

Table 3-1d. Measured noble gas isotopic concentrations in $CaO-SiO_2$ and $MgO-SiO_2$ system (cm^3STP/g)

sample run#	temp. (°C)	pressure (kbars)	time (hours)	weight (mg)	^{4}He	^{20}Ne	^{22}Ne	^{40}Ar	^{84}Kr	^{132}Xe
								cm^3STP/g*		
CS1										
G156 #1[a]	1600	1.10	2.0	0.62	9.23(-7)	4.47(-6)	4.38(-8)	6.07(-6)	1.56(-9)	3.51(-11)
G156 #1[b]	1600	1.10	2.0	0.62	7.19(-4)	7.81(-4)	8.17(-5)	1.40(-2)	4.02(-6)	6.83(-8)
G156 #2	1600	1.10	2.0	1.38	5.01(-4)	7.07(-4)	7.34(-5)	1.32(-2)	3.91(-6)	6.62(-8)
G156 #3	1600	1.10	2.0	1.10	4.23(-4)	7.08(-4)	7.49(-5)	1.36(-2)	3.97(-6)	7.13(-8)
CS2										
G156 #1	1600	1.10	2.0	1.46	9.75(-4)	1.62(-3)	1.73(-4)	3.95(-2)	1.34(-5)	2.56(-7)
G156 #2[a]	1600	1.10	2.0	2.08	2.85(-7)	6.84(-8)	4.26(-9)	1.33(-6)	1.17(-9)	4.75(-11)
G156 #2[b]	1600	1.10	2.0	2.08	8.52(-4)	1.33(-3)	1.40(-4)	3.28(-2)	1.09(-5)	2.05(-7)
G156 #3	1600	1.10	2.0	2.08	1.16(-3)	1.66(-3)	1.81(-4)	3.91(-2)	1.37(-5)	2.51(-7)
CS3										
G156 #1[a]	1600	1.10	2.0	0.80	8.59(-5)	1.25(-4)	1.24(-5)	3.76(-4)	2.16(-7)	9.81(-9)
G156 #1[b]	1600	1.10	2.0	0.80	2.39(-3)	3.32(-3)	3.41(-4)	1.09(-1)	4.25(-5)	9.27(-7)
G156 #2[a]	1600	1.10	2.0	1.49	4.36(-4)	9.34(-4)	9.65(-5)	2.00(-2)	1.19(-5)	5.26(-7)
G156 #2[b]	1600	1.10	2.0	1.49	2.61(-3)	3.33(-3)	3.48(-4)	1.16(-1)	4.56(-5)	9.80(-7)
G156 #3[a]	1600	1.10	2.0	3.79	5.05(-4)	1.77(-3)	1.87(-4)	3.46(-2)	2.05(-5)	8.51(-7)

G156 #3[b]	1600	1.10	2.0	3.79	1.83(-3)	2.63(-3)	2.86(-4)	1.08(-1)	4.06(-5)	9.15(-7)
MS1										
G156 #1	1600	1.10	2.0	0.64	1.35(-3)	1.52(-3)	1.58(-4)	3.40(-2)	1.19(-5)	2.23(-7)
G156 #2[a]	1600	1.10	2.0	0.79	5.37(-8)	3.40(-8)	3.07(-9)	3.15(-6)	2.41(-9)	1.93(-10)
G156 #2[b]	1600	1.10	2.0	0.79	7.18(-4)	8.56(-4)	9.09(-5)	1.88(-2)	6.76(-6)	1.32(-7)

All gases were extracted by fusion at 1630°C.

*: The numerical value in the parentheses is exponent factor.

[a]: These values were estimated from released gases by crushing the samples (300 kgf•cm) in a high vacuum line.

[b]: These gases were extracted by fusion at 1630°C after crushing extraction.

Hot Blanks at 1630°C (cm^3STP) ^{4}He: (5.7-440) x10^{-12}; ^{20}Ne: (1.1-8.2) x10^{-11}; ^{22}Ne: (5.7-7.1) x10^{-12}; ^{40}Ar: (1.3-37) x10^{-9}; ^{84}Kr: (1.7-12) x10^{-11}; ^{132}Xe: (1.6-36) x10^{-13}.

Table 3-2. Fugacities during the dissolution experiments. The fugacities are calculated by using a Redlich-Kwong equation of state [*Ferry and Baumgartner*, 1987].

run#	He	Ne	Ar	Kr	Xe
			bar		
G156	6.36	12.4	1250	1.33	0.141
G205	12.5	2.15	2540	2.69	0.301
G206	12.9	2.21	2620	2.77	0.311
G209	13.0	2.24	2650	2.80	0.314
G211	12.0	2.10	2460	2.59	0.289
G212	12.8	2.18	2600	2.75	0.309
G215	12.3	2.12	2510	2.64	0.296

Table 3-3a. Noble gas solubilities in Na_2O-SiO_2 system (cm^3STP/g-bar). All values of noble gases are normalized by each fugacity of synthetic conditions.

sample run#	He	Ne	Ar	Kr	Xe
			x 10^{-5} cm^3STP/g-bar		
NS1					
G205	31.3 ±0.7	64.3 ±15.3	8.73 ±0.69	4.32 ±0.46	2.17 ±0.05
G206	37.8	49.9	8.98	4.65	2.02
G209	40.4 ±7.2	70.5 ±15.1	8.74 ±2.04	4.32 ±1.47	2.44 ±0.44
G211	52.9 ±23.7	83.6 ±1.5	10.2 ±1.1	4.56 ±0.31	1.56 ±1.05
NS2					
G205	51.2 ±15.7	69.6 ±13.8	10.9 ±3.0	4.98 ±3.13	1.58 ±1.61
G206	41.8	64.5	4.66	1.28	0.190
G209	53.8 ±13.1	86.3 ±6.8	15.4 ±0.8	7.70 ±0.11	3.32 ±0.21
G211	69.8 ±6.5	95.0 ±5.5	15.0 ±2.4	8.92 ±1.36	6.39 ±0.50
NS3					
G205	16.3 ±8.6	89.0 ±13.0	15.8 ±0.5	6.65 ±2.52	2.37 ±2.23
G206	27.3	84.0	9.26	2.92	2.56
G209	34.7 ±8.4	105 ±15	20.6 ±0.2	11.6 ±0.2	5.13 ±2.08
G211	42.4 ±21.9	111 ±12	22.9 ±0.3	13.5 ±0.2	7.57 ±0.43

Errors are the reproducibility of the noble gas analyses for each sample, and show 1 σ. Errors of the G206 sample could not be calculated because only one analysis of noble gas was performed in the sample.

Table 3-3b. Noble gas solubilities in Na_2O-CaO-SiO_2 system (cm^3STP/g-bar). All values of noble gases are normalized by each fugacity of synthetic conditions.

sample run#	He	Ne	Ar	Kr	Xe
			x 10^{-5} cm^3STP/g-bar		
NCS1					
G205	43.3 ±12.2	44.5 ±2.0	8.08 ±0.68	4.47 ±0.43	2.26 ±0.36
G206	60.6	48.9	7.91	3.44	1.26
G209	55.1 ±7.0	58.3 ±19.1	8.26 ±1.63	4.60 ±0.73	1.80 ±0.11
G211	51.2 ±1.8	70.4 ±8.7	12.1 ±0.2	6.84 ±0.00	3.41 ±0.02
NCS2					
G205	37.1 ±10.9	35.0 ±3.6	5.24 ±0.58	2.48 ±0.63	0.770 ±0.324
G206	41.9	31.6	3.62	1.37	0.391
G209	36.5 ±22.8	42.9 ±15.7	6.23 ±0.36	3.35 ±0.15	1.47 ±0.11
G211	60.7 ±6.9	49.5 ±8.0	7.78 ±0.67	4.28 ±0.42	1.87 ±0.42
NCS3					
G211	32.7 ±14.8	22.5 ±8.5	3.50 ±1.03	1.81 ±0.50	0.818 ±0.081

Errors are the reproducibility of the noble gas analyses for each sample, and show 1 σ. Errors of the G206 sample could not be calculated because only one analysis of noble gas was performed in the sample.

Table 3-3c. Noble gas solubilities in CaO-MgO-SiO_2 system (cm^3STP/g-bar). All values of noble gases are normalized by each fugacity of synthetic conditions.

sample run#	He	Ne	Ar	Kr	Xe
			x 10^{-5} cm^3STP/g-bar		
CMS1					
G212	18.2 ±4.8	12.2 ±2.2	1.53 ±0.03	0.792 ±0.071	0.631 ±0.045
G215	23.0 ±3.5	14.0 ±1.6	1.82 ±0.07	0.902 ±0.047	0.361 ±0.100
CMS2					

G212	23.8 ±1.9	12.0 ±0.7	1.63 ±0.06	0.839 ±0.020	0.424 ±0.067
CMS3					
G212	20.6 ±1.1	16.3 ±5.1	1.86 ±0.26	0.951 ±0.114	0.488 ±0.149
G215	28.4 ±0.3	17.2 ±0.2	2.43 ±0.06	1.30 ±0.03	0.488 ±0.73

Errors are the reproducibility of the noble gas analyses for each sample, and show 1 σ.

Table 3-3d. Noble gas solubilities in $CaO\text{-}SiO_2$ and $MgO\text{-}SiO_2$ system ($cm^3STP/g\text{-}bar$). All values of noble gases are normalized by each fugacity of synthetic conditions.

sample run#	He	Ne	Ar	Kr	Xe
			x 10^{-5} $cm^3STP/g\text{-}bar$		
CS1					
G156	8.64 ±2.41	6.54 ±0.37	1.09 ±0.03	0.524 ±0.007	0.181 ±0.006
CS2					
G156	15.6 ±2.4	13.7 ±1.6	2.98 ±0.30	1.66 ±0.19	0.626 ±0.074
CS3					
G156	35.8 ±6.3	27.6 ±3.5	8.92 ±0.35	5.67 ±0.33	2.48 ±0.09
MS1					
G156	16.3 ±7.0	10.6 ±3.9	2.12 ±0.89	1.23 ±0.48	0.469 ±0.170

Errors are the reproducibility of the noble gas analyses for each sample, and show 1 σ.

3-1 Equilibrium Condition

We evaluated the equilibrium condition by comparing the typical diffusive length of a noble gas atom with the typical grain size of the glasses. We can write the equilibrium condition as

$$\sqrt{D_i t} \geq r,$$

where D_i is the diffusion coefficient for noble gas "i" in silicate melts, t is the time duration of the solubility experiment, and r is the radius of glass pieces. It is sufficient to examine the equilibrium condition for Xe which has the lowest diffusivity among five noble gases. *Lux* [1987] obtained the value of the diffusion coefficient, 3 x 10^{-6} cm^2/s, at 1350 °C for Xe in tholeiite basalt at an atmospheric pressure. Since the diffusion coefficient of Ar in SiO_2 glass is independent of pressure up to 4 kbars [*Carroll and Stolper,* 1991], it would be no serious problem to use the diffusion coefficient under an atmospheric pressure for estimating the typical diffusive length. We could obtain a typical diffusion length of 1000 μm for one hour from the value of 3 x 10^{-6} cm^2/s. This value is larger than the typical grain size (r = 500-1000 μm) in this experiment. However, since all the samples have finally been melted, it is unclear whether the equilibrium condition could be confirmed by comparing the typical diffusive length of a noble gas atom with the typical grain size of the glasses. Therefore, I measured time variation of noble gas solubility for NS1, NS2, NS3, NCS1 and NCS2 at 1200 °C (See Figures 3-1 a-e). For all the samples, almost all the data of solubilities for 3 hours are within 1σ of the solubilities for 13 hours, which is the reproducibility of the noble gas analyses for each sample. Therefore, it can be concluded that 3 hours are enough to attain solubility equilibrium in the all samples. The conclusion from experiments of time variation supports the result of equilibrium condition estimated by comparing the typical diffusive length of a noble gas atom with the typical grain size of glasses. Although we did not examine the time variation of noble gas solubility in the other sample, we expected that the solubility equilibrium of noble gases was attained in the other samples because of above discussion.

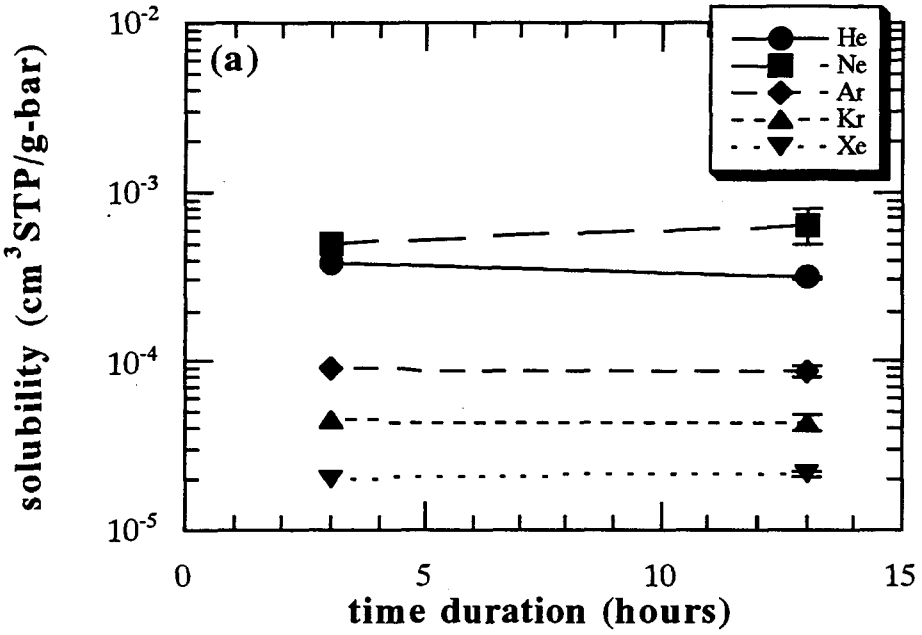

Figure 3-1. Noble gas solubility at 1200 °C is plotted against the duration time. Almost all the data of solubilities for 3 hours are within 1σ of the solubilities for 13 hours. Therefore, it can be concluded that 3 hours are enough to attain solubility equilibrium in all the samples. Errors are the reproducibility of the noble gas analyses for each sample, and show 1 σ. Errors of samples for 3 hours can not be calculated because only one analysis of noble gas was performed in the sample. Silicate melt samples are: (a) NS1; (b) NS2; (c) NS3; (d) NCS1; (e) NCS2. Helium data in the present study may not be reliable because of possibility helium loss.

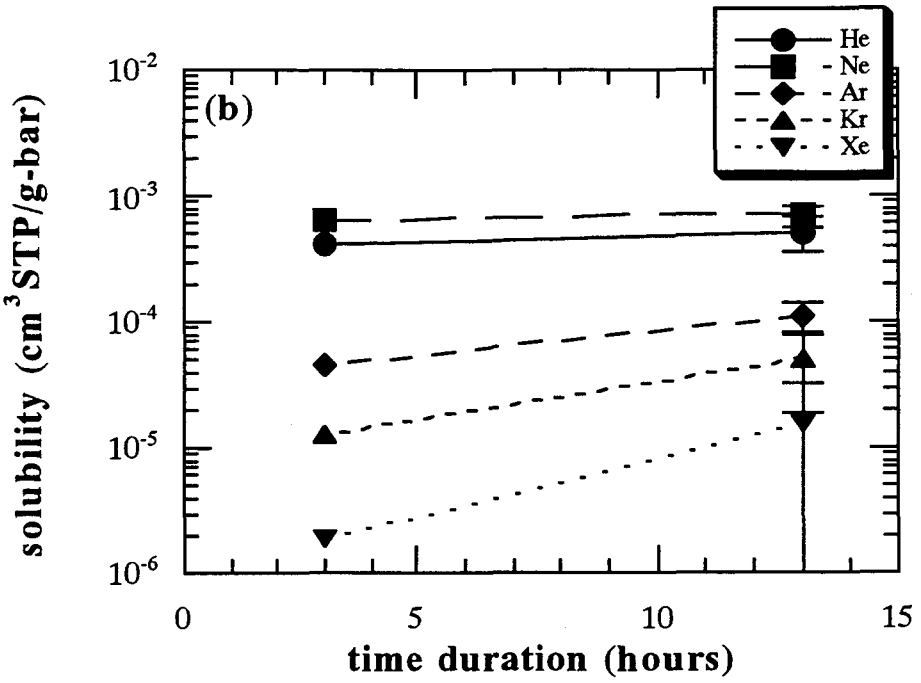

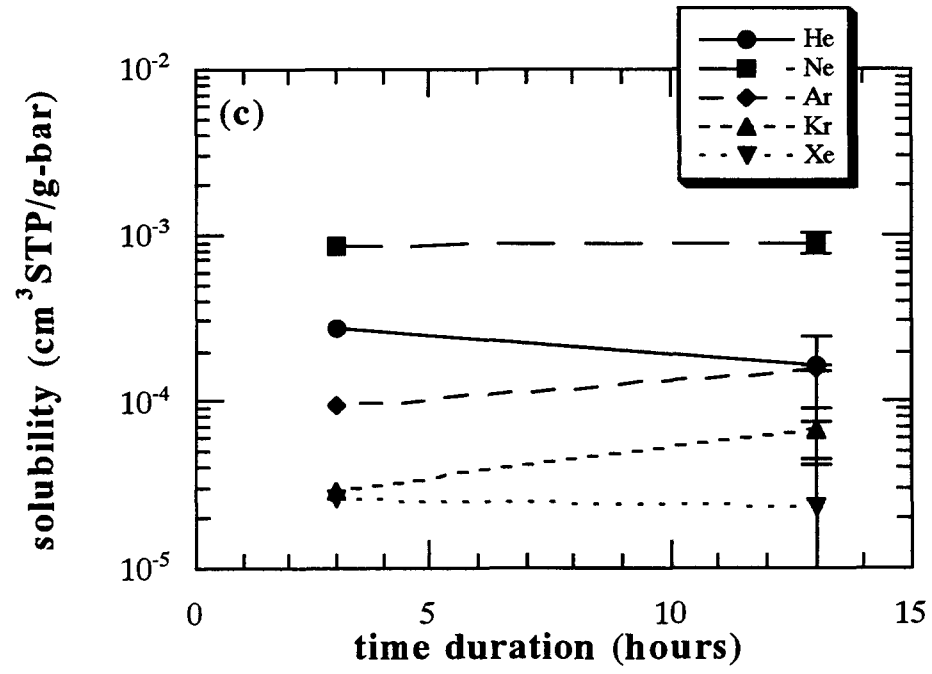

Figures 3-1 (b) and (c).

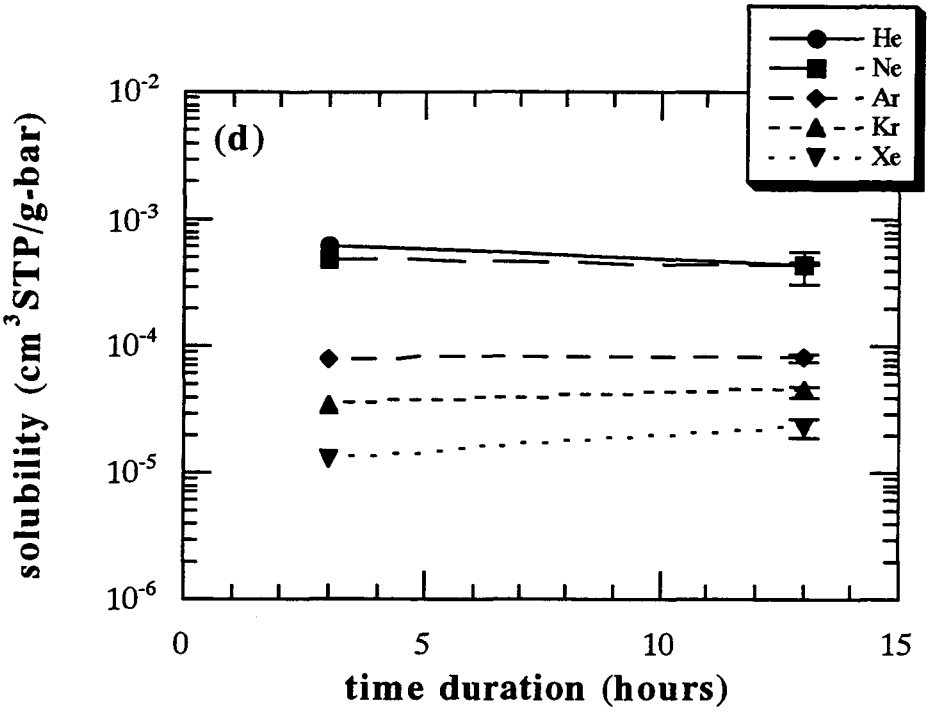

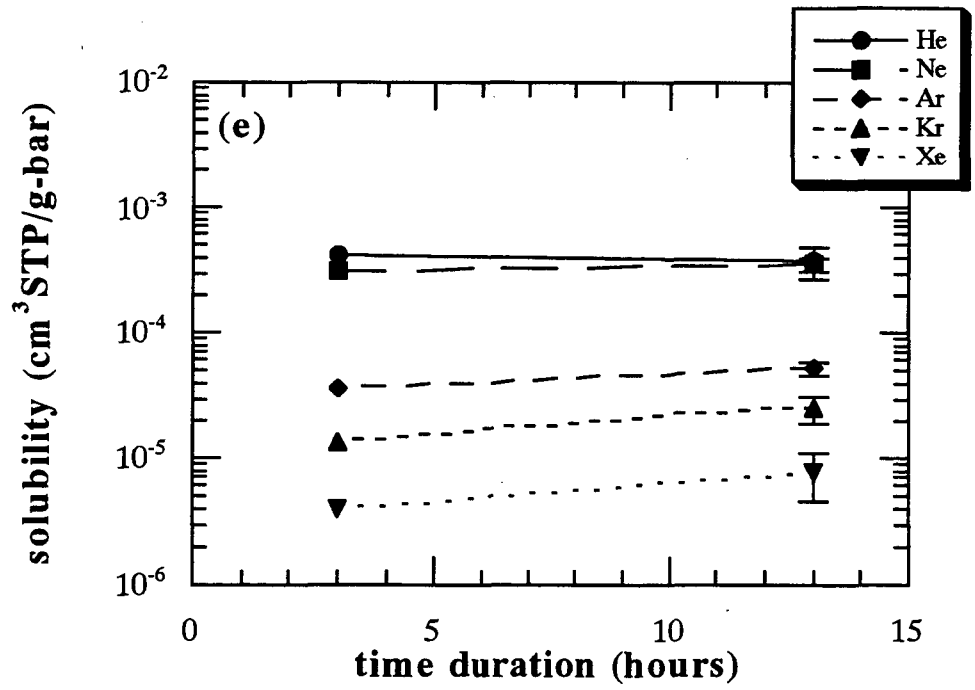

Figures 3-1 (d) and (e).

3-2 Noble Gas Solubility

Noble gas solubilities, which were measured at various temperature conditions, were plotted in Figures 3-2 a-h. The obtained solubility data of helium may not be reliable because helium loss could have occurred from the samples. The possibility of helium loss from the sample was inferred from the high hot blank of helium during the measurement period. Therefore, we will discuss the solution data for noble gases except for helium in this thesis, although we show the results of helium data in this section. In Figure 3-2, we can see that there is little change of the solubilities with temperature, but there is a significant change of the solubilities with noble gas radius; the solubility decreases with increasing atomic size of noble gases. The solubility in all the melts dramatically decreases from neon to argon but it gradually decreases from argon to xenon. Figures 3-3 a-d show the relation between noble gas radius and noble gas solubility in (a) Na_2O-SiO_2 system at 1300°C, (b) Na_2O-CaO-SiO_2 system at 1400°C, (c) CaO-MgO-SiO_2 system at 1500°C and (d) CaO-SiO_2 and MgO-SiO_2 system at 1600°C, respectively. The variation of the solubility is mainly due to atomic size of gas. The Van der Waals radius of gas changes largely from neon (1.54 Å) to argon (1.88 Å), but the Van der Waals radius changes slightly from argon (1.88 Å) to xenon (2.16 Å) [*Bondi,* 1964]. Figures 3-4 a-e show that the solubility of all the four gases and system increases with increasing the concentration of SiO_2. Such a relation between the solubility in this experiment and the concentration of SiO_2 is compatible with previous data [e.g., *Doremus,* 1966; *Shackelford et al.,* 1972; *Shelby,* 1974, 1976; *Jambon et al.,* 1986; *Lux,* 1987; *Broadhurst et al.,* 1990, 1992; *Carroll and Stolper,* 1991, 1993; *Roselieb et al.,* 1992]. Detailed discussions are given in the following section.

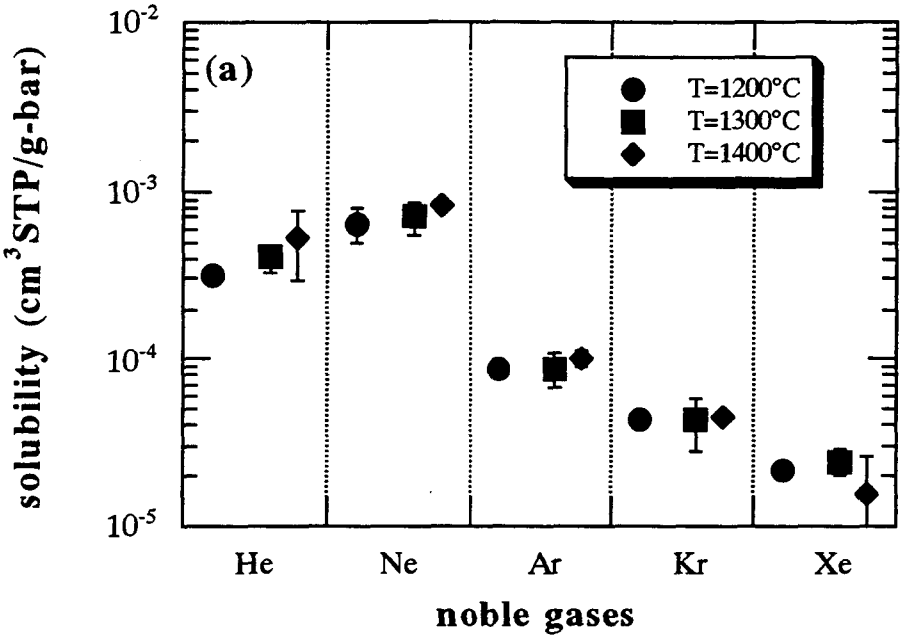

Figure 3-2. Noble gas solubility of the present work. Helium data in the present study may not be reliable because of possibility helium loss. Effect of temperature on the solubility is very little. Errors are the reproducibility of the noble gas analyses for each sample, and show 1 σ. Silicate melt samples are: (a) NS1; (b) NS2; (c) NS3; (d) NCS1; (e) NCS2; (f) NCS3; (g) CMS1; (h) CMS2; (i) NCS2; (j) CS1, CS2, CS3 and MS1.

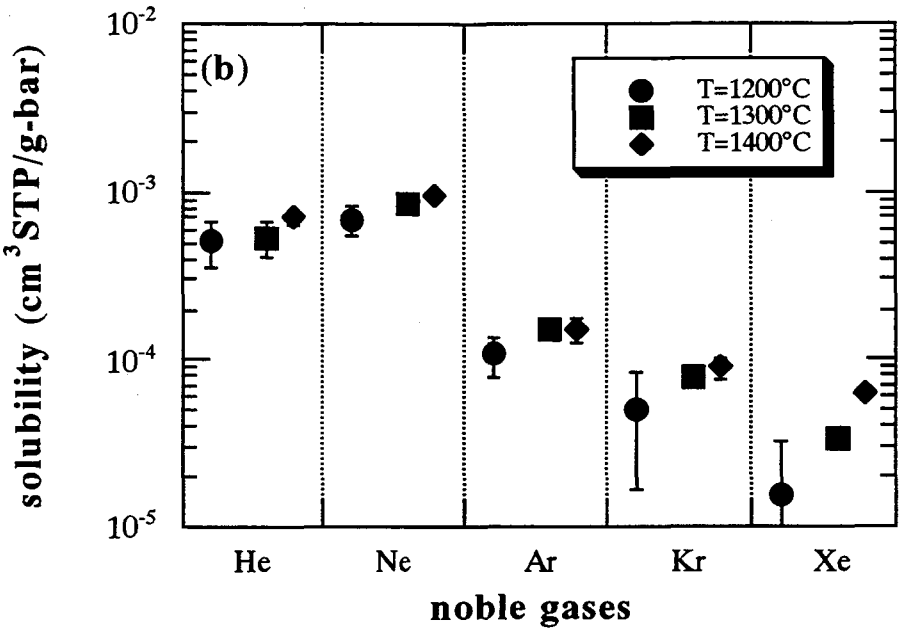

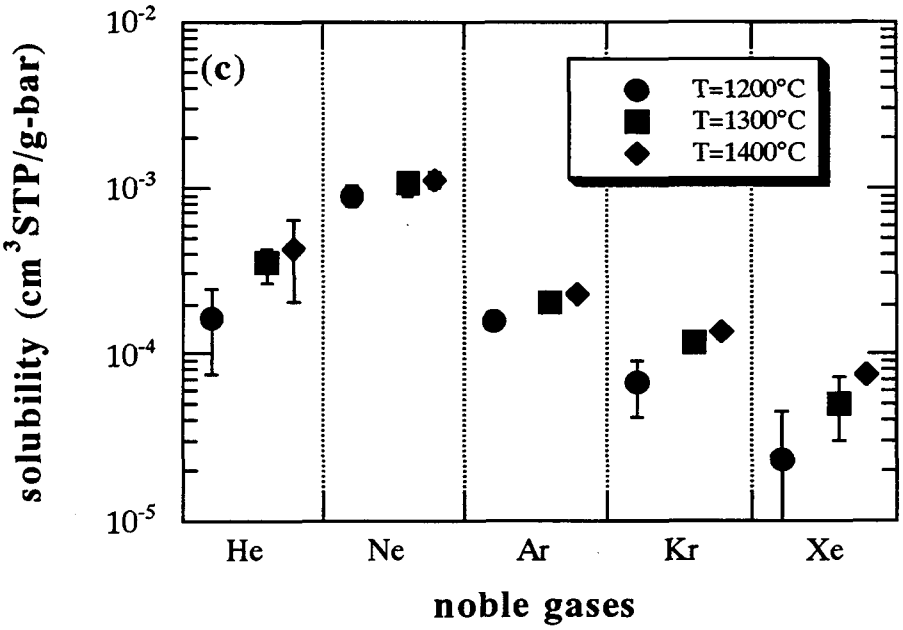

Figures 3-2 (b) and (c).

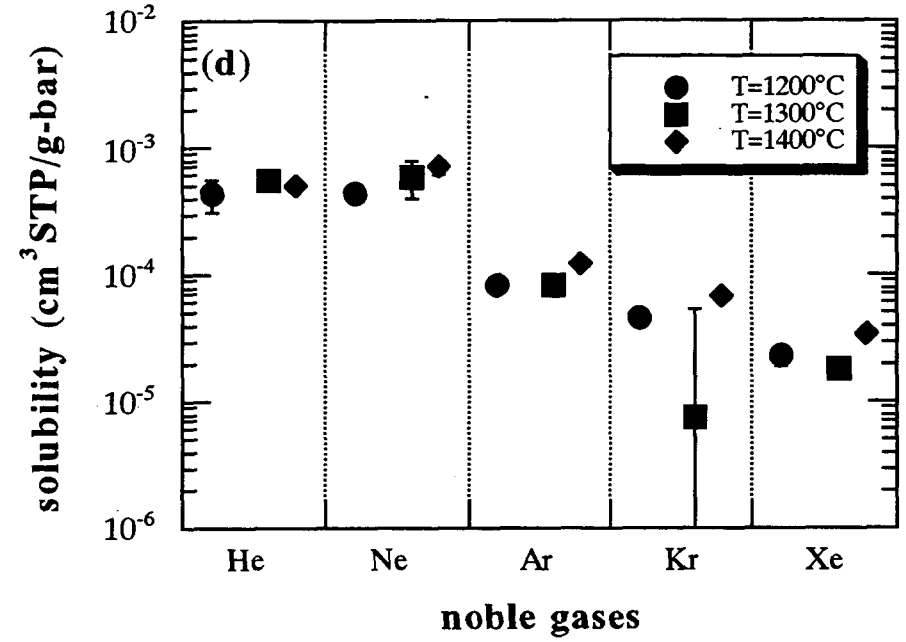

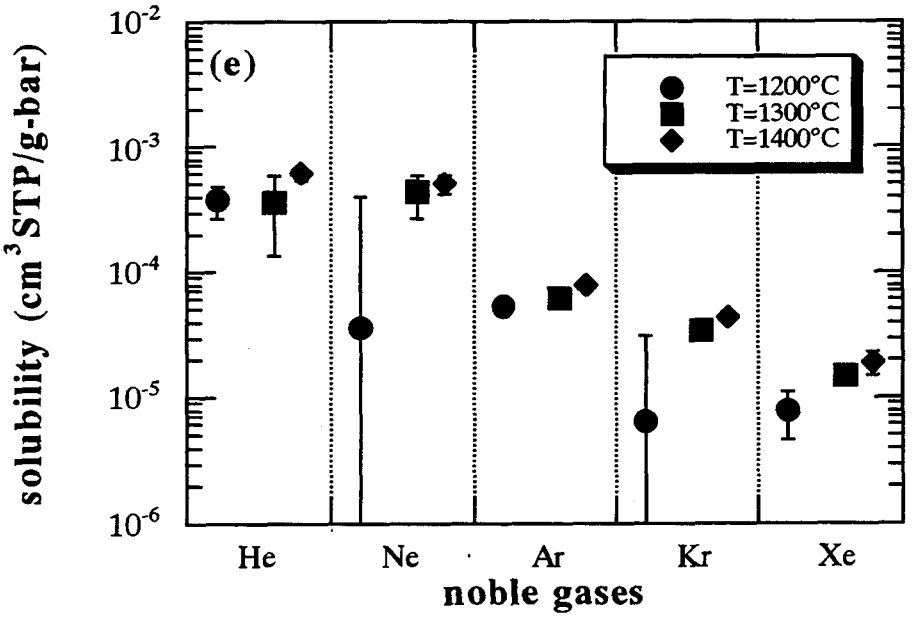

Figures 3-2 (d) and (e).

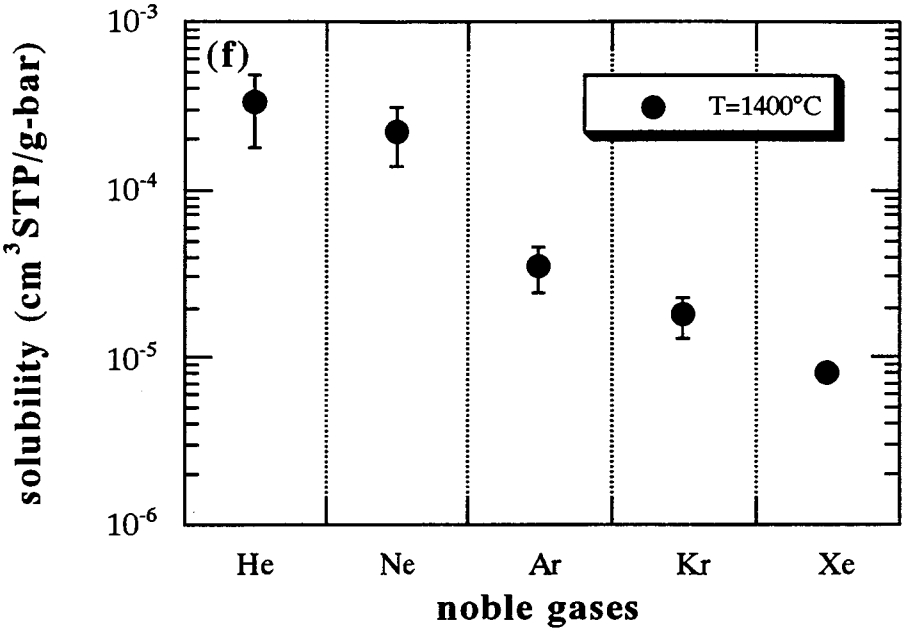

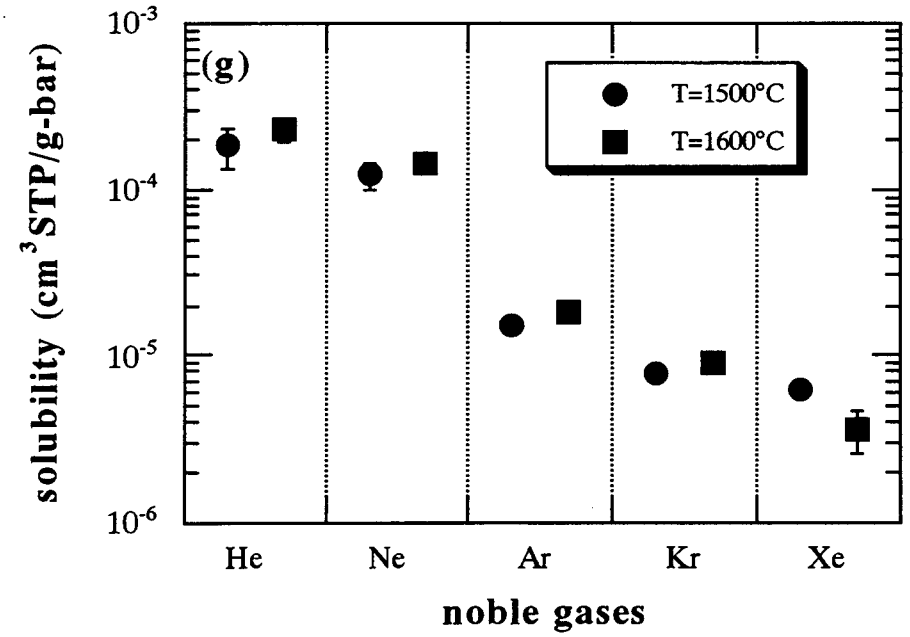

Figures 3-2 (f) and (g).

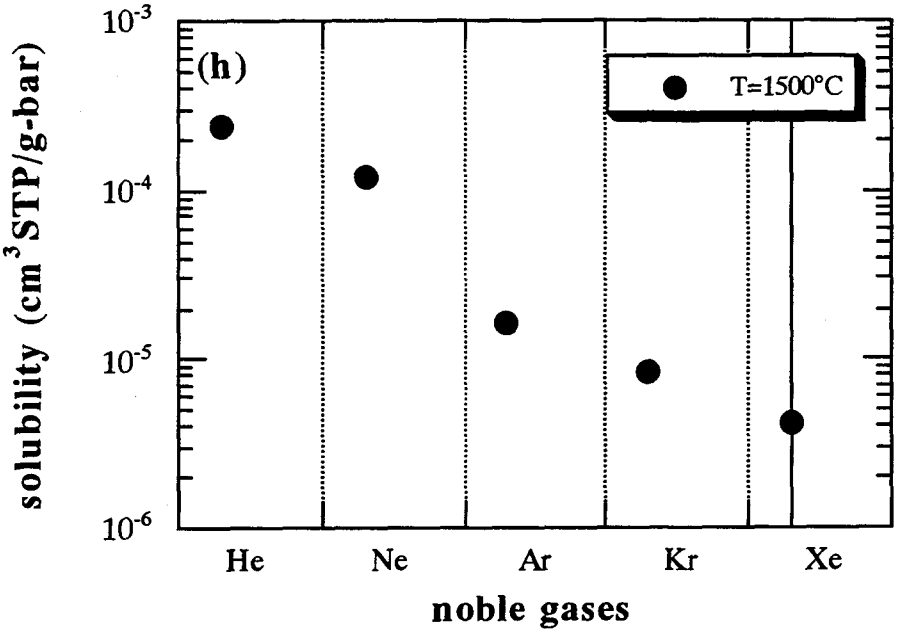

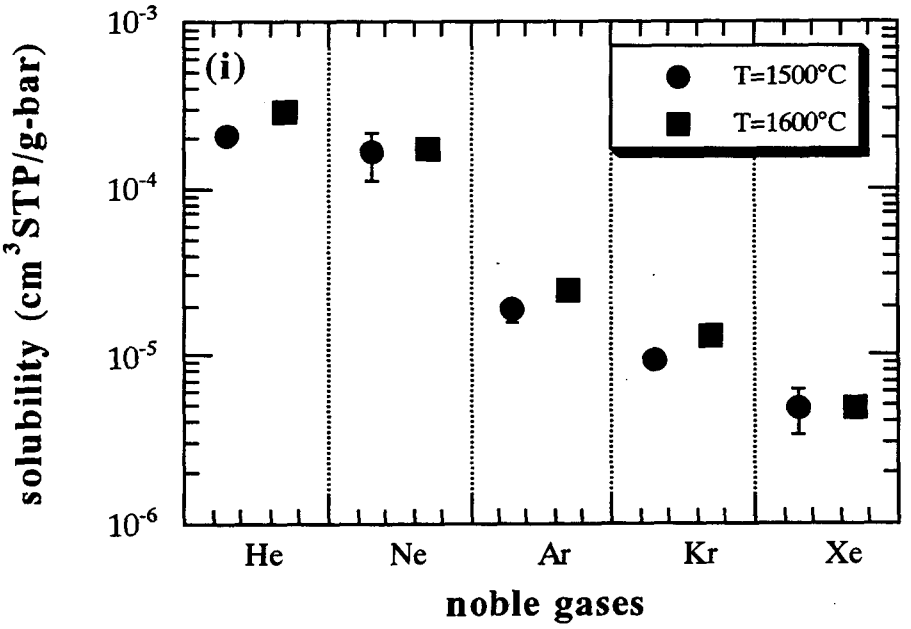

Figures 3-2 (h) and (i).

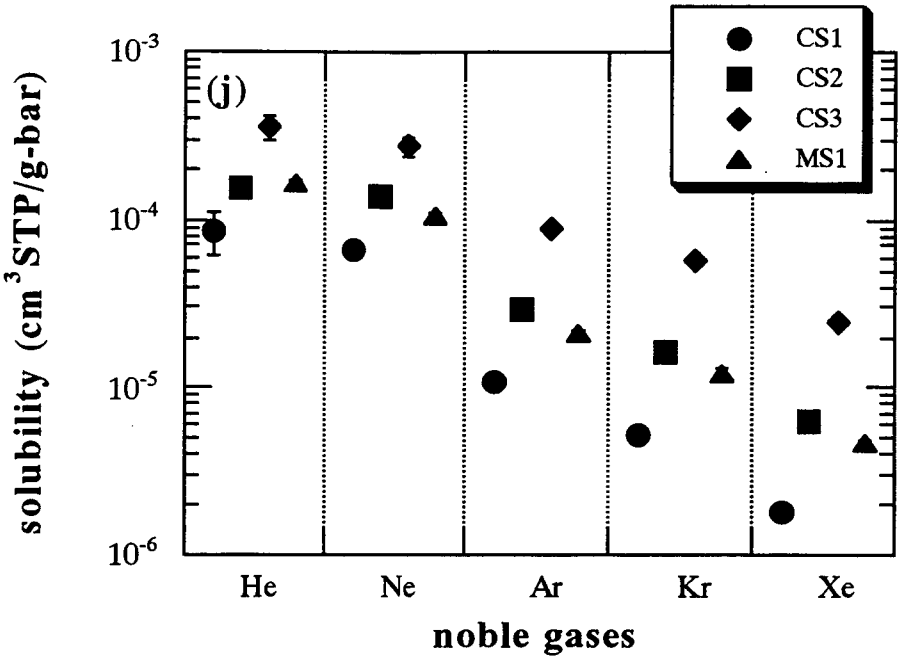

Figure 3-2 (j). The temperature is 1600 °C.

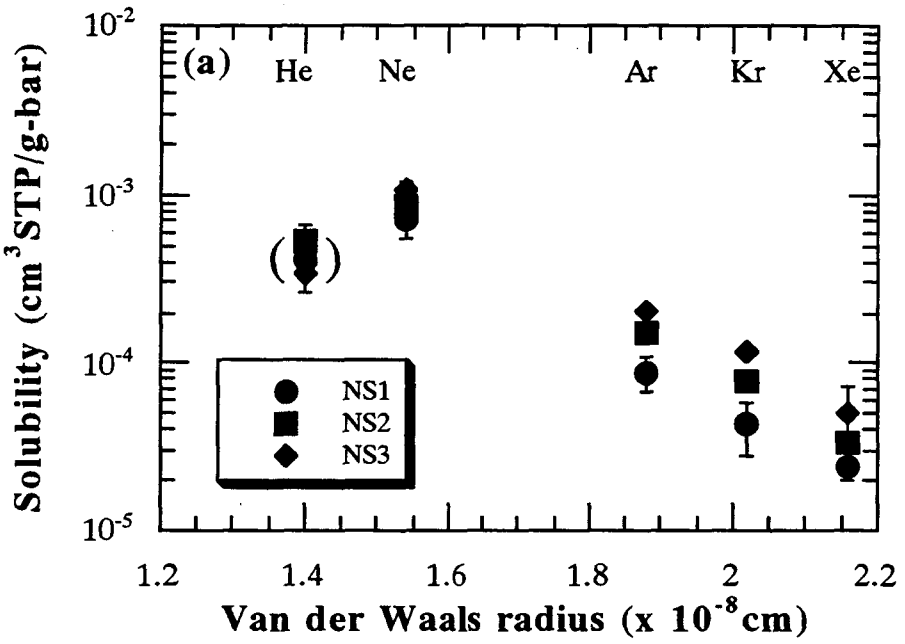

Figure 3-3. Correlation between solubility and Van der Waals radius [*Bondi*, 1964] of noble gas. Helium data in the present study may not be reliable because of possibility helium loss. Noble gas solubility in all the systems is lower with increasing Van der Waals radius of noble gas. Errors are the reproducibility of the noble gas analyses for each sample, and show 1 σ. Silicate melt systems are: (a) Na_2O-SiO_2 system at 1300°C; (b) Na_2O-CaO-SiO_2 system at 1400°C; (c) CaO-MgO-SiO_2 system at 1500°C; (d) CaO-SiO_2 and MgO-SiO_2 system at 1600°C.

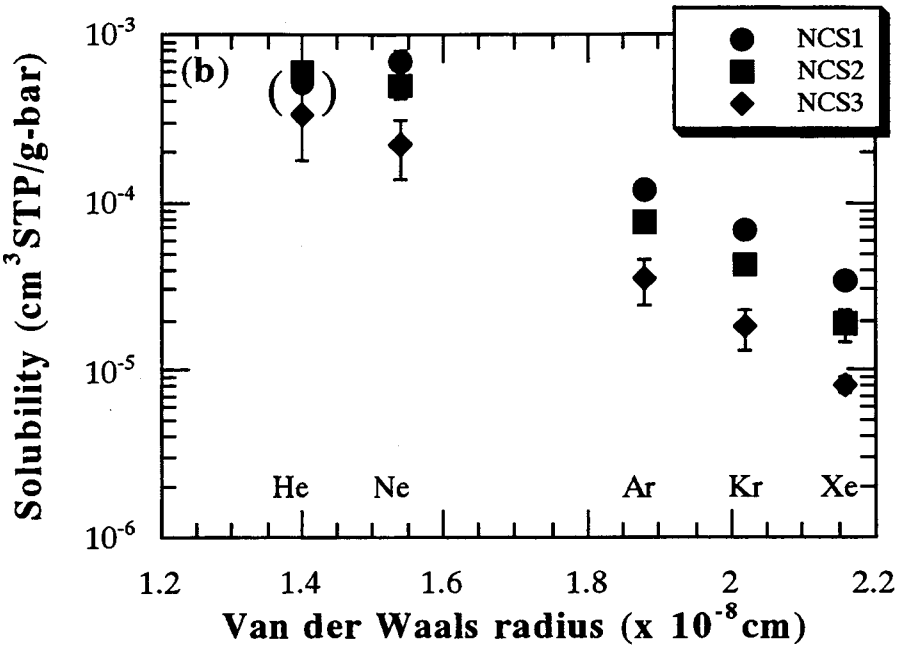

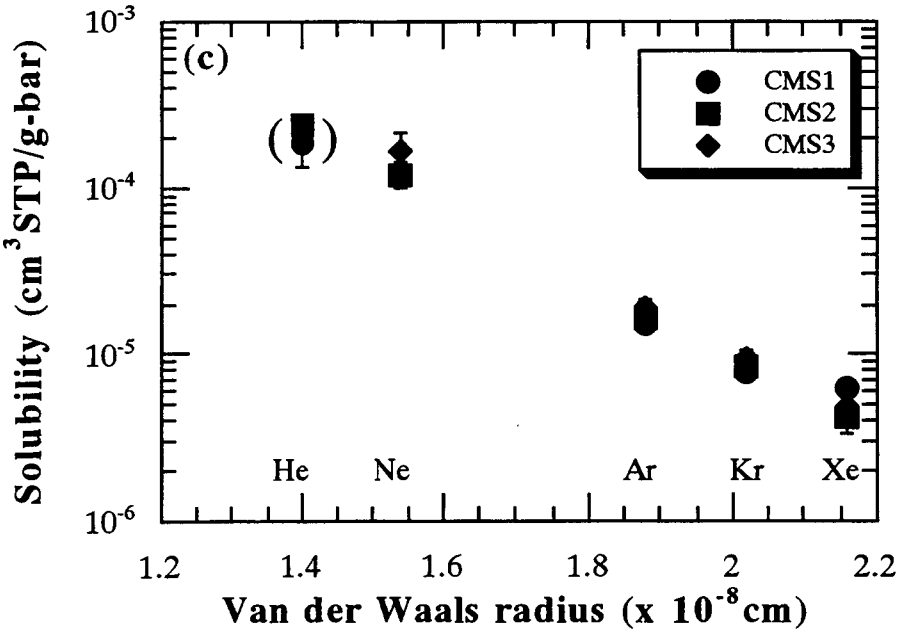

Figures 3-3 (b) and (c).

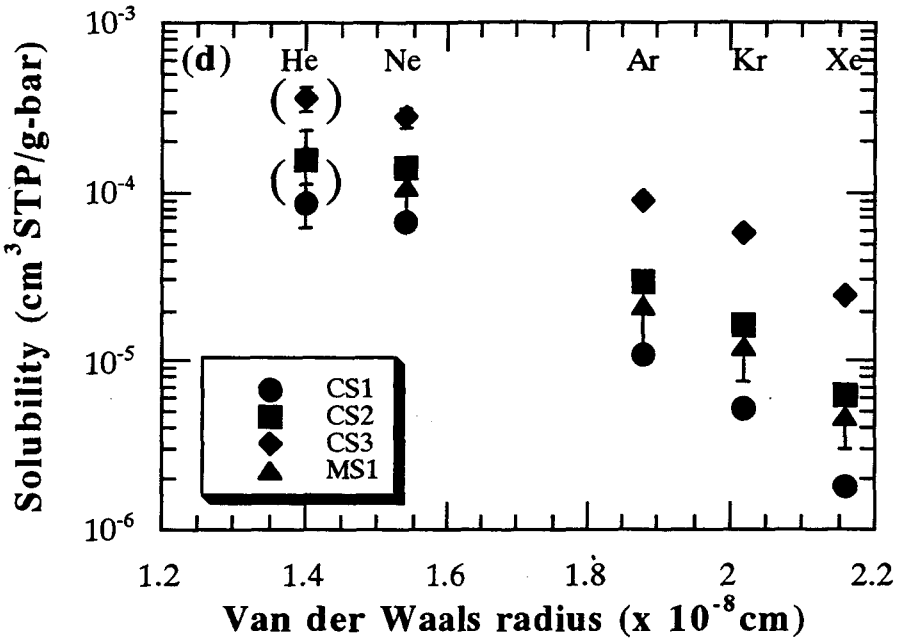
(d)
He
Ne
Ar
Kr
Xe
CS1
CS2
CS3
MS1
Solubility (cm3STP/g-bar)
Van der Waals radius (x 10-8cm)
10-3
10-4
10-5
10-6
1.2
1.4
1.6
1.8
2
2.2

Figure 3-3 (d).

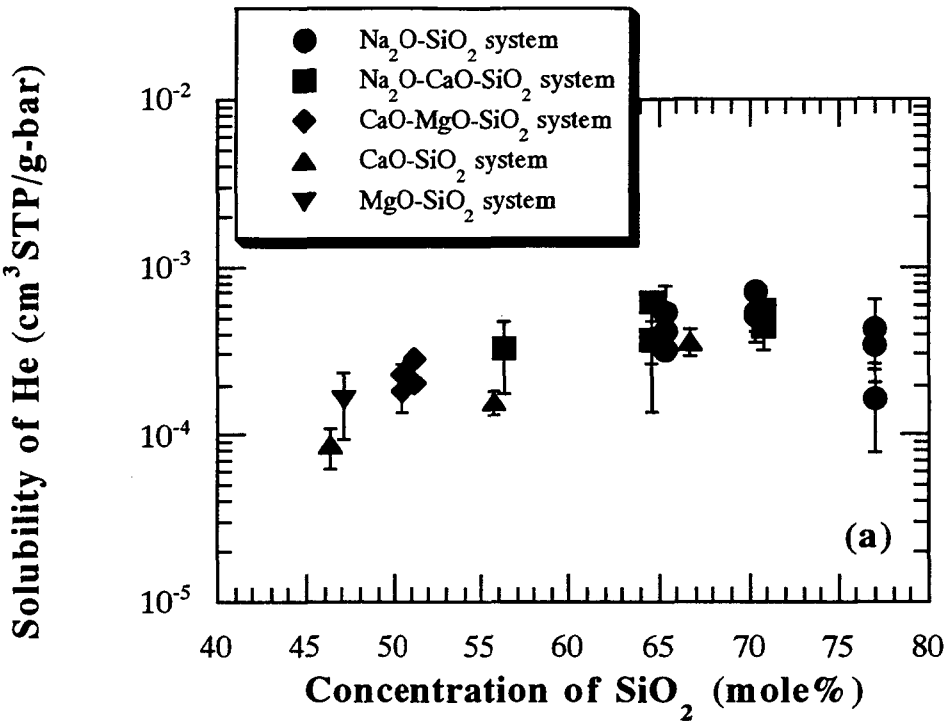

Figure 3-4. Correlation between noble gas solubility and concentration of SiO_2. All obtained data are plotted in the figures. The solubility is higher with increasing concentration of SiO_2. There is a linear trend for a wide range of melt compositions for all the noble gases. Errors are the reproducibility of the noble gas analyses for each sample, and show 1 σ. Figures (a), (b), (c), (d) and (e) show solubilities of He, Ne, Ar, Kr and Xe, respectively. Helium data in the present study may not be reliable because of possibility helium loss.

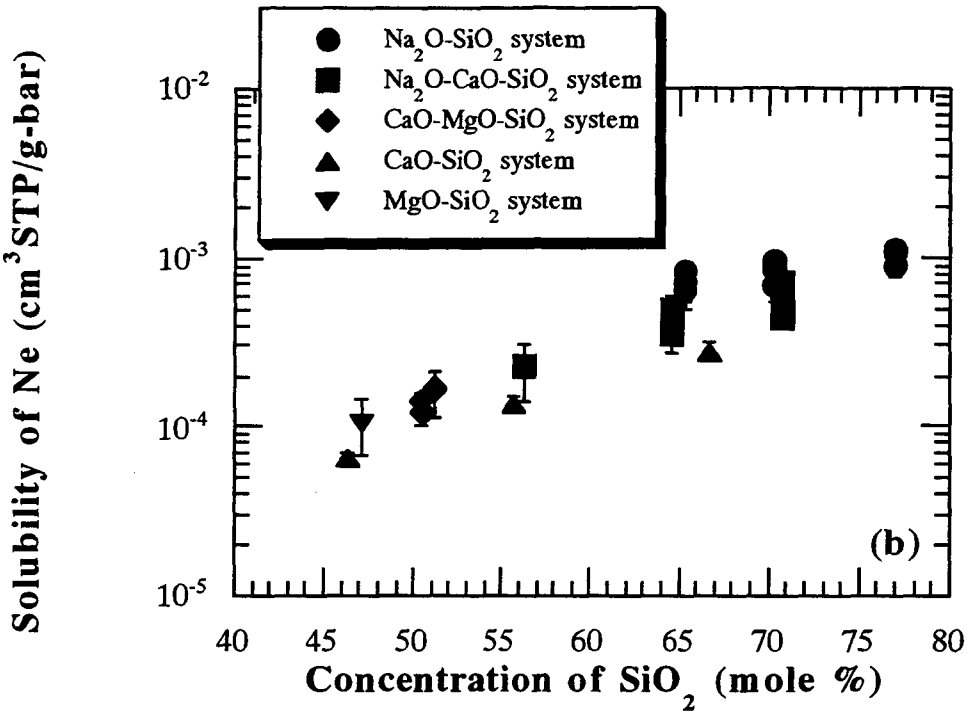

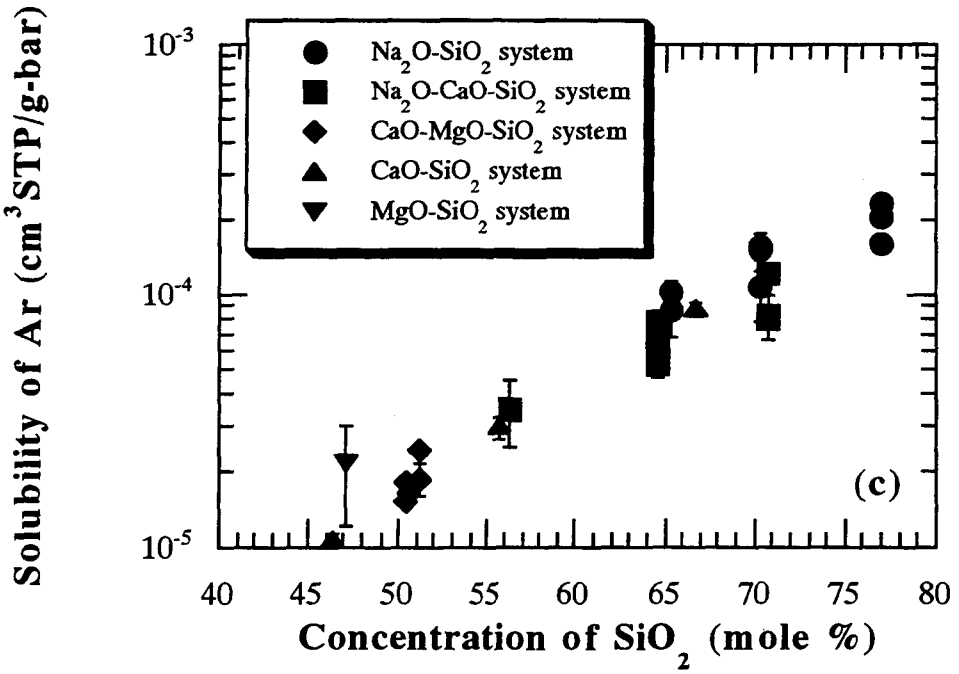

Figures 3-4 (b) and (c).

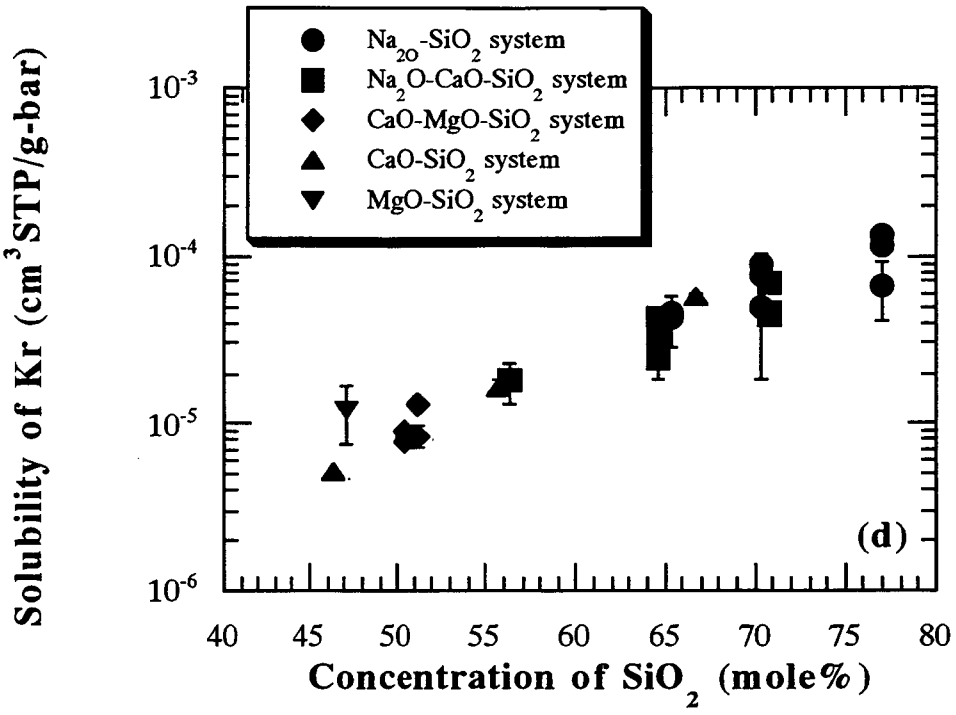

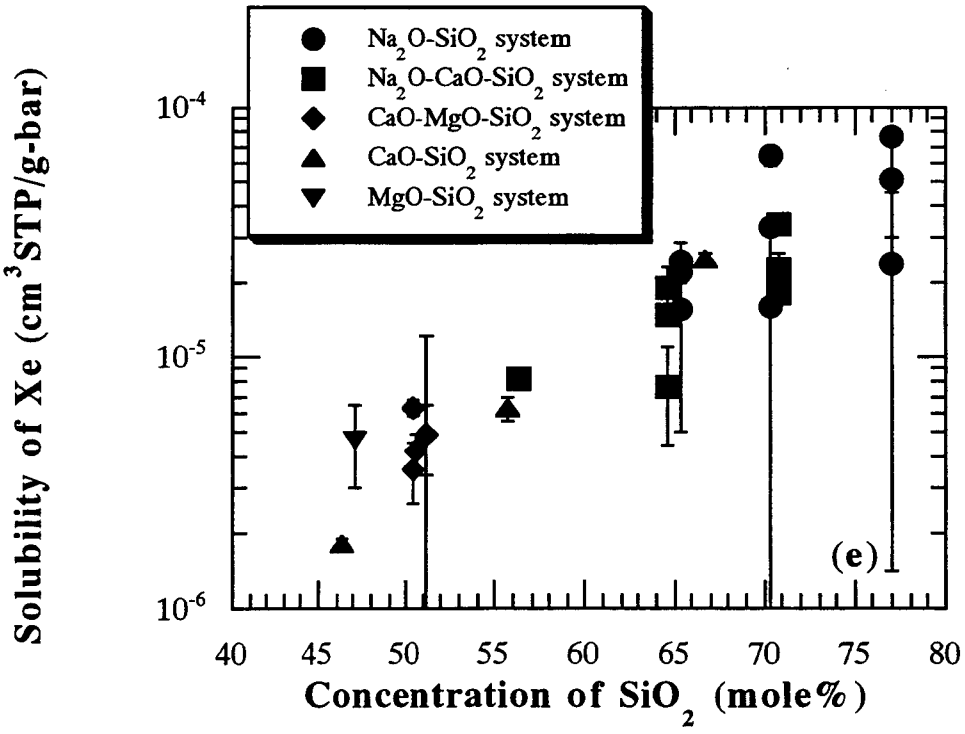

Figures 3-4 (d) and (e).

4. DISCUSSIONS

4-1 Thermodynamics

The equilibrium condition between liquid and gas is represented by

$$\mu_i^g = \mu_i^l , \qquad (4\text{-}1\text{-}1)$$

where μ_i^g and μ_i^l refer to the chemical potential of component "i" in gas and liquid phases, respectively. Equation (4-1-1) can be recast using chemical thermodynamics into the following relation:

$$d(\ln \frac{a^l}{a^g}) = -(\frac{V^0{}_m{}^l}{RT} - \frac{V^0{}_m{}^g}{RT})\, dP + \frac{\Delta H^0}{RT^2}\, dT , \qquad (4\text{-}1\text{-}2)$$

where a is the activity of solute, V^0_m is the standard-state molar volume, R is the gas constant, T is the absolute temperature, ΔH^0 (= H^l - H^g) is the standard enthalpy of solution, and superscript "l" and "g" represent liquid and gas phase, respectively. From the thermodynamical definition, $\frac{a^l}{a^g}$ can be rewritten by

$$\frac{a^l}{a^g} = K , \qquad (4\text{-}1\text{-}3)$$

where K is the equilibrium constant. We can derive a formula for the equilibrium constant from (4-1-2) and (4-1-3):

$$d(\ln K) = -(\frac{V^0{}_m{}^l}{RT} - \frac{V^0{}_m{}^g}{RT})\, dP + \frac{\Delta H^0}{RT^2}\, dT . \qquad (4\text{-}1\text{-}4)$$

This equation shows change of the equilibrium constant, when the pressure and the temperature change infinitesimally. If the pressure is constant (dP = 0), the equilibrium constant is given by

$$d(\ln K) = \frac{\Delta H^0}{RT^2}\, dT. \qquad (4\text{-}1\text{-}5)$$

If we rewrite (4-1-5), we obtain the van't Hoff equation

$$\left(\frac{\partial \ln K}{\partial T}\right)_P = \frac{\Delta H^0}{RT^2} \qquad (4\text{-}1\text{-}6)$$

or

$$\left(\frac{\partial \ln K}{\partial (1/T)}\right)_P = -\frac{\Delta H^0}{R}\ . \qquad (4\text{-}1\text{-}7)$$

The thermodynamic properties of the solution can be determined from standard thermodynamic manipulation, e.g.,

$$\Delta G^0{}_m = -\,R\,T \ln K = \Delta H^0 - T\,\Delta S^0 \qquad (4\text{-}1\text{-}8)$$

or

$$\ln K = -\frac{\Delta H^0}{RT} + \frac{\Delta S^0}{R}\ , \qquad (4\text{-}1\text{-}9)$$

where ΔS^0 is the standard entropy of solution. The equilibrium constant, K, is given by,

$$K = \frac{a^l}{a^g} = \frac{f^l}{f^g} \approx \frac{C^l}{C^g}\ , \qquad (4\text{-}1\text{-}10)$$

where f is the fugacity of solute in the mixture, C is the concentration of solute and superscript "l" and "g" represent liquid and gas phase. Using (10), we can rewrite (9) in the form

$$\ln \frac{C^l}{C^g} \approx -\frac{\Delta H^0}{RT} + \frac{\Delta S^0}{R}\ . \qquad (4\text{-}1\text{-}11)$$

C^l was obtained from the noble gas measurement and melt volume (cm^3/g) of the glass. The melt volume was calculated from the composition of the glass using the oxide partial molar volume of *Lange and Carmichael* [1987]. C^g was calculated with a Redlich-Kwong equation of state at the solubility experiment using the pressure apparatus [*Ferry and Baumgartner,* 1987]. Consequently, the

equilibrium constants are equal to the solubilities. Estimated equilibrium coefficients are listed in Table 4-1.

The effect of temperature on noble gas solubility was studied over the range 1200-1400 °C at 100° intervals in five of the liquids. The results indicate that the temperature dependence for all the noble gases is very weak and, for the most parts, lost in the experimental scatter. Figure 4-1 shows the results of the five studied liquids. In general, solubility increases with the increasing temperature yielding the positive enthalpies of solution, but because of the large uncertainties it is not possible to identify the positive trends. The ΔH^0 can be calculated from the slope, and ΔS^0 can be determined from the intercept of the line in Figure 4-1. These values are given in Table 4-2. Although the obtained values are scattered, the values are close to those obtained by *Lux* [1987] who found ΔH^0 (2.3- 80 kJ/mol) and ΔS^0 (-84- -130 J/mol-K) in natural silicate melts at 1275-1500 °C.

Table 4-1a. Equilibrium constants ($K = \frac{C^l}{C^g}$) of noble gases in Na_2O-SiO_2 system. C^l is obtained from the noble gas measurement in the glass. C^g at the synthetic condition is calculated with a Redlich-Kwong equation of state. Errors show 1 σ of the reproducibility of the noble gas analyses for each sample.

sample run#	Ne	Ar	Kr	Xe
		x 10^{-3}		
NS1				
G205	12.5 ±3.0	1.90 ±0.15	0.990 ±0.106	0.541 ±0.014
G209	14.5 ±3.1	2.02 ±0.47	1.05 ±0.36	0.645 ±0.115
G211	17.5 ±0.3	2.38 ±0.25	1.12 ±0.08	0.412 ±0.277
NS2				
G205	13.5 ±2.7	2.37 ±0.65	1.14 ±0.72	0.393 ±0.400
G209	17.7 ±1.4	3.55 ±0.18	1.88 ±0.03	0.879 ±0.06
G211	19.9 ±1.2	3.49 ±0.55	2.18 ±0.33	1.69 ±0.13

NS3				
G205	17.3 ±2.5	3.45 ±0.11	1.53 ±0.58	0.590 ±0.556
G209	21.5 ±3.1	4.78 ±0.04	2.83 ±0.05	1.36 ±0.55
G211	23.2 ±2.6	5.34 ±0.06	3.31 ±0.06	2.00 ±0.11

Table 4-1b. Equilibrium constants ($K = \frac{C^l}{C^g}$) of noble gases in Na_2O-CaO-SiO_2 system. C^l is obtained from the noble gas measurement in the glass. C^g at the synthetic condition is calculated with a Redlich-Kwong equation of state. Errors show 1 σ of the reproducibility of the noble gas analyses for each sample.

sample run#	Ne	Ar	Kr	Xe
		x 10^{-3}		
NCS1				
G205	8.93 ±0.39	1.82 ±0.15	1.06 ±0.10	0.580 ±0.094
G209	12.4 ±4.1	1.97 ±0.39	1.16 ±0.18	0.492 ±0.029
G211	15.2 ±1.9	2.92 ±0.06	1.73 ±0.01	0.930 ±0.005
NCS2				
G205	7.30 ±0.75	1.23 ±0.13	0.611 ±0.156	0.206 ±0.087
G209	9.48 ±3.46	1.55 ±0.09	0.876 ±0.379	0.418 ±0.047
G211	11.1 ±1.8	1.95 ±0.17	1.13 ±0.11	0.531 ±0.119
NCS3				
G211	5.28 ±2.00	0.915 ±0.269	0.495 ±0.136	0.242 ±0.024

Table 4-1c. Equilibrium constants ($K = \frac{C^l}{C^g}$) of noble gases in CaO-MgO-SiO_2 system. C^l is obtained from the noble gas measurement in the glass. C^g at the synthetic condition is calculated with a Redlich-Kwong equation of state. Errors show 1 σ of the reproducibility of the noble gas analyses for each sample.

sample run#	Ne	Ar	Kr	Xe
		x 10^{-3}		
CMS1				
G212	3.22 ±0.57	0.450 ±0.099	0.245 ±0.022	0.211 ±0.015

G215	3.81 ±0.44	0.547 ±0.022	0.285 ±0.015	0.123 ±0.034
CMS2				
G212	3.15 ±0.19	0.477 ±0.018	0.258 ±0.006	0.141 ±0.022
CMS3				
G212	4.24 ±1.33	0.540 ±0.074	0.290 ±0.035	0.161 ±0.049
G215	4.59 ±0.05	0.722 ±0.018	0.405 ±0.010	0.164 ±0.024

Table 4-1d. Equilibrium constants ($K = \frac{C^l}{C^g}$) of noble gases in $CaO\text{-}SiO_2$ and $MgO\text{-}SiO_2$ system. C^l is obtained from the noble gas measurement in the glass. C^g at the synthetic condition is calculated with a Redlich-Kwong equation of state. Errors show 1 σ of the reproducibility of the noble gas analyses for each sample.

sample run#	Ne	Ar	Kr	Xe
		x 10^{-3}		
CS1				
G156	1.54 ±0.09	0.272 ±0.008	0.134 ±0.002	0.0481 ±0.0018
CS2				
G156	3.12 ±0.36	0.715 ±0.072	0.412 ±0.050	0.160 ±0.019
CS3				
G156	6.00 ±0.78	2.05 ±0.08	1.34 ±0.08	0.609 ±0.022
MS1				
G156	2.47 ±0.98	0.517 ±0.211	0.310 ±0.121	0.123 ±0.044

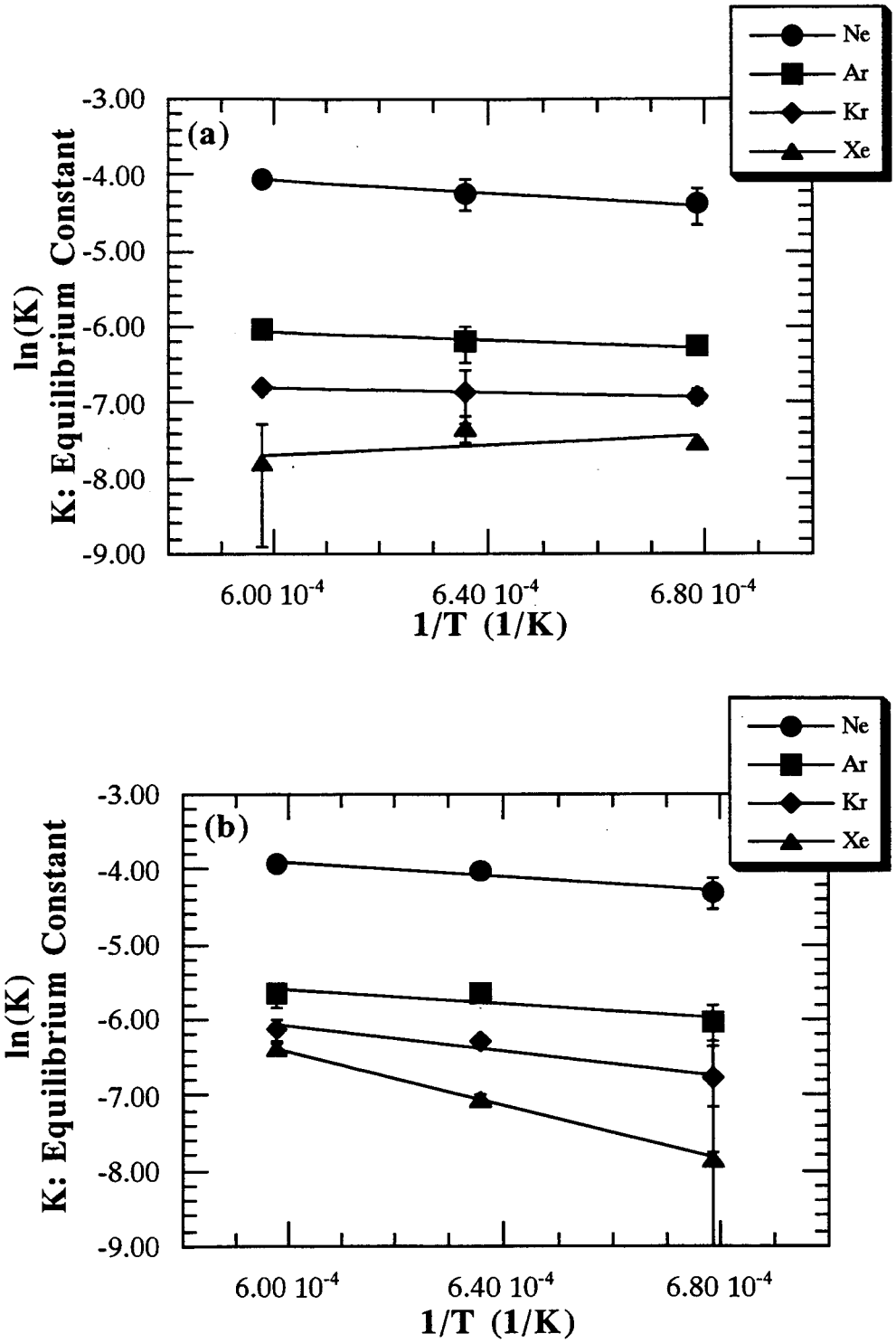

Figure 4-1. Temperature dependence of equilibrium constants. Noble gas solubility in all the five melts slightly increases with increasing temperature. Errors show 1 σ of the reproducibility of the noble gas analyses for each sample. Silicate melts are: (a) NS1; (b) NS2; (c) NS3; (d) NCS1; (e) NCS2.

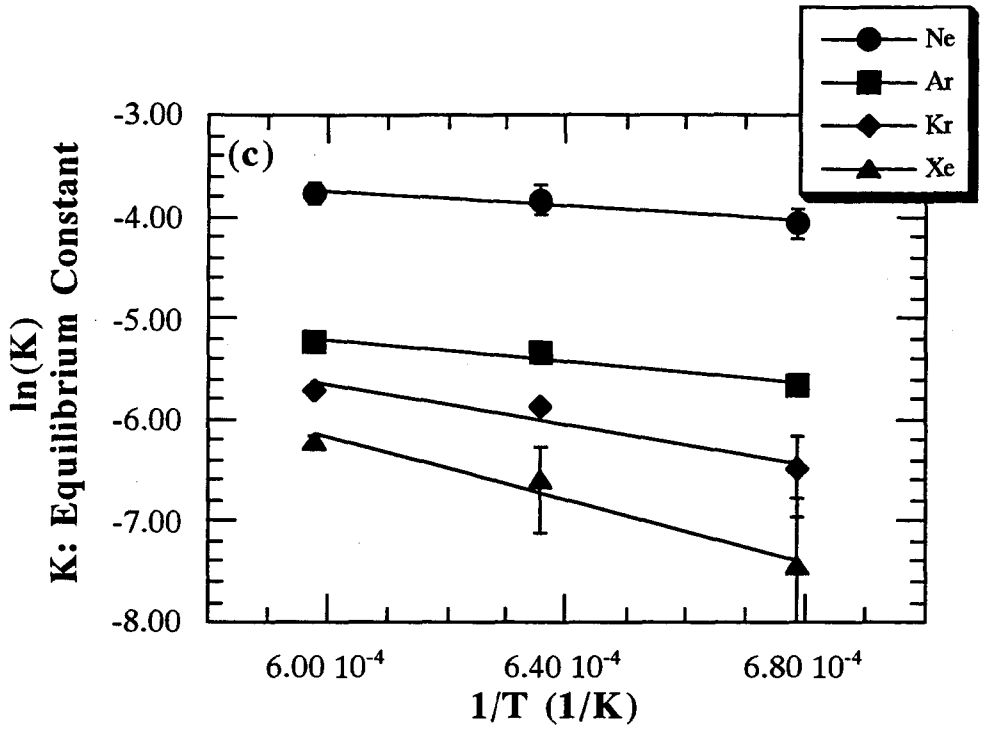

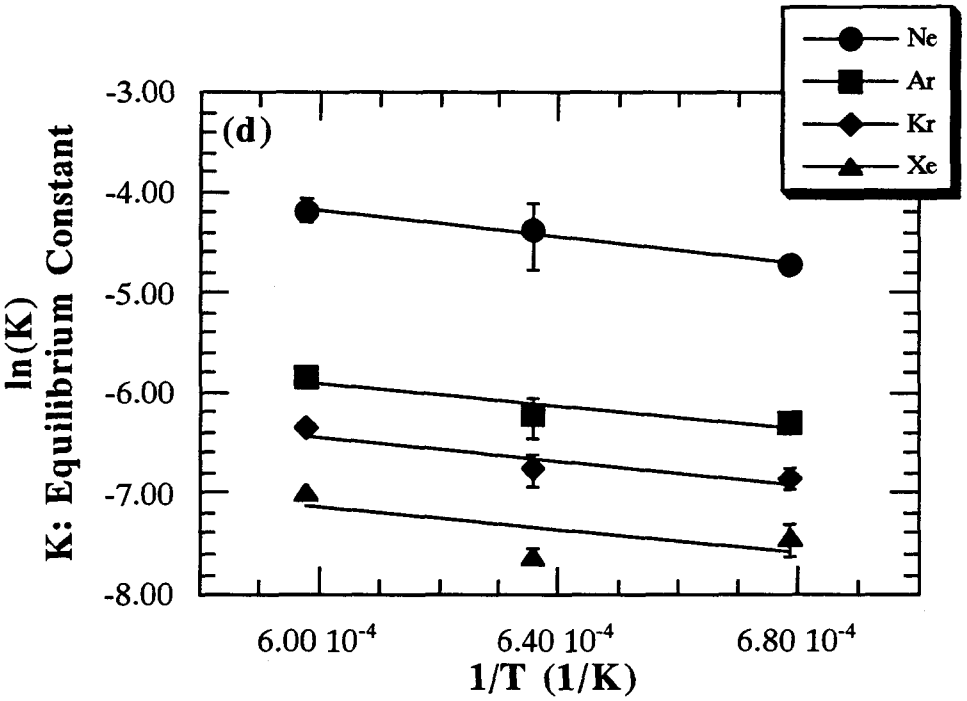

Figures 4-1 (c) and (d).

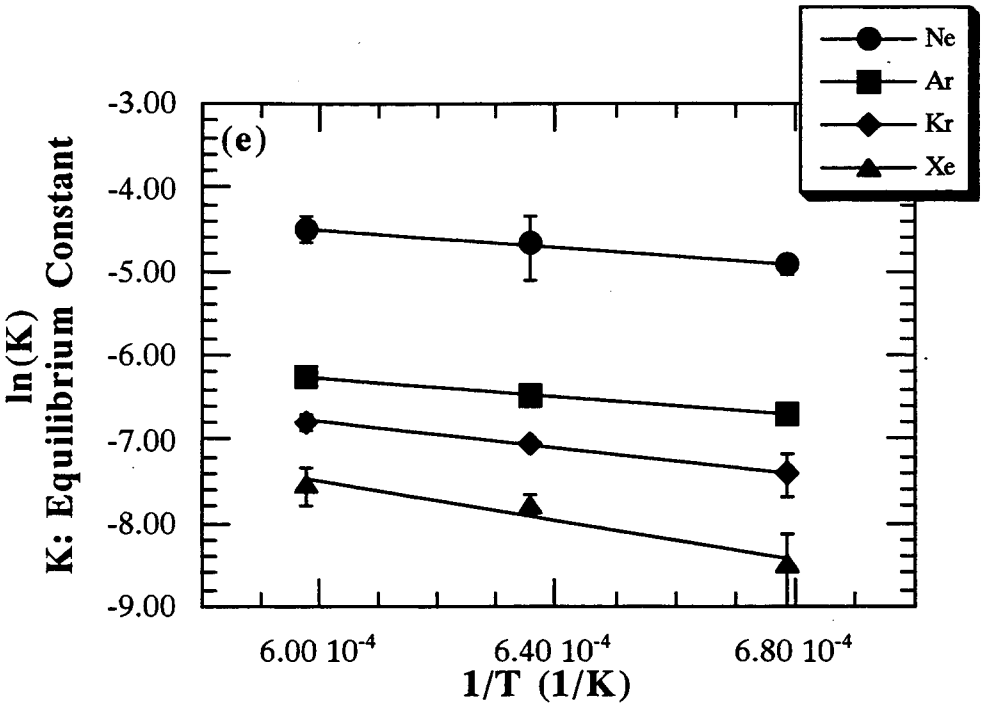
Ne
Ar
Kr
Xe
(e)
-3.00
-4.00
-5.00
-6.00
-7.00
-8.00
-9.00
ln(K)
K: Equilibrium Constant
6.00 10-4
6.40 10-4
6.80 10-4
1/T (1/K)

Figure 4-1 (e).

Table 4-2. Enthalpy and entropy change on solution of noble gases in silicate liquids.

	ΔH^0 (kJ/mol)					ΔS^0 (J/mol-K)				
	NS1	NS2	NS3	NCS1	NCS2	NS1	NS2	NS3	NCS1	NCS2
Ne	34.4	40.1	30.3	55.0	43.5	-13.2	-8.42	-13.0	-1.79	-11.3
	±3.6	±7.8	±7.4	±5.1	±4.4	±2.3	±4.97	±4.7	±3.27	±2.8
Ar	22.6	40.5	45.3	47.6	47.3	-34.4	-22.3	-16.1	-20.6	-23.7
	±6.9	±23.5	±11.1	±20.1	±1.7	±4.4	±15.0	±7.1	±12.9	±1.1
Kr	12.1	67.1	80.2	49.5	62.8	-49.3	-10.4	1.04	-23.8	-18.8
	±0.2	±17.9	±24.3	±20.4	±4.3	±0.1	±11.4	±15.53	±13.1	±2.7
Xe	-26.6	149	126	46.5	97.9	-79.7	36.5	24.2	-31.5	-3.58
	±38.1	±3	±22	±49.1	±24.3	±24.3	±2.2	±13.9	±31.3	±15.52

4-2 Melt Composition Dependence of Noble Gas Solubility

Solubilities of noble gases obtained in this study are higher in more silica-rich melts (See Figure 3-4). In the given melts, the solubility decreases in the order Ne > Ar > Kr > Xe; the larger the gas atom, the lower the solubility (See Figure 3-3). These results of the solubility are consistent with the previous results [*Kirsten,* 1968; *Shackelford et al.,* 1972; *Doremus,* 1966; *Hayatsu and Waboso,* 1985; *Jambon et al.,* 1986; *Lux,* 1987; *Broadhurst et al.,* 1992; *Roselieb et al.,* 1992]. Such feature has been interpreted to indicate an interstitial model of solution mechanism where noble gas occupies the centers of rings of tetrahedra [*Doremus,* 1966; *Shelby,* 1974; *Shackelford,* 1972]. In general, we refer to such interstitial locations for dissolved gas atoms as "holes" or "solubility site". The decrease of the gas solubility with increasing the gas atom size suggests that there is a continuous distribution of hole sizes with a greater number of small holes in which atoms such as He and Ne may be accommodated. In this suggestion, it is required that the time scale of the statistical variation for the hole size is longer than that of the motion of the noble gas atom in silicate melts, which we suppose can be satisfied. For simple materials such as vitreous silica it is possible to use solubility variations with gas atom size to estimate the size frequency distribution of holes or solubility sites [e.g., *Shackelford and Brown,* 1980, 1981; *Shackelford,* 1982]. The increase of the content of network forming oxide tends to increase the openness of the melt structure, and thus to increase the concentration of holes into which gas atoms can fit.

Previous studies of inert gas solubility in a range of melt compositions have shown that solubility variations may be roughly correlated with density [*Lux,* 1987] and with molar volume [*Broadhurst et al.,* 1990, 1992] of silicate melt.

Recently, *Carroll and Stolper* [1993] have shown that noble gas solubility is also well correlated with ionic porosity, IP = 100 (1 - V_{io}/V_m), where V_{io} is the total volume of spherical cations plus anions in 1 g of melt, calculated using ionic radii by *Shannon and Prewitt* [1969], and V_m is the melt volume (cm^3/g) calculated using the oxide partial molar volumes of *Lange and Carmichael* [1987] on the basis of appendix in *Carroll and Stolper* [1993]. The ionic porosity is considered to be one measure of the integrated "hole" space in a melt.

In this study we examined the effect of not only holes in silicate melt and glass but also oxygen atoms combining with silicon atoms and also a state of network structure in silicate melt and glass, since it is generally supposed that silicate glass and melt are formed by polymer of silicon atoms combining oxygen atoms [e.g., *Zachariasen,* 1932; *Masson,* 1977; *Mysen et al.,* 1980]. *Brawer and White* [1975] indicated that degree of polymerization in silicate melt and glass is shown by NBO/Si (or NBO/T) ratio which is the number of nonbridging oxygens per silicon (or tetrahedrally coordinated cation) in the melt. Therefore, we use the NBO/Si (or NBO/T) ratio as one measure of state of network structure to explain the relationship between noble gas solubility and melt compositions.

The bulk NBO/Si (or NBO/T) ratio of silicate melt is based on electrical charge balance. The number of tetrahedrally coordinated cations (from molar or atomic proportions) is calculated first. The NBO is the difference between the total negative electrical charge of oxygen (O x 2) and the positive charge of tetrahedrally coordinated cations (T x 4). For melts with several types of potential tetrahedrally coordinated cations (e.g., Al^{3+} and Fe^{3+}), calculation of the NBO/T ratio from a chemical analysis relies on knowledge of the melt structural role of all cations. Increasing value of the NBO/Si (or NBO/T) ratio leads to depolymerization of silicon atoms in the silicate glass and melt.

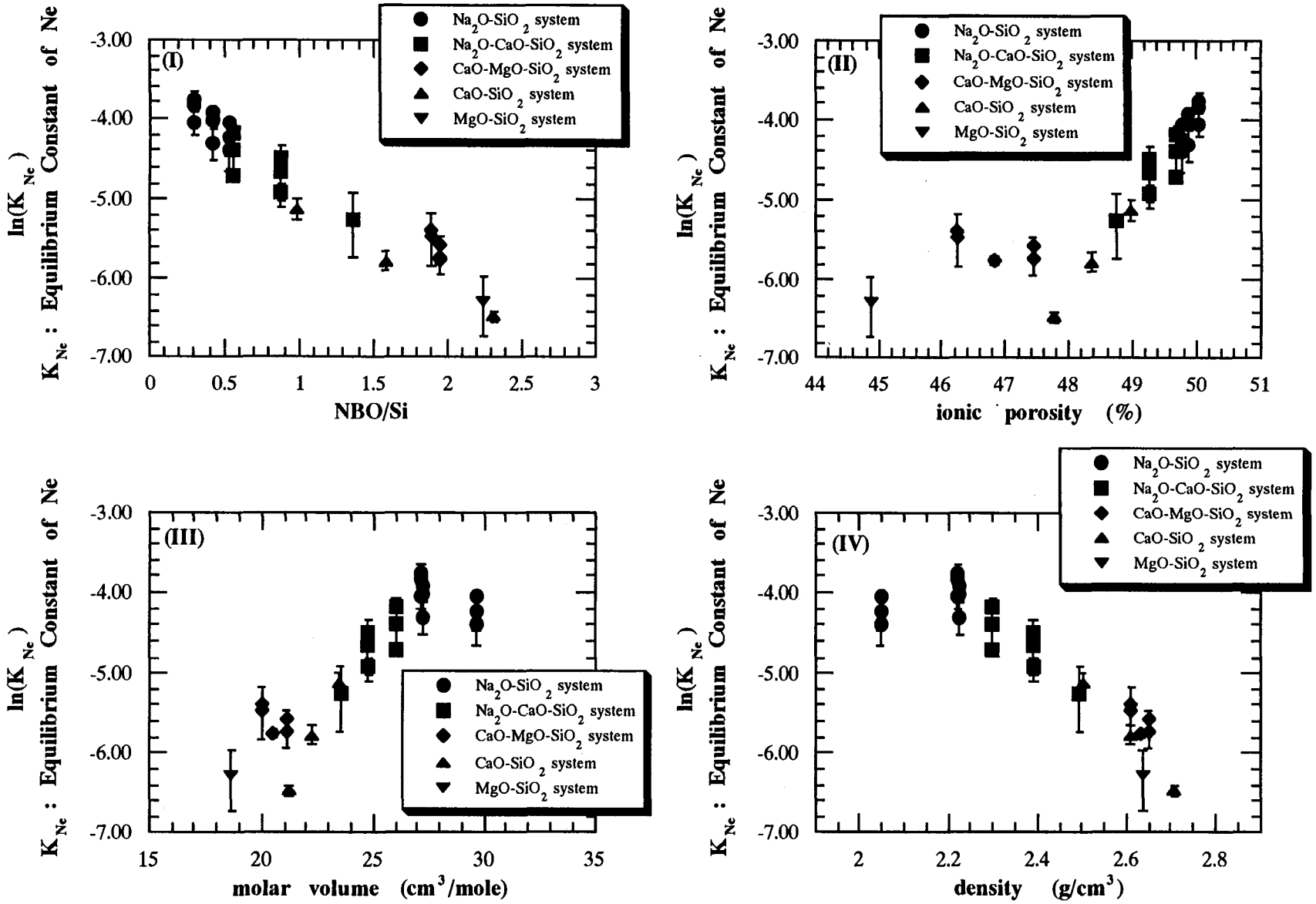

Figure 4-2a. Comparisons of correlation between the natural logarithm of equilibrium constant of Ne and (I) NBO/Si, (II) ionic porosity, (III) molar volume, and (IV) density.

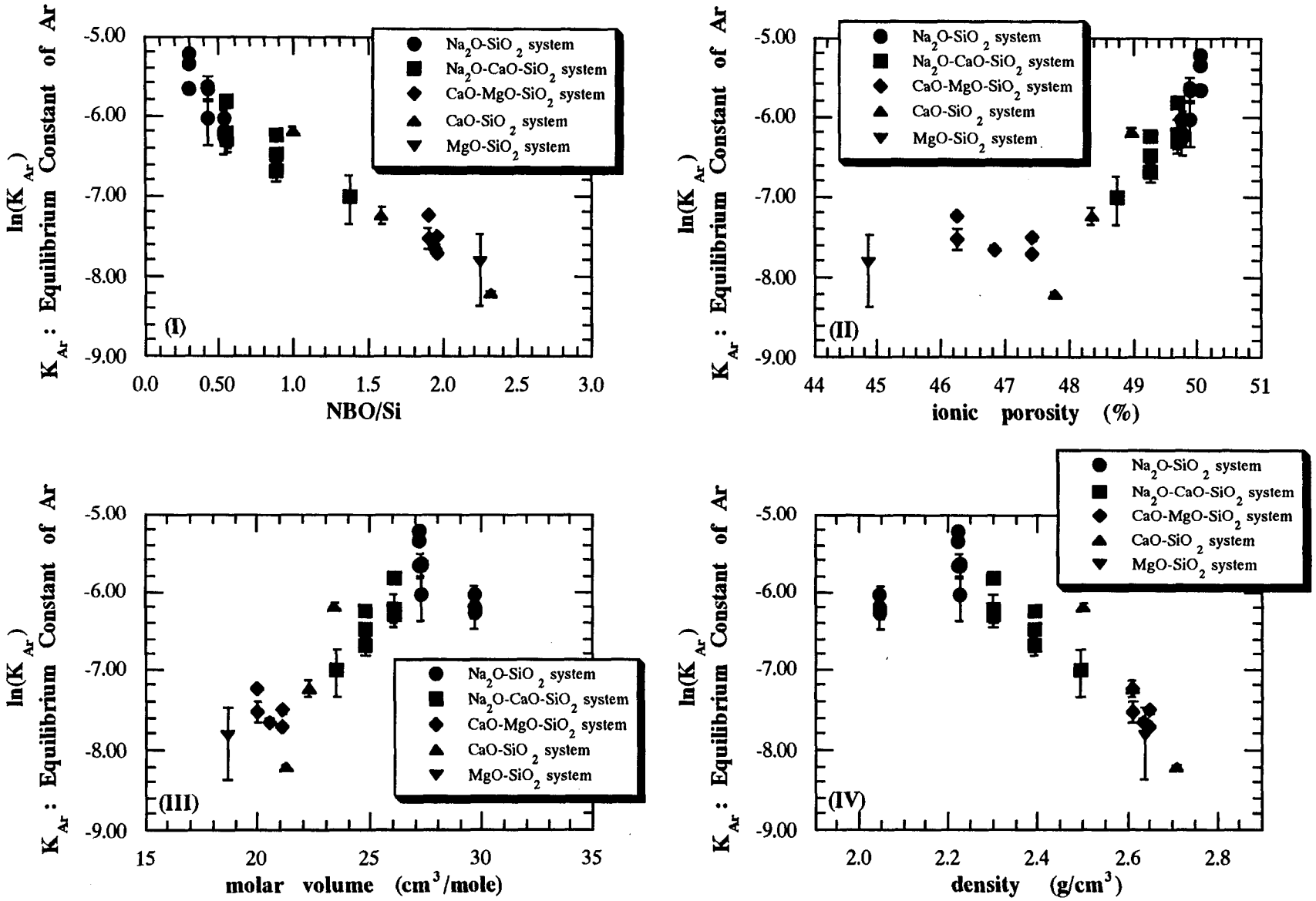

Figure 4-2b. Comparisons of correlation between the natural logarithm of equilibrium constant of Ar and (I) NBO/Si, (II) ionic porosity, (III) molar volume, and (IV) density.

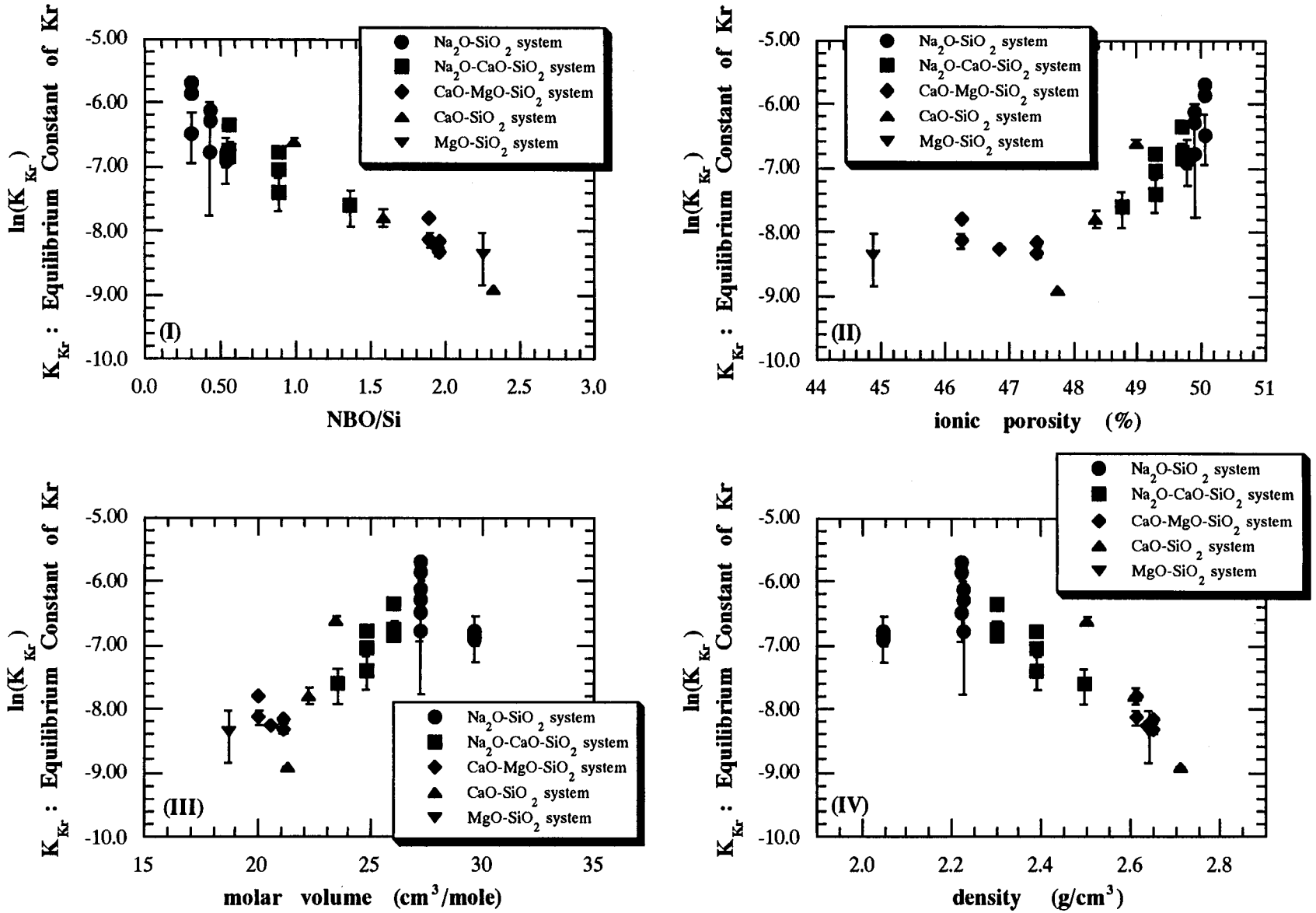

Figure 4-2c. Comparisons of correlation between the natural logarithm of equilibrium constant of Kr and (I) NBO/Si, (II) ionic porosity, (III) molar volume, and (IV) density.

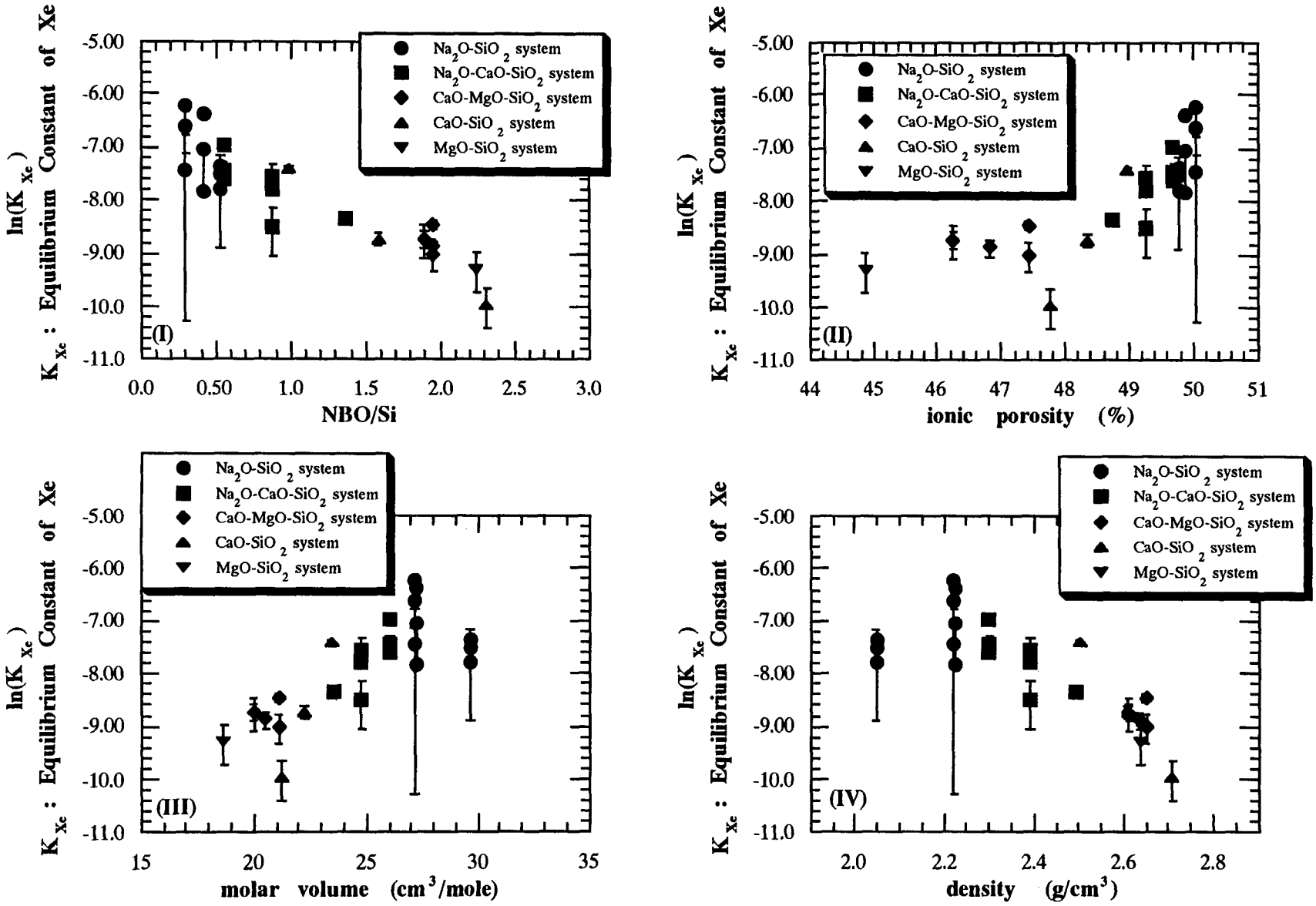

Figure 4-2d. Comparisons of correlation between the natural logarithm of equilibrium constant of Xe and (I) NBO/Si, (II) ionic porosity, (III) molar volume, and (IV) density.

Figure 4-2 shows the logarithm of all equilibrium constants of Ne, Ar, Kr and Xe obtained from this work versus NBO/Si ratio, ionic porosity, melt density and molar volume, respectively; the latter three variables have previously been suggested as predictors of rare gas solubility by other authors [*Lux,* 1987; *White et al.,* 1989; *Broadhurst et al.,* 1990, 1992; *Carroll and Stolper,* 1993].

NBO/Si ratio, ionic porosity, density and molar volume are all correlated with the noble gas solubility, but the NBO/Si ratio is clearly the best predictor based on the quality of the linear fit shown in Figure 4-2. Ionic porosity is well correlated with noble gas solubility in Na_2O-SiO_2, Na_2O-CaO-SiO_2 and CaO-SiO_2 systems. However, the data of MgO-SiO_2 and CaO-MgO-SiO_2 systems deviate from the correlation line (See diamond and downward triangle symbol in Figure 4-2). In the case of CaO-MgO-SiO_2 system, ionic porosity decreases as the concentration of MgO increases in the sequence of CMS1 (12.1 mole%), CMS2 (24.0 mole%) and CMS3 (35.5 mole %) but the concentration of SiO_2 does not change (~50 mole%). This indicates that the solubilities in CaO-MgO-SiO_2 melts do not change with ionic porosity but are related to concentration of SiO_2. In general, there are two kinds of region in silicate melt and glass: one is made up by network formers and the other is made up by network modifier. Cation cluster of network modifier is called as "percolation channel" [*Greaves*, 1985]. The idea of ionic porosity does not distinguish the regions in the network former from those of network modifier. Most previous data and my data indicate that noble gas solubility is higher in more silica rich melts, so it is estimated that noble gas dissolves into free volume formed by network forming oxide. The noble gas solubility in Na_2O-SiO_2, Na_2O-CaO-SiO_2 and CaO-SiO_2 systems can be well correlated with the ionic porosity, since the change of ionic porosity in these systems would indicate the change of the free volume formed by network former and modifier. Meanwhile, the amount of the free volume formed by network former will be approximately constant in CaO-MgO-SiO_2 melts, because the

concentration of SiO_2 does not change (~50 mole%). The change of ionic porosity in the melts would mainly indicate the change of the free volume formed by only network modifier. Therefore, the solubility in the melts will be poorly correlated with the ionic porosity. Consequently, ionic porosity will not be suitable for explaining the noble gas solubility for many silicate melts.

Molar volume has a good correlation except for the data of low and high values (See Figure 4-2). Molar volume reflects a kind of density that has a good liner trend except for data of the lowest value in my experiment. It is surprising that density has the good liner trend in Figure 4-2, since density depends on atomic mass and number of atoms in a given volume of melt. *Lux* [1987] indicated a good linear relationship between the density and the solubility in the range 2.1-2.7 g/cm^3. The data obtained in this study also indicate the relationship in the same range. However, the solubilities less than density of 2.1 g/cm^3 fall off the linear trend. The good correlation of the molar volume and the density with the solubility will indicate the noble gas solubility is related to network structure. However, molar volume and density have indirect information of network structure in silicate melt, so it is not clear how noble gas solubility is related to the network structure and what in silicate melt accommodates noble gases.

As a whole, the NBO/Si ratio has the best relation with noble gas solubility. The NBO/Si ratio exhibits polymeric degree of melt structure. In general the polymerization of melt structure increases as the amount of the network former increases. From Figure 4-2, it can be seen that the noble gas solubility increases with decreasing the NBO/Si ratio. In other word, the noble gas solubility increases as the amount of network structure by network formers increases. Consequently, the correlation between the noble gas solubility and the NBO/Si ratio allows that noble gas dissolves in the network structure by network former rather than the free-volume by the network modifier. Additionally the noble gas solubility is not dependent on the type of network modifying cations in silicate

melt, but the noble gas solubility is affected by the network structure formed by network forming atoms.

4-3 Relation between Melt Structure and Solubility

As is described above, noble gas solubility is affected by the network structure. In this section we will describe the detailed relation between noble gas solubility and network structure in silicate melt and glass. The network structure is constructed by silicon atoms combining with oxygen atoms. The feature of the combination between silicon and oxygen atom has been studied. As results of Raman spectroscopy studies, only limited shapes, which are called as anionic structural units, exist in silicate melts [e.g., *Brawer,* 1975; *Brawer and White,* 1975, 1977; *Virgo et al.,* 1980; *Mysen et al.,* 1980, 1982; *Furukawa et al.,* 1981]. These units are SiO_2 (three-dimensional network structure), $Si_2O_5^{2-}$ (sheets), $Si_2O_6^{4-}$ (chains), $Si_2O_7^{6-}$ (dimers) and SiO_4^{4-} (monomer). The structural units will show not the long-range structure but the random network by combination between silicon and oxygen atoms. The features of these units are shown in Figure 1-4.

Na_2O-SiO_2 System

As the anionic structure units for Na_2O-SiO_2 glass have been observed by Raman spectroscopy studies [*Brawer,* 1975; *Brawer and White,* 1977; *Furukawa et al.,* 1981], Na_2O-SiO_2 glasses with the NBO/Si ratio of 0-1.4 are constituted by limited three units: SiO_2 (three-dimensional network structure), $Si_2O_5^{2-}$ (sheets) and $Si_2O_6^{4-}$ (chains) (See figure 4-3). We use their data to the model of noble gas solubility related to anion structure units. Figure 4-4 shows the relation between proportion of anionic structure units and equilibrium constants of Ne, Ar, Kr and Xe. As can be seen in Figure 4-4, the equilibrium constant of the all four noble

gases increases continuously as the proportion of three-dimension structure unit increases or the proportion of sheet and chain units decreases. The correlation between structural units and the equilibrium constant supports that noble gases dissolve in more polymerized network structure. Additionally it is likely that noble gases dissolving in melts are always coupling together with oxygens bridging only silicon.

If we assume that the noble gas dissolving in silicate melts is accommodated by the limited structure units, it is possible to estimate the contribution of each unit to the noble gas solubility. If the noble gases in the units are in equilibrium with those on the gaseous phase and the other units, the bulk equilibrium constant is given by

$$K_i^{bulk} = A^{3D} \bullet K_i^{3D} + A^{she} \bullet K_i^{she} + A^{cha} \bullet K_i^{cha} \quad , \qquad (4\text{-}3\text{-}1)$$

where A is abundance proportion of each unit, K_i is the equilibrium constant of noble gas "i", and superscripts "3D", "she" and "cha" represent three-dimension, sheet and chain units, respectively. Three sets of K_i^{bulk}, A^{3D}, A^{she}, and A^{cha} are obtained from the data of my experiment and the abundance of units estimated from Figure 4-3 for three Na_2O-SiO_2 melts (NS1, NS2 and NS3). From three sets of equations, three equilibrium constants can be calculated. However, this analysis yielded negative equilibrium constants for sheet units ($Si_2O_5^{2-}$) and chain units ($Si_2O_6^{4-}$). The negative values would indicate that these species play a less significant role for noble gas solubility. Therefore, after discarding the sheet and chain units we estimated equilibrium constants for the three dimensional units. In conclusion, noble gas dissolves in most polymerized structure units (three-dimensional units) among three units. This conclusion supports the results obtained from the correlation of the noble gas solubility with the NBO/Si ratio. Table 4-3 shows the estimated values of equilibrium constants in three-dimensional units.

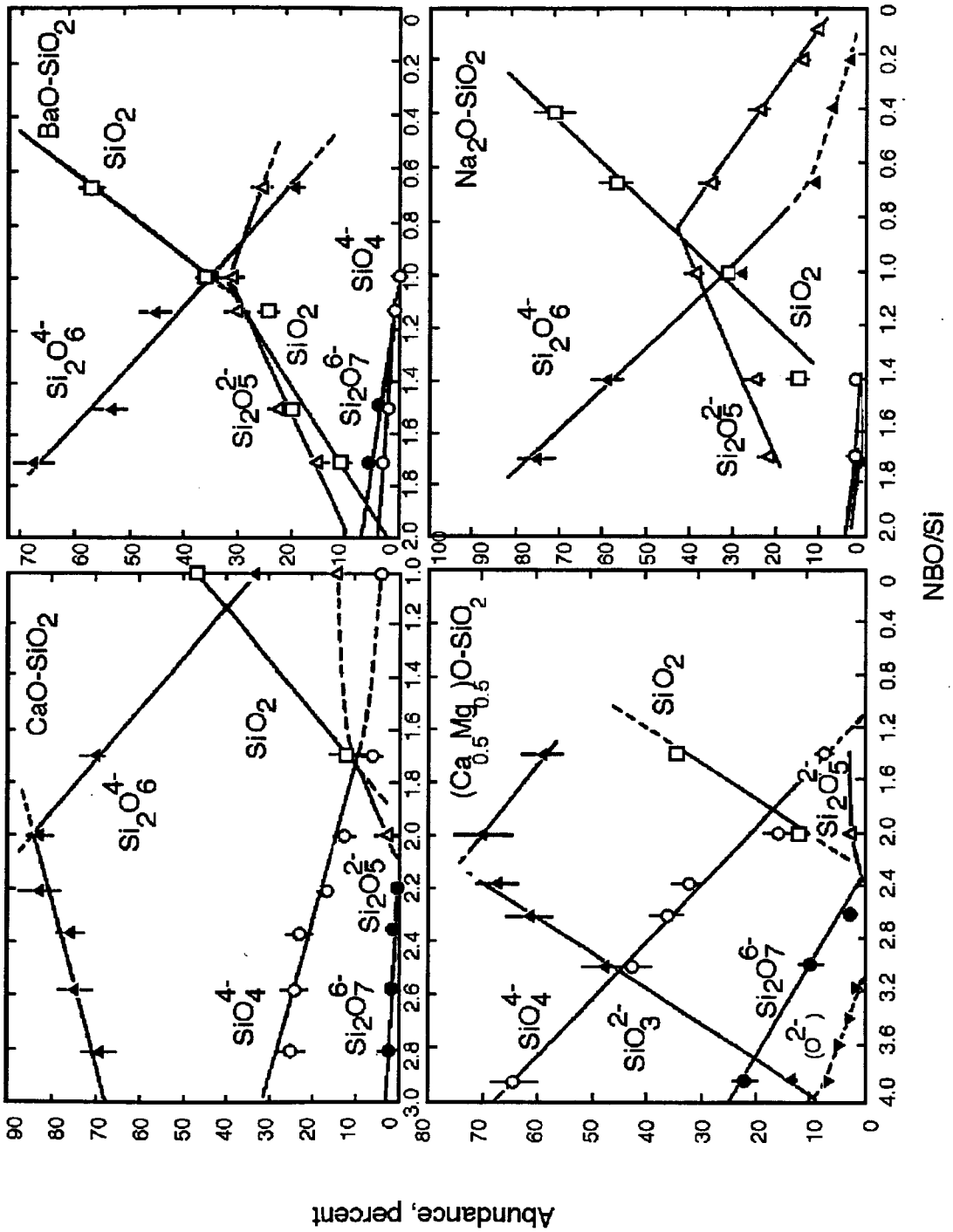

Figure 4-3. Abundance of structural units in binary metal oxide-silica melts as a function of bulk NBO/Si and type of metal cation [From *Mysen et al.*, 1982].

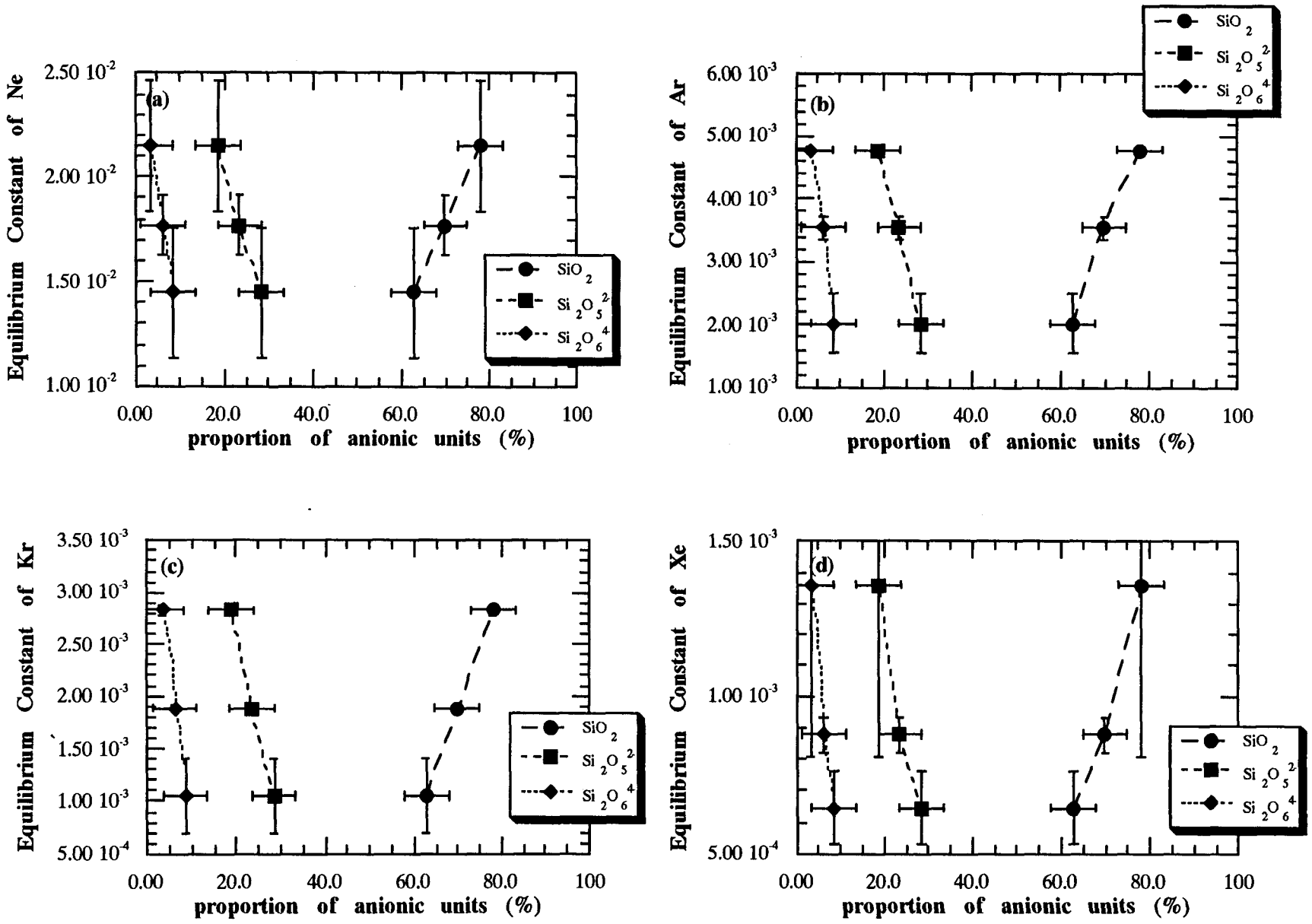

Figure 4-4. Equilibrium constant for (a) Ne, (b) Ar, (c) Kr and (d) Xe in binary Na_2O-SiO_2 melts as a function of proportion of structure units. The equilibrium constants of the noble gases increase with increasing abundance of three-dimensional structure unit.

Table 4-3. Estimated values of equilibrium constants in three-dimensional (3D) and chain units for Na_2O-SiO_2 and CaO-SiO_2 systems. Errors show 1 σ.

	Ne	Ar	Kr	Xe
		x 10^{-3}		
Na_2O-SiO_2 system				
chain units -	-	-	-	-
3D units	25.3	4.81	2.66	1.34
	(±2.3)	(±1.47)	(±0.97)	(±0.36)
CaO-SiO_2 system				
chain units	1.96	0.349	0.171	0.0613
	(±0.11)	(±0.010)	(±0.002)	(±0.0023)
3D units	11.3	4.05	2.68	1.23
	(±0.1)	(±0.16)	(±0.12)	(±0.07)

CaO-SiO_2 System

The structure of CaO-SiO_2 system has also been studied by Raman spectroscopy. *Mysen et al.* [1982] also observed and estimated the proportion of these units in binary CaO-SiO_2 system. CaO-SiO_2 glasses with the NBO/Si ratio of 1.0-2.3 are constituted by limited four units: SiO_2 (three-dimensional network structure), $Si_2O_5^{2-}$ (sheets), $Si_2O_6^{4-}$ (chains) and SiO_4^{4-} (monomer) (See Figure 4-3). Figure 4-5 shows the relation between the proportion of anionic structure units and the equilibrium constant of four noble gases. Figure 4-5 indicates that the equilibrium constants of noble gases increase as the fraction of three-dimensional structure units increases.

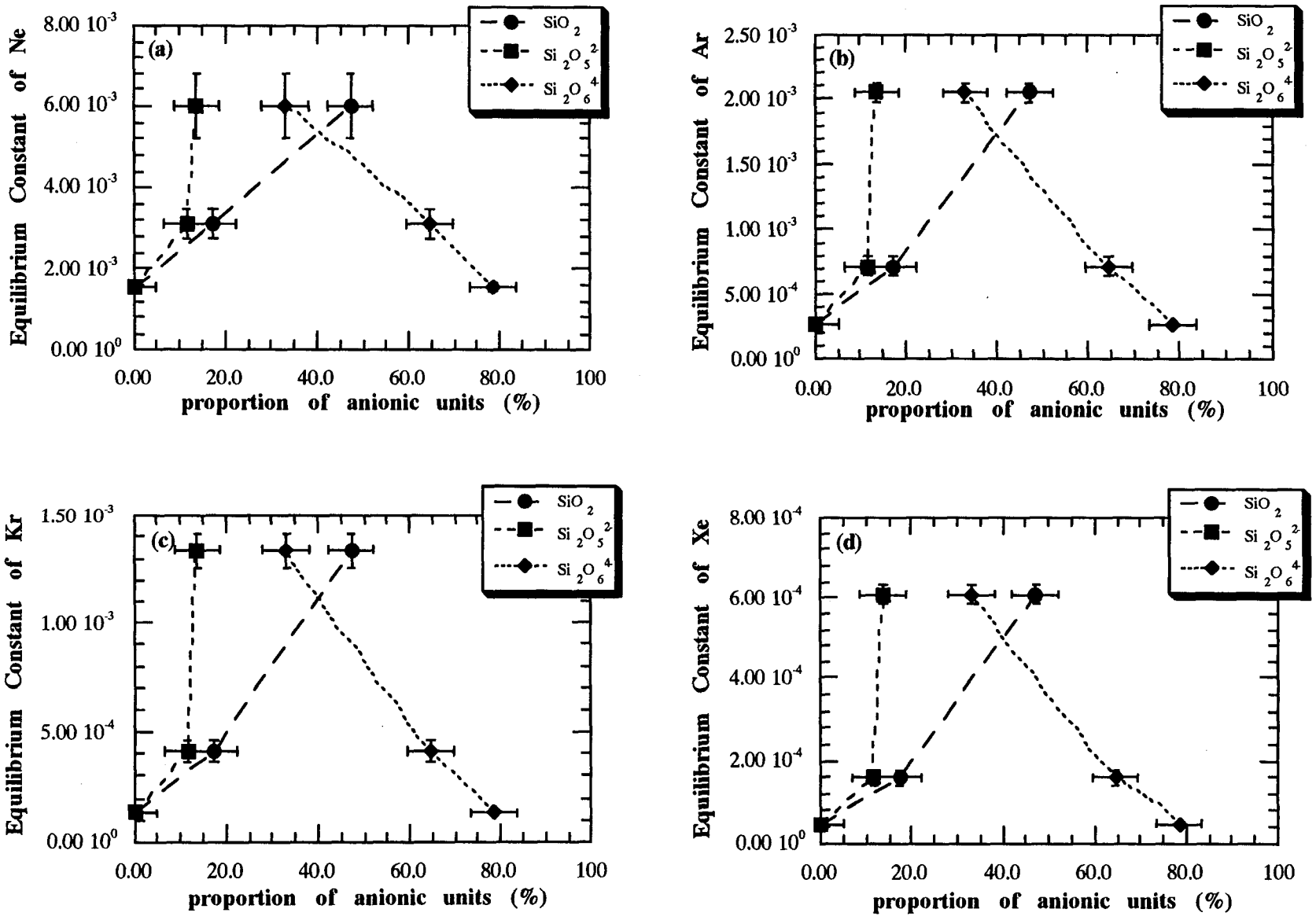

Figure 4-5. Equilibrium constant for (a) Ne, (b) Ar, (c) Kr and (d) Xe in binary $CaO\text{-}SiO_2$ melts as a function of proportion of structure units. The equilibrium constants of the noble gases increase with increasing abundance of three-dimensional structure unit.

As the glasses of $CaO\text{-}SiO_2$ system are constituted by four limited structure units, the bulk equilibrium constant is given by

$$K_i^{bulk} = A^{3D} \bullet K_i^{3D} + A^{she} \bullet K_i^{she} + A^{cha} \bullet K_i^{cha} + A^{mon} \bullet K_i^{mon} \quad , \qquad (4\text{-}3\text{-}2)$$

where A^{mon} and K_i^{mon} are the proportion and the equilibrium constant of noble gas "i" of monomer units. Because monomer units (SiO_4^{4-}) can not accommodate gases in their interior due to their simple structure (See Figure 1-4), we neglect their contribution to gas solubility (See Figure 4-5). Hence, we can rewrite (4-3-2) as follows,

$$K_i^{bulk} = A^{3D} \bullet K_i^{3D} + A^{she} \bullet K_i^{she} + A^{cha} \bullet K_i^{cha} \qquad (4\text{-}3\text{-}3)$$

or

$$\frac{K_i^{bulk}}{A^{3D}} = K_i^{3D} + \frac{A^{she}}{A^{3D}} \bullet K_i^{she} + \frac{A^{cha}}{A^{3D}} \bullet K_i^{cha}. \qquad (4\text{-}3\text{-}4)$$

Three sets of K_i^{bulk}, A^{3D}, A^{she}, and A^{cha} are obtained from the data of our experiment and the proportion of units estimated from Figure 4-3 for three $CaO\text{-}SiO_2$ melts (CS1, CS2 and CS3). From three set equations, three equation constants can be calculated. This analysis yields negative equilibrium constant for sheet units ($Si_2O_5^{2-}$) for noble gas solubility. *Mysen et al.* [1982] also showed that sheet units played a less significant role in these melts. Therefore, we discarded the sheet units. Additionally, since CS1 melt is constructed by only a chain unit, equilibrium constant of chain unit is easily obtained from that of CS1 melt. Then, we estimated equilibrium constants of chain and three-dimensional units which are very close to those obtained without neglecting the sheet units. The estimated equilibrium constants are listed in Table 4-3. Most important are the observations that (a) the equilibrium constants in three-dimension units are much higher than in chain units and (b) the equilibrium constants are greater for smaller gases. The estimated equilibrium constants in three-dimension units of Ar, Kr and Xe are close to those in $NaO\text{-}SiO_2$ system.

We will apply the estimated equilibrium constants to $CaO-MgO-SiO_2$ (CMS2) melt. The NBO/Si ratio in the $CaO-MgO-SiO_2$ (CMS2) melt used in our experiment is 1.94. As seen in Figure 4-3 that is the same as figure 10 in *Mysen et al.* [1982], the proportion of three-dimension units in the $CaO-MgO-SiO_2$ (CMS2) melt is ~11.5%. If we assume that all noble gases dissolving in the $CaO-MgO-SiO_2$ (CMS2) melt are accommodated by only three-dimension network, we can calculate bulk equilibrium constants in the $CaO-MgO-SiO_2$ (CMS2) melt using the proportion and the equilibrium constants of three-dimension units. Obtained values of Ar, Kr and Xe from noble gas measurement are very close to the values estimated from $NaO-SiO_2$ and $CaO-SiO_2$ system (See Table 4-4). This result supports that most noble gas dissolves in three-dimensional network units and is always coupling together with oxygen bonding two silicon atoms.

Table 4-4. Observed and estimated values of equilibrium constants in $CaO-MgO-SiO_2$ (CMS2) melt.

	Ne	Ar	Kr	Xe
			x 10^{-3}	
Obtained values from noble gas measurement				
	3.15	0.477	0.258	0.141
	(±0.19)	(±0.181)	(±0.006)	(±0.022)
Estimated values from Na_2O-SiO_2 system				
	2.91	0.553	0.306	0.154
	(±0.26)	(±0.169)	(±0.112)	(±0.042)
Estimated values from $CaO-SiO_2$ system				
	1.30	0.466	0.308	0.142

(±0.09) (±0.019) (±0.014) (±0.008)

Proportion of three-dimensional units is 11.5% in CMS2 melt.

4-4 Application for Relation between Solubility and Structure to Natural Silicate Melts

Solubilities obtained in this study indicate that noble gas solubility in silicate melts and glasses is sensitive to the silicate composition. Table 4-5 presents a compilation of solubility data of noble gases at 1 bar, 800-1600°C; in some cases, these values are based on extrapolation to this temperature range and pressure using the enthalpies of solution and molar volume derived from the published results. As has been discussed above, the noble gases would dissolve into more polymerized network structure and would be always coupling with oxygens bonding network formers. The NBO/T ratio, which is the average number of nonbridging oxygens per tetrahedral cation in the melt, is one measure expressing the state of bonding between network formers and oxygens [*Brawer,* 1975; *Brawer and White,* 1975, 1977; *Mysen et al.,* 1982]. We can estimate the NBO/T ratio from the compositions of silicate melts and glasses. Increasing the value of the NBO/T ratio tend to increase the depolymerization of silicon atoms in the silicate glass and melt. Al^{3+} may occur both as a network former and as a network modifier in silicate melts. Most authors have suggested that whenever sufficient metal cations of the type M^{2+} or M^{+} are present in a melt to charge-compensate Al^{3+} as an $M_{0.5}Al^{4+}$ or MAl^{4+} complex, so that aluminum is in tetrahedral coordination in silicate melts [e.g., *Riebling,* 1964, 1966; *Bottinga and Weill,* 1972; *Wood and Hess,* 1980; *Mysen et al.,* 1980]. However, if Al^{3+}/M^{+} or $Al^{3+}/0.5M^{2+}$ is greater than 1, some Al^{3+} may no longer be in tetrahedral coordination. Since Al^{3+}/M^{+} or $Al^{3+}/0.5M^{2+}$ is less than 1 in all the melts in Table 4-5, we treat Al^{3+} as a network former such as an $M_{0.5}Al^{4+}$ or MAl^{4+} complex.

Table 4-5. Input data and results of noble gas solubility for melt compositions.

Input Data		solubility				
Composition	T [°C]	Ne	Ar	Kr	Xe	Reference
		x 10^{-5} cm^3STP/g-bar				
NS1	1300	70.5	8.74	4.32	2.44	This study
NS2	1300	86.3	15.4	7.70	3.32	This study
NS3	1300	105	20.6	11.6	5.13	This study
NCS1	1400	58.3	8.26	4.60	1.80	This study
NCS2	1400	42.9	6.23	3.35	1.47	This study
NCS3	1400	22.5	3.50	1.81	0.818	This study
CMS1	1500	12.2	1.53	0.792	0.631	This study
CMS2	1500	12.0	1.63	0.839	0.424	This study
CMS3	1500	16.3	1.86	0.951	0.488	This study
CS1	1600	6.54	1.09	0.524	0.181	This study
CS2	1600	13.7	2.98	1.66	0.626	This study
CS3	1600	27.6	8.93	5.67	2.48	This study
MS1	1600	10.6	2.11	1.23	0.469	This study
tholeiite	1200	18.4	4.68	0.789	-	Hayatsu and Waboso [1985]
alkali oliv basalt	1200	21.2	5.98	1.58	-	Hayatsu and Waboso [1985]

basaltic andesite	1200	25.2	10.8	2.07	-	Hayatsu and Waboso [1985]
tholeiite	1300	25.0	5.90	3	1.70	Jambon et al. [1986]
andesite	1350	-	15.2	11.3	8.19	Lux [1987]
leucite basanite	1350	41.5	12.0	9.17	3.45	Lux [1987]
tholeiite	1350	34.5	8.59	6.21	2.66	Lux [1987]
alkali oliv basalt	1350	25.7	6.32	4.34	1.48	Lux [1987]
ugandite	1350	20.7	4.44	2.96	0.987	Lux [1987]
albite	1300	-	28.8	-	-	White et al. [1989]
anorthite	1300	-	2.57	-	-	White et al. [1989]
$Alb_{50}An_{50}$	1300	-	13.1	-	-	White et al. [1989]
sanidine	1300	-	19.5	-	-	White et al. [1989]
$K_2Si_4O_9$	1300	-	23.9	-	-	White et al. [1989]
diopside	1300	-	0.600	-	-	White et al. [1989]
$Di_{25}Alb_{75}$	1600	-	16.4	-	-	White et al. [1989]
$Di_{50}Alb_{50}$	1600	-	8.97	-	-	White et al. [1989]
$Di_{75}Alb_{25}$	1600	-	4.49	-	-	White et al. [1989]
An_9Qz_{91}	1600	-	22.4	-	-	White et al. [1989]
$An_{40}Qz_{60}$	1600	-	7.85	-	-	White et al. [1989]
$An_{23}Qz_{77}$	1600	-	15.7	-	-	White et al. [1989]
granite	1300	-	39.1	-	-	White et al. [1989]
olivine tholeiite	1300	-	4.73	-	-	White et al. [1989]

CMAS[7an]	1300	3.36	1.18	0.602	0.33	Broadhurst et al. [1990]
CMAS[1di]	1300	5.13	0.99	1.88	3.55	Broadhurst et al. [1990]
CMAS[2di]	1300	5.92	2.12	1.66	1.05	Broadhurst et al. [1990]
SiO_2	1000	-	69.1	-	-	Carroll and Stolper [1991]
albite	1000	150	23.6	18.5	-	Roselieb et al. [1992]
albite	1300	-	-	-	8.77	Montana et al. [1993]
sanidine	1300	-	-	-	9.03	Montana et al. [1993]
$K_2Si_4O_9$	1300	-	-	-	11.5	Montana et al. [1993]
albite	1300	-	20.8	-	-	Carroll and Stolper [1993]
orthoclase	1300	-	11.7	-	-	Carroll and Stolper [1993]
rhyolite	1300	-	34.8	-	-	Carroll and Stolper [1993]
tholeiite [EMS]	1300	-	9.94	-	-	Carroll and Stolper [1993]
tholeiite [BU, RE]	1300	-	3.98	-	-	Carroll and Stolper [1993]
albite	800	-	-	14.4	-	Carroll et al. [1993]
SiO_2	800	-	-	37.9	-	Carroll et al. [1993]

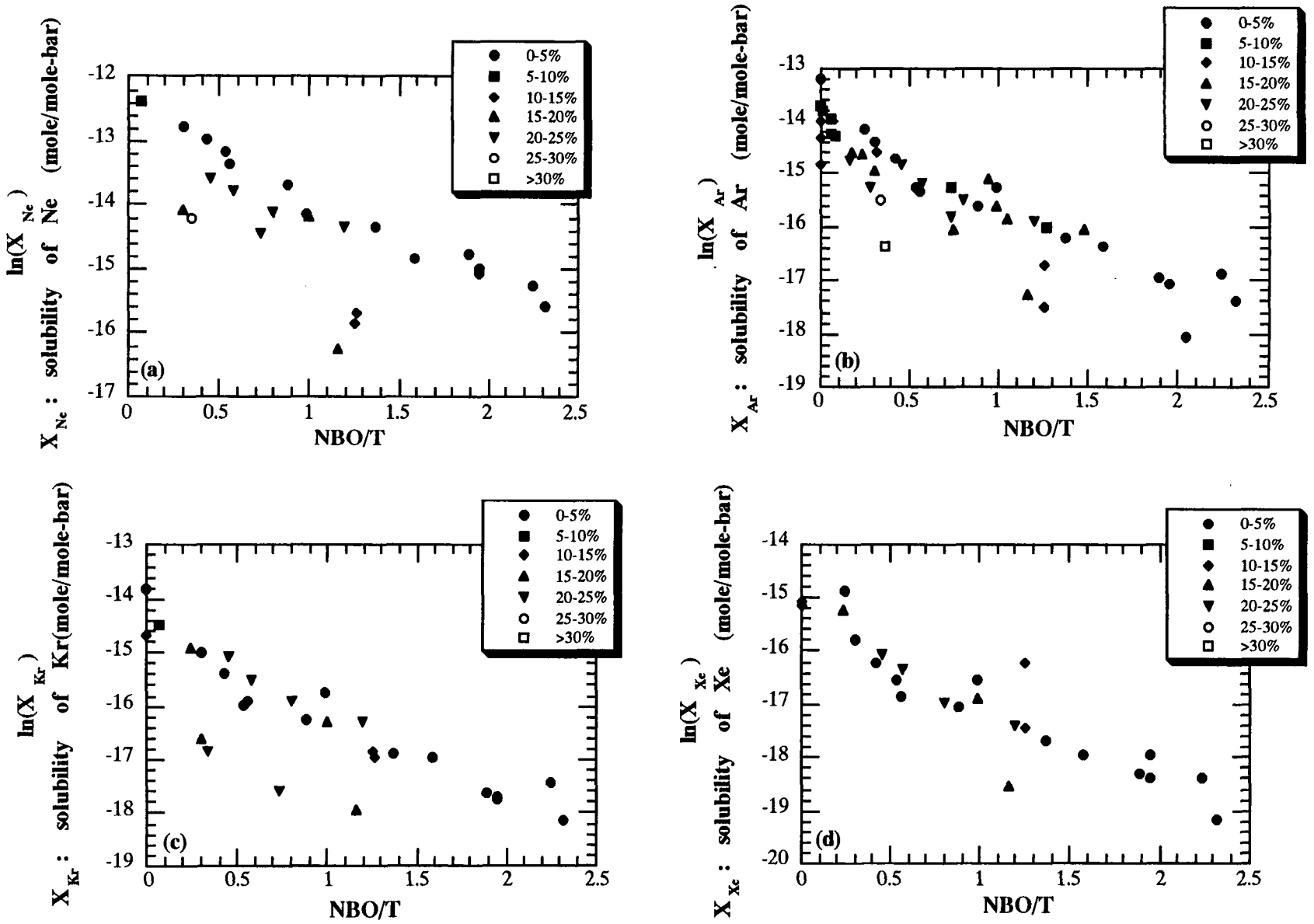

Figure 4-6. Correlation between NBO/T and the natural logarithm of mole fraction at 1 bar of noble gases; (a) Ne, (b) Ar, (c) Kr and (d) Xe. Silicate melts are divided by T/(T + Si) into seven classes, which T is number of network former cations except for Si. The seven classes are following: T/(T + Si) = 0-5%, 5-10%, 10-15%, 15-20%, 20-25%, 25-30% and >30%.

Figure 4-6 shows the logarithm of the 1 bar solubility of Ne, Ar, Kr and Xe, expressed as mole fractions versus the NBO/T ratio for a wide range of silicate melt compositions (given in Table 4-5). The silicate melt compositions are classified with the T/(T + Si) ratio where T is amount of network former except silicon, for example Al^{3+}, Fe^{3+}, P^{5+} and Ti^{4+}. Noble gas solubilities in silicate melts with small T (T/(T + Si) < ~0.15) have a good correlation with the NBO/T ratio. However, the silicate melts with large T (T/(T + Si) > ~0.15) fall off the linear trend. The deviation from the linear trend is not surprising since the added network forming cations except Si change the state of bonding between network formers and oxygens, and give effect on the network structure in the melt. Most network forming cations except Si in silicate melts listed in Table 4-5 are supposed to be aluminum.

The structural roles of Al^{3+} in the silicate melts have been studied [*Riebling,* 1964, 1966; *Taylor and Brown,* 1979a, 1979b; *Seifert et al.,* 1982; *Mysen et al.,* 1985]. It is commonly concluded that Al^{3+} is in tetrahedral coordination in aluminosilicate melts with sufficient M^{+} and M^{2+} cations for charge-balance. The results of Raman spectroscopic studies indicate substitution of Al^{3+} for Si^{4+} in structure units [*Brawer and White,* 1977]. The random substitution of Al for Si in melts, which was inferred from the Raman data, would result in increasing T-O distance with increasing the Al/(Al + Si) ratio [*Seifert et al.,* 1982]. Furthermore, *Mysen et al.* [1985] indicated that the relative abundance of three-dimensional network units increased with increasing the Al/(Al + Si) ratio of the melt even though its bulk NBO/T ratio was unchanged.

It has been proposed that noble gas dissolves in three-dimensional network units in this study. If the model is right, we could infer that the increase of the Al/(Al + Si) ratio in melt gives the increase of noble gas solubility because Raman study indicates that three-dimensional network units increase with increasing the Al/(Al + Si) ratio. However, Figure 4-6 shows that noble gas solubility decreases

with increasing the Al/(Al + Si) ratio. The estimation of noble gas solubility seems to be inconsistent with the expectation from results of Raman study. However, we suppose that this discrepancy is due to the structural difference by between Si^{4+} and Al^{3+}. Al^{3+} accompanying with M^{+} or M^{2+} cations for charge-balance enters the anionic structure units. It is possible that the added cations in the structure units occupy solubility sites of noble gases. Actually, Figure 4-6 indicates that noble gas solubility decreases with adding aluminum oxide to fully polymerized melts, for example Ar solubility in SiO_2 (69.1×10^{-5} cm^3STP/g-bar, and NBO/T = 0) is higher than that in $NaAlSi_3O_8$ (23.6×10^{-5} cm^3STP/g-bar, and NBO/T = 0) [*Carroll and Stolper,* 1991; *Roselieb et al.,* 1992]. The accommodation of M^{+} or M^{2+} cations in the structure units could decrease the noble gas solubility in the melt, although direct experiments for noble gas solubility in aluminosilicate melts are very rare. It is necessary to examine the relation between the noble gas solubility and the structure of aluminosilicate melts further.

Noble gas solubility is related to the network structure that is depend on the coordination number of Si. *Xue et al.* [1991] observed the occurrence of five- and six-coordinated Si species in $Na_2Si_4O_9$ glass at high pressure (6 GPa) and that the abundance of the these species increased with the pressure. Such highly coordinated Si species could contribute to the increase of melt density and decrease the abundance of free-volume in silicon oxide network accommodating noble gases. Therefore, we can expect that noble gas solubility decreases below the transition zone in upper mantle.

SUMMARY

New experimental results and consideration presented in this study allow a comprehensive characterization of noble gas solubility variation with a wide range of silicate melt compositions. We find a systematic relationship between the noble gas solubility and the network structure in melts, leading to quantitative and qualitative characterization of the solubility of noble gases as a function of melt composition. The results and conclusions of this work can be summarized as follows:

1. Noble gas solubilities in binary silicate melts (Na_2O-SiO_2, CaO-SiO_2 and MgO-SiO_2) and ternary silicate melts (Na_2O-CaO-SiO_2 and CaO-MgO-SiO_2) are mostly sensitive to the fraction of SiO_2. The solubilities are related to the network structure in silicate melt, and are higher in more polymerized melts.

2. Noble gas solubility is not governed by cations induced holes or channels but is governed by the tetrahedral network structure. Therefore, noble gas solubility in silicate melts could be defined by the degree of polymerization in silicate melt. Specifically, the most important unit among network anionic structure units is three-dimensional unit. In fact, we can expect equilibrium constants of Ar, Kr, and Xe in CaO-MgO-SiO_2 melts using both the proportion of three-dimensional unit in the melts and the equilibrium constants of three-dimensional unit estimated from Na_2O-SiO_2 and CaO-SiO_2 systems.

3. There is a correlation between noble gas solubility and the NBO/T ratio in for a wide range of silicate melt compositions. However, the noble gas solubility

in the melts falls off the linear correlation line, as the network forming cations except for silicon in the melts increases. This deviation from the linear trend would be due to existence of network modifying cations accompanying with Al^{3+} in network structure units, since most of the network forming cations are supposed to be aluminum.

4. The proposed model is very important for understanding the process of noble gas solution into silicate melts and glass. The model could predict the change of noble gas solubility together with the change of coordination number of Si under high pressure. Therefore, we could expect that noble gas solubility decreases below the transition zone in upper mantle.

These findings and ideas will hopefully contribute to study of Earth evolution.

Acknowledgments

This thesis could not have been written without the assistance of Professor J. Matsuda who acted as supervisor and gave constructive suggestions, criticism of the work and continuous encouragement.

I would also like to thank Professor E. Takahashi of Tokyo Institute of Technology, for his aid in a series of this experiment and many invaluable discussions and comments and Professor K. Kawamura of Tokyo Institute of Technology for their advice of production of silicate melts. I thank Dr. A. Tsuchiyama for many discussions and assistance with the operation of analysis by electron micro probe analysis.

Professor M. Ozima is acknowledged because he guided me to the field of noble gas geochemistry at the beginning of this study. I thank Dr. H. Sato for many discussions and comments. Professor S. Shimokawa at Hokkaido National Agricultural Research Institute and Dr. H. Maekawa in Hokkaido University offered helpful comments regarding structure units in silicate melts. I also acknowledge Dr. I. Miyagi, Dr. A. Tomiya and Dr. K. Funakoshi in Tokyo Institute of Technology for provided kindly advice and assistance with operation of an internally heated gas medium high-pressure apparatus with quench device. I also express my thank to Mr. S. Tachibana, Mr. T. Yoshida, Mr. O. Hamano and my colleagues in my laboratory for their helpful cooperation.

This research was supported by Grant-in-Aid for Scientific Research on JSPS Research Fellowships for Young Sciences from the Japanese Ministry of Education, Science and Culture.

Finally, I thank my family for encouragement.

References

Benson B. B. and D. J. Krause, Empirical laws for dilute aqueous solutions of non-polar gases. *J. Chem. Phys., 64,* 689-709, 1976.

Bockris J. O. and F. Kojonen, The compressibility of certain molten alkali silicates and borates. *J. Am. Chem. Soc., 82,* 4493-4497, 1960.

Bockris J. O., J. D. MacKenzie, and J. A. Kitchner, Viscous flow in silica and binary liquid silicates. *Trans. Faraday Soc., 51,* 1734-1748, 1955.

Bockris J. O., J. W. Tomlinson, and J. L. White, The structure of liquid silicates. *Trans. Faraday Soc., 52,* 299-311, 1956.

Bondi A., Van der Waals Volumes and Radii. *J. Phys. Chem., 68,* 441-451, 1964.

Bottinga Y. and D. F. Weill, The viscosity of magmatic silicate liquids: A model for calculation. *Am. J. Sci., 272,* 438-475, 1972.

Brawer S. A., Theory of vibrational spectra of some network and molecular glasses, *Phys. Rev. B11,* 3173-3194, 1975.

Brawer S. A. and W. B. White, Raman spectroscopic investigation of the structure of silicate glasses, I, The binary silicate glasses. *J. Chem. Phys., 63,* 2421-2432, 1975.

Brawer S. A. and W. B. White, Raman spectroscopic investigation of the structure of silicate glasses, II, Soda-alkaline earth-alumina ternary and quaternary glasses. *J. Non Cryst. Solids, 23,* 261-278, 1977.

Broadhurst C. L., M. J. Drake, B. E. Hagee, and T. J. Bernatowicz, Solubility and partitioning of Ar in anorthite, diopside, forsterite, spinel, and synthetic basaltic liquids. *Geochim. Cosmochim. Acta , 54,* 299-309, 1990.

Broadhurst C. L., M. J. Drake, B. E. Hagee, and T. J. Bernatowicz, Solubility and partitioning of Ne, Ar, Kr, and Xe in minerals and synthetic basaltic liquids. *Geochim. Cosmochim. Acta*, *56*, 709-723, 1992.

Brown G. E. Jr., F. Farges and G. Calas, X-ray scattering and x-ray spectroscopy studies of silicate melts. *In Mineralogical Society of America Review in Mineralogy*, *32*, 318-410, 1995.

Carroll M. R. and E. M. Stolper, Argon solubility and diffusion in silica glass: Implications for the solution behavior of molecular gases. *Geochim. Cosmochim. Acta*, *55*, 211-225, 1991.

Carroll M. R. and E. M. Stolper, Noble gas solubilities in silicate and glasses: New experimental results for argon and the relationship between solubility and ionic porosity. *Geochim. Cosmochim. Acta*, *57*, 5039-5051, 1993.

Carroll M. R., S. R. Sutton, M. L. Rivers, and D. S. Woolum, An experimental study of krypton solubility and diffusion in silicic glasses. *Chem. Geol., 109,* 9-28, 1993.

Dent Glasser L. S., Non-existent silicates. *Zeit. Krist., 149,* 291-305, 1979.

Dietzel A., Die kationenfeldstärken und ihre beziehungen zu entglasungs-vorgängen, zur verbindungsbildung und zu den schmelzpunkten von silikaten. *Zeit Electrochemie, 48,* 9-23, 1942.

Doremus R. H., Physical solubility of gases in fuse silica. *J. Amer. Ceram. Soc., 49,* 461-462, 1966.

Ferry J. M. and L. Baumgartner, Thermodynamic models of molecular fluids at the elevated pressures and temperatures of crustal metamorphism. *In Mineralogical Society of America Review in Mineralogy, 17,* 323-365, 1987.

Frankenheim M. L., Die lehre von der cohäsion. *Breslau, p389,* 1835 (as quoted in Wright, 1994).

Furukawa T, S. A. Brawer and W. B. White, The structure of lead silicate glasses determined by vibrational spectroscopy. *J. Mat. Sci., 13,* 268-282, 1978.

Furukawa T., K. E. Fox and W. B. White, Raman spectroscopic investigation of structure of silicate glasses. III. Raman intensities and structure units in sodium silicate glasses *J. Chem. Phys., 75,* 3226-3237, 1981.

Greaves G. N., EXAFS and the structure of glass. *J. Non Cryst. Solids, 71,* 203-217, 1985.

Goldschmidt V. M. Geochemische verteilungsgesetze der elemente. Skrifter Norske Videnskaps Akademy (Oslo), *I. Math-naturwiss Kl. No. 8* 7-156 1926 (as quoted in Brown et al., 1995).

Hayatsu A. and C. E. Waboso, The solubility of rare gases in silicate melts and implications for K-Ar dating. *Chem. Geol., 52,* 97-102, 1985.

Jambon A., H. Weber and O. Braun, Solubility of he, Ne, Ar, Kr and Xe in a basalt melt in the range 1250-1600 °C. Geochemical implications. *Geochim. Cosmochim. Acta , 50,* 401-408, 1986.

Kirsten T., Incorporation of rare gases in solidifying enstatite melts. *J. Geophys. Res., 73,* 2807-2810, 1968.

Kuroda K. and C. Kato, Trimethylsilylation of hemimorphite. *J. Inorg. Nucl. Chem., 41,* 947-951, 1979.

Kushiro I., Changes in viscosity and structure of melt of $NaAlSi_2O_6$ composition at high pressures. *J. Geophys. Res., 81,* 6347-6350, 1976.

Kushiro I., Viscosity and structural changes of albite ($NaAlSi_3O_8$) melt at high pressures. *Earth Planet. Sci. Lett., 41,* 87-91, 1978.

Lange R. M. and I. S. E. Carmichael, Densities of Na_2O-K_2O-CaO-MgO-FeO-Fe_2O_3-Al_2O_3-TiO_2-SiO_2 liquids: New measurements and derived partial molar properties. *Geochim. Cosmochim. Acta, 51,* 2931-2946, 1987.

Lebedev A. A., Trudy Gos. *Otical Institute, 2,* 1, 1921 (as quoted in Brown et al., 1995).

Lux G., The behavior of noble gases in silicate liquids: Solution, diffusion, bubbles, and surface effects, with applications to natural samples. *Geochim. Cosmochim. Acta, 51,* 1549-1560, 1987.

MacKenzie J. D., Structure of some inorganic glasses from high-temperature studies. *In Modern Aspects of the Vitreous State, ed. by J. D. MacKenzie,* pp. 188-218, Butterworths, Woburn, Mass., 1960 (as quoted in Mysen et al., 1982).

Masson C. R., An approach to the problem of ionic distribution in liquid silicates. *Proc. Roy. Soc., A287,* 201-221, 1965.

Masson C. R., Anionic constitution of glass-forming melts. *J. Non Cryst. Solids, 25,* 3-42 1977.

Montana A., Q. Guo, S. Boettcher, B. S. White and M. Brearley, Xe and Ar in high-pressure silicate liquids. *Am. Mineral., 78,* 1135-1142, 1993.

Morioka M., cation diffusion in olivine- I. Cobalt and magnesium. *Geochim. Cosmochim. Acta, 44,* 759-762, 1980.

Mysen B. O., D. Virgo, and C. M. Scarfe, Relations between the anionic structure and viscosity of silicate melts- a Raman spectroscopic study. *Am. Mineral., 65,* 690-710, 1980.

Mysen B. O., D. Virgo, and F. A. Seifert, The structure of silicate melts: Implications for chemical and physical properties of natural magma. *Reviews of Geophysics and Space Physics, 20,* 353-383, 1982.

Mysen B. O., D. Virgo, and F. A. Seifert, Relationships between properties and structure of aluminosilicate melts. *Am. Mineral., 70,* 88-105, 1985.

Navrotsky A., R. Hon, D. F. Weill and D. J. Henry, Thermochemistry of glasses and liquids in the systems $CaMgSi_2O_6$-$CaAl_2Si_2O_8$-$NaAlSi_3O_8$, SiO_2-$CaAl_2Si_2O_8$-$NaAlSi_3O_8$ and SiO_2-Al_2O_3-CaO-Na_2O. *Geochim. Cosmochim. Acta, 44,* 1409-1423, 1980.

Pauling L., The principles determining the structure of complex ionic crystals. *J. Am. Chem. Soc., 51,* 1010-1026, 1929.

Pierotti R. A., The solubility of gases in liquids. *J. Phys. Chem., 67,* 1840-1845, 1963.

Pierotti R. A. and G. D. Halsey, The interaction of krypton with metals. An appraisal of several interaction theories. *J. Phys. Chem., 63,* 680-686, 1959.

Randall J. T., H. P. Rooksby and B. S. Cooper, X-ray diffraction and the structure of vitreous solid-I. *Zeit. Krist., 75,* 196-214, 1930.

Rawson H., Inorganic glass-forming systems. pp. 267, Academic Press, New York, 1967 (as quoted in Brown et al., 1995).

Redlich O. and J. N. S. Kwong, On the thermodynamics of solutions. V. An equation of state. Fugacities of gaseous solutions. Chem. Rev., 44, 233-244, 1949.

Riebling E. F., Structure of magnesium aluminosilicate liquids at 1700 °C. *Can. J. Chem., 42,* 2811-2821, 1964.

Riebling E. F., Structure of sodium aluminosilicate melts containing at least 50 mole % silica at 1500 °C. *J. Chem. Phys., 44,* 2857-2865, 1966.

Riebling E. F., Structural similarities between a glass and its melt. *J. Am. Ceram. Soc., 51,* 143-149, 1968.

Roselieb K., W. Rammensee, H. Büttner, and M. Rosenhauer, Solubility and diffusion of noble gases in vitreous albite. *Chem. Geol., 96,* 241-266, 1992.

Seifert F. A., B. O. Mysen and D. Virgo, Three-dimensional network melt structure in the systems SiO_2-$NaAlO_2$, SiO_2-$CaAl_2O_4$ and SiO_2-$MgAl_2O_4$. *Am. Mineral., 67,* 696-718, 1982.

Shackelford J. F., A gas probe analysis of structure in bulk and surface layers of vitreous silica. *J. Non Cryst. Solids, 49,* 299-307 1982.

Shackelford J. F. and B. D. Brown, A gas-probe analysis of structure in silicate glasses. *J. Am. Ceram. Soc., 63,* 562-565, 1980.

Shackelford J. F. and B. D. Brown, The lognormal distribution in the random network structure. *J. Non Cryst. Solids, 44,* 379-382 1981.

Shackelford J. F., P. L. Studt and R. M. Fulrath, Solubility of gases in glass. II. He, Ne, and H_2 in fused silica. *J. Appl. Phys., 43,* 1619-1626, 1972.

Shannon R. D. and C. T. Prewitt, Effective ionic radii in oxides and fluorides. *Acta. Cryst., B25,* 925-946, 1969.

Shartsis L., S. Spinner and W. Capps, Density, expansivity and viscosity of molten alkali silicates. *J. Am. Ceram. Soc., 35,* 155-160, 1952.

Shelby J. E., Helium diffusion and solubility in K_2O-SiO_2 glasses. *J. Am. Ceram. Soc., 57,* 236-263, 1974.

Shelby J. E., Pressure dependence of helium and neon solubility in vitreous silica. *J. Appl. Phys., 47,* 135-139, 1976.

Shelby J. E. and R. J. Eagan, Helium migration in sodium aluminosilicate glasses. *J. Am. Ceram. Soc., 47,* 420-425, 1976.

Shibata T., E. Takahashi, and M. Ozima, Noble gas partition between basaltic melt and olivine crystals at high pressure. *In Noble Gas Geochemistry and Cosmochemistry, ed. by J. Matsuda,* pp. 343-354, Terra Scientific Publishing Company, Tokyo, 1994.

Sun K. H., Fundamental condition of glass formation. *J. Am. Ceram. Soc., 30,* 277-281, 1947.

Sweet J. R. and W. B. White, Study of sodium silicate glasses and liquids by infrared spectroscopy. *Phys. Chem. Glasses., 10,* 246-251, 1969.

Takahashi E. and A. Tomiya, An internally heated gas-medium high-pressure apparatus with quench device (SMC-2000) (Abstract D31-P83) *Program and abstracts the Volcanological Society of Japan, at Kyoto, 1992: 28,* 1992.

Taylor M. and G. E. Brown Jr., Structure of mineral glasses. I. The feldspar glasses $NaAlSi_3O_8$, $KAlSi_3O_8$ and $CaAl_2Si_2O_8$. *Geochim. Cosmochim. Acta, 43,* 61-75, 1979a.

Taylor M. and G. E. Brown Jr., Structure of mineral glasses. II. The SiO_2-$NaAlSiO_4$ join. *Geochim. Cosmochim. Acta, 43,* 1467-1473, 1979b.

Taylor M, G. E. Brown Jr. and P. M. Fenn, Structure of mineral glasses. III. $NaAlSi_3O_8$ supercooled liquid at 805 °C and the effects of thermal history. *Geochim. Cosmochim. Acta, 44,* 109-117, 1980.

Valenkov N and E. Porai-Koshits, X-ray investigation of glassy state. *Zeit. Krist., 95,* 196-214, 1936.

Verweij H., Raman study of the structure of alkali germanosilicate glasses II. Lithium, sodium and potassium digermanosilicate glasses. *J. Non Cryst. Solids, 33,* 55-69, 1979.

Virgo D., B. O. Mysen, and I. Kushiro, Anionic constitution of 1-atmosphere silicate melts: Implication for the structure of igneous melts. *Science, 208,* 1371-1373, 1980.

Warren B. E., X-ray diffraction of vitreous silica. *Zeit. Krist., 86,* 349-358, 1933.

White B. S., M. Brearley, and A. Montana, Solubility of Argon in silicate liquids at high pressure *Am. Mineral., 74,* 513-529, 1989.

Wood M. I., and P. C. Hess, The structural role of Al_2O_3 and TiO_2 in immiscible silicate liquids in the system SiO_2-MgO-CaO-FeO-TiO_2-Al_2O_3, *Contrib. Mineral. Petrol., 72,* 319-328, 1980.

Wright A. C., Neutron scattering from vitreous silica. V. The structure of vitreous silica: What have we learned from 60 years of diffraction studies? *J. Non Cryst. Solids, 179,* 84-115, 1994.

Xue X., J. F. Stebbins, M. Kanzaki, P. F. McMillan, and B. Poe, Pressure-induced silicon coordination and tetrahedral structure changes in alkali oxide-silica melts up to 12 GPa: NMR, Raman, and infrared spectroscopy. Am. Mineral., 76, 8-26, 1991.

Zachariasen W. H., The atomic arrangement in glass. *J. Am. Chem. Soc., 54,* 3841-3851, 1932.

Zachariasen W. H., The vitreous state. *J. Chem. Phys., 3,* 162-163, 1935.

APPENDIX A

Noble Gas Mass Spectrometry

Two systems used for noble gas analysis consist of (1) main sample handing system, extraction of gases from samples, which can be subdivided in to four sections: (a) gas extraction, (b) purification of extracted gases, (c) separation of noble gases, and (d) the standard gas pipette system, and (2) measurement of noble gases. The systems of quadrupole mass spectrometer and sector type mass spectrometer are shown in Figure A-1 and Figure A-2. In the case of a noble gas analytical system with the quadrupole mass spectrometer, a good vacuum (~ 10^{-9} torr) was obtained. This system was used to analyze noble gas in binary CaO-SiO_2 and MgO-SiO_2 melts. The other silicate melt systems were analyzed by noble gas analytical system with the sector type mass spectrometer. This analytical system was especially assembled in order to measure a large amount of noble gases in synthetic samples, so that the analytical system of sector type mass spectrometer, which consist of very simple section, is in vacuum (~ 10^{-7} torr) lower than that of the quadrupole mass spectrometer. However, it is good enough to measure noble gas in silicate glasses. The followings are details of each mass spectrometer.

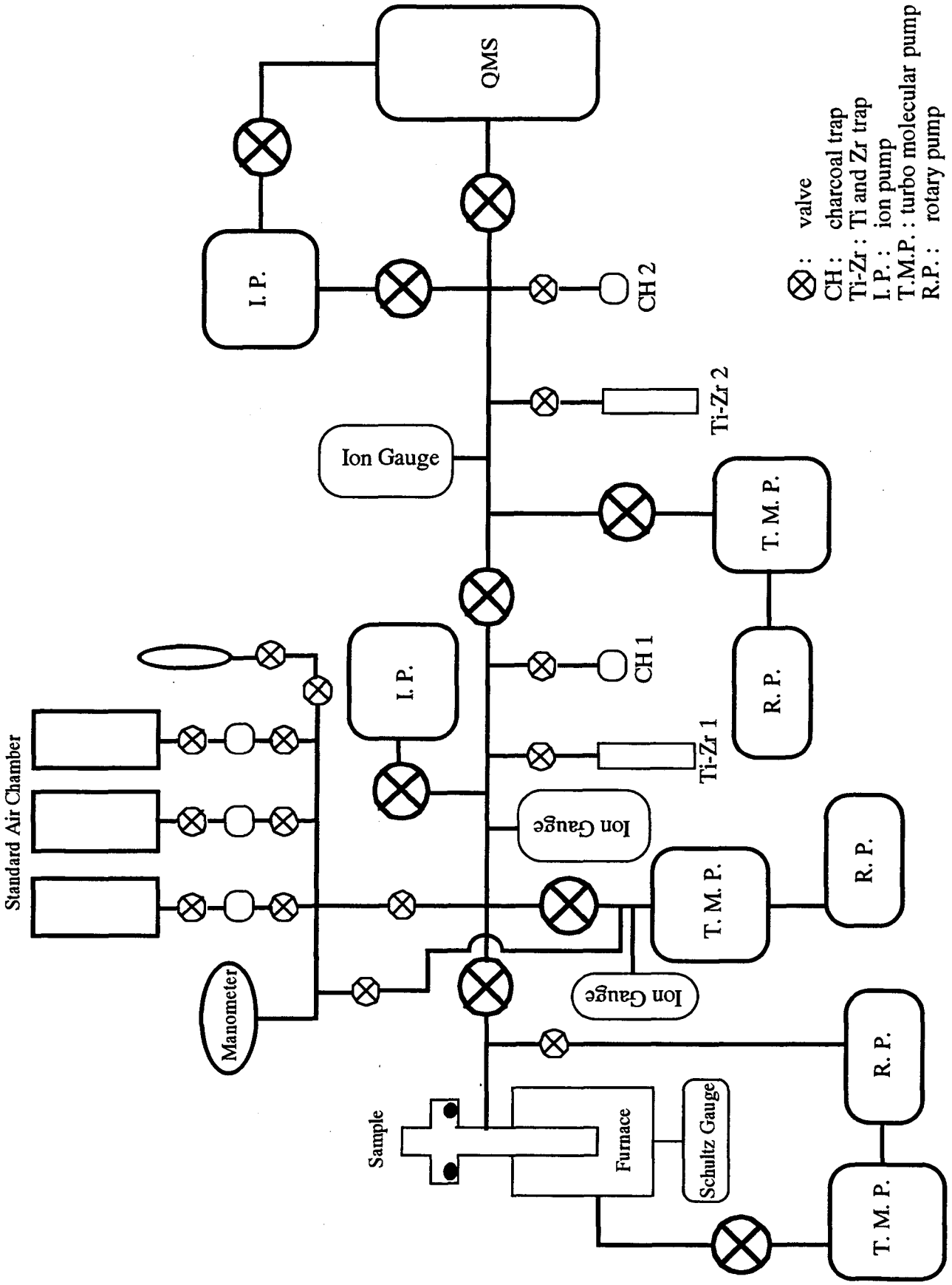

Figure A-1. Noble gas analyzing system of quadrupole mass spectrometer.

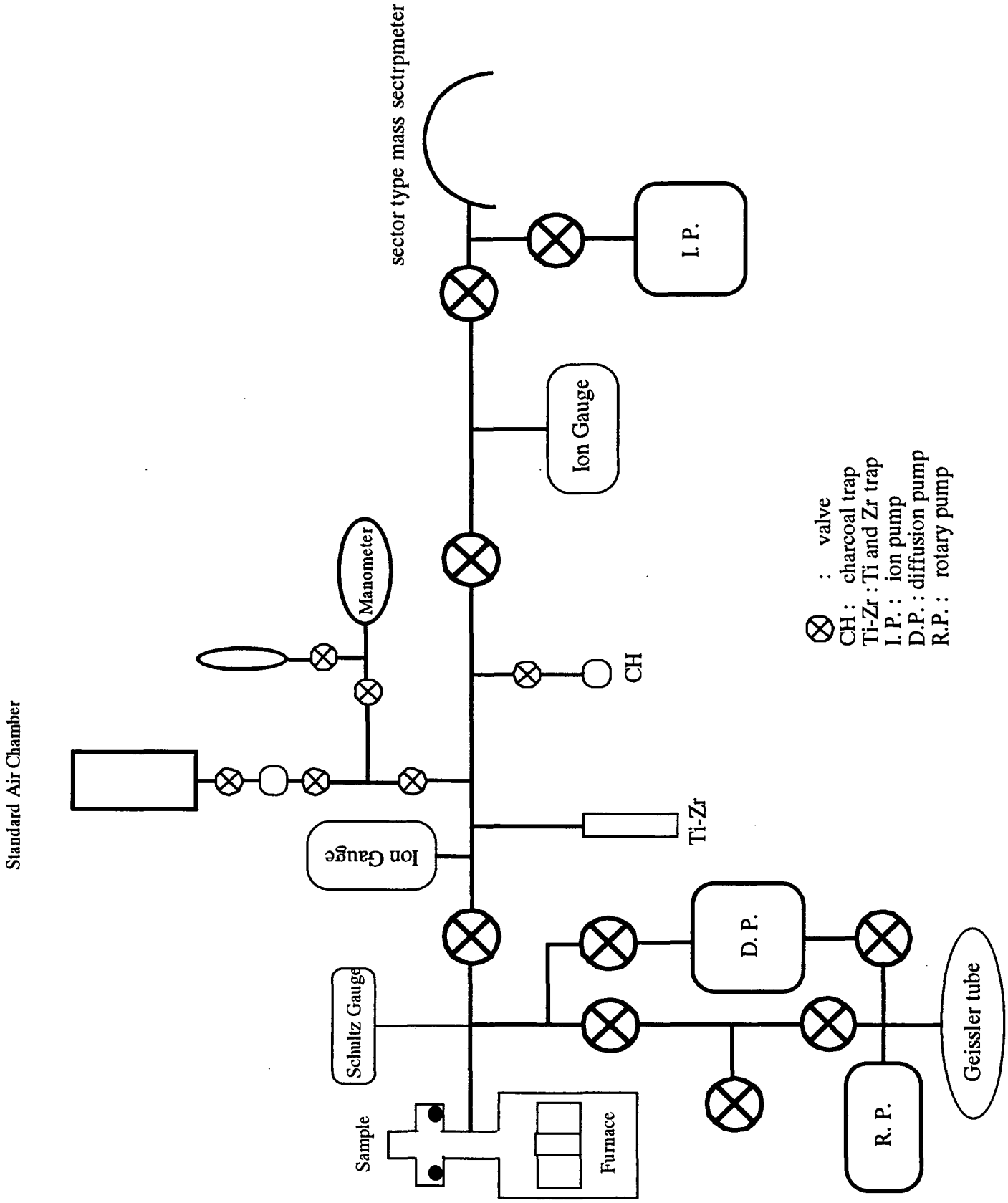

Figure A-2. Noble gas analysis system of sector type mass spectrometer.

I. Noble Gas Analytical System with Quadrupole Mass Spectrometer

A quadrupole mass spectrometer (BALZERS QMG421) was used for the quantitative noble gas analysis. The mass spectrometer has a crossbeam ion source, where emission current is 1 mA, and is fitted with two collectors: a Faraday collector with on-axis and a 17-stage secondary electron multiplier (SEM) with 90° off-axis. The Faraday collector is connected to an amplifier which has three input resistors of 10^6, 10^8, and 10^{10} ohms. One of three resisters was chosen depending on beam intensity. In the case of analysis by the SEM, measured ions are deflected by an electric field to enter the SEM. The followings are details of the procedure.

(a) Gas Extraction

The gas extraction section includes a tantalum crucible and connecting tabulation. The tantalum crucible is radiatively heated with a tantalum resistive heater housed in a separately pumped vacuum chamber. The heating element is constructed by tantalum sheets in a cylindrical shape and is surrounded by radiation shields of tantalum sheets. To protect the crucible from corrosion by reaction with samples, a molybdenum crucible with a thickness of 1 mm connecting with a pipe made of molybdenum sheet is placed inside the tantalum crucible, so that samples are melted in the molybdenum crucible. Temperature of crucible is monitored by a thermocouple (W•5%Re-W•26%Re) at the edge of the crucible, and calibrated beforehand with a pyrometer.

The samples dropped into the furnace were heated as follows; for the first 20 minutes, the furnace was heated up gradually to the required temperature, for

the next 20 minutes, the temperature was kept constant, and for the final 10 minutes, the furnace was cooled down gradually to the room temperature.

(b) Purification of Extracted Gases

When gases are released from the samples, they consist of various gas species, e.g., noble gases, CO_2, H_2O hydrocarbons and so on. Gases other than noble gases must be removed because they interfere the measurement of noble gases. This is why purification is very important part in the noble gas measurement.

Two titanium-zirconium getters containing 20 sheets of titanium and zirconium foils (Ti: 5 mm in width and 80 mm in length, Zr: 5 mm in width and 10.5 mm in length) were used for purification. Hot titanium and zirconium (about 800 °C) chemically absorb active gases other than noble gases. Purification of extracted gases was performed in two steps. First, the extracted gases were purified by only a titanium-zirconium getter during gas extraction and 15 minutes after the extraction. After the purification the titanium-zirconium getter was cooled down to room temperature gradually to absorb H_2 and so on, physically. After the first purification the remaining gases were again purified by the second titanium-zirconium getter with the same procedure as the first purification.

(c) Separation of Noble Gases

After purification, in order to make precise measurement of all noble gases, the extracted noble gases are separated into two fractions: helium and neon fraction and argon, krypton and xenon fraction. They were separated with cold traps of charcoal kept at liquid nitrogen boiling temperature. Two chambers containing charcoal grains (2-3 mm in diameter, and total weight is about 2 g) were used for the separation. Argon, krypton and xenon were adsorbed on the

charcoal at the liquid nitrogen boiling temperature. While argon, krypton and xenon species were trapped on the charcoal, the amounts of helium and neon were measured by mass spectrometer. After measurement of the helium and neon species, argon, krypton and xenon fraction was desorbed from charcoal at 100 °C. After all the fractions were released from the charcoal, the amounts of argon, krypton and xenon were measured.

(d) Standard Gas Pipette System

Three pipettes are attached to the sample system and used to deliver the known aliquots of standard gases so as to calibrate instrument sensitivity. Two of them were prepared by purified air. One pipette was used in this experiment. The amounts of ^{4}He, ^{20}Ne, ^{40}Ar, ^{84}Kr and ^{132}Xe in the first pipette were 2.91 x 10^{-9}, 9.13 x 10^{-9}, 5.14 x 10^{-6}, 3.61 x 10^{-10} and 1.30 x 10^{-11}(cm^3STP), respectively.

(e) Measurement

Cold blank corresponds to residual gases in the high vacuum line on a static condition. A cold blank in the high vacuum line was measured before the sample was crushed. The amounts of ^{4}He, ^{20}Ne, ^{40}Ar, ^{84}Kr and ^{132}Xe in cold blanks during the experiments ranged (7.2-34) x 10^{-12}, (0.78-18) x 10^{-11}, (0.41-8.8) x 10^{-10}, (2.5-4.1) x 10^{-12} and (1.4-2.3) x 10^{-13} cm^3STP, respectively. Meanwhile, hot blank indicates gases evolved during a complete experiment procedure without a sample. The hot blanks were measured before and after two or three samples were run. The amounts of ^{4}He, ^{20}Ne, ^{40}Ar, ^{84}Kr and ^{132}Xe in hot blanks (at 1630°C) during the experiments of these systems ranged on (5.7-440) x 10^{-12}, (1.1-8.2) x 10^{-11}, (1.3-37) x 10^{-9}, (1.7-12) x 10^{-11} and (1.6-36) x 10^{-13} cm^3STP, respectively. These amounts of hot blank do not influence the amounts of noble gas dissolving in silicate melts.

I measured not only ^{20}Ne but also ^{40}Ar during He and Ne fraction to avoid effect of interferences of double-charged ions of ^{40}Ar on ^{20}Ne peak. The production ratio of $^{40}Ar^{++}/^{40}Ar^{+}$ is about 13%.

II. Noble Gas Analytical System with Sector Type Mass Spectrometer

Noble gases in all samples except for $CaO\text{-}SiO_2$ system and $MgO\text{-}SiO_2$ system were analyzed by a sector type mass spectrometer which was a single focusing instrument with 150 mm radius of both incident and exit angle of 55°. It has an ion collector of a secondary electron multiplier (SEM). I set up this analytical system to measure the large amounts of noble gases in my synthetic samples. The purification of extracted gases was performed in a single step. The procedure of noble gas analysis is almost the same as the case of quadrupole mass spectrometer. The different procedures from those of the quadrupole mass spectrometer are described in the followings.

(a) Gas Extraction

The gas extraction chamber includes a heater of an internally heated type, which is made by tantalum sheets. Because of the internally heated type, values of hot blanks in this system are higher than those in line for the quadrupole mass spectrometer. An appearance of the heater is shown in Figure A-3. The tantalum crucible itself plays a role of resistive heater in the gas extraction chamber. To protect the crucible from corrosion by reaction with samples, a molybdenum crucible with a molybdenum chimney is placed in the crucible, so that samples are melted inside the crucible (See Figure A-3). Temperature of crucible was related with a voltage applied on the crucible. The relation between the temperature and

the voltage was investigated by a thermocouple (W•5%Re-W•26%Re) which was put into alumina (Al_2O_3) powder in the crucible (Figure A-4).

The samples dropped into the furnace were heated as follows; for the first 20 minutes, the furnace was heated up gradually to the required temperature, for the next 20 minutes, the temperature was kept constant, and for the final 10 minutes, the furnace was cooled down gradually to the room temperature.

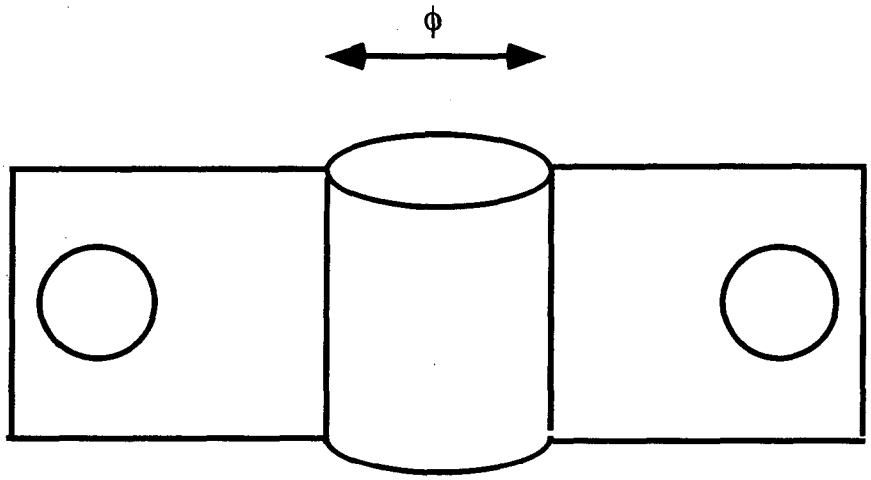

A tantalum heater of an internally heated type

ϕ = 20 mm M-type
= 10 mm S-type

Figure A-3. An appearance of a tantalum heater of an internally heated type. There are two kinds of the heater with the different diameter of the crucible; one is 20 mm and the other is 10 mm.

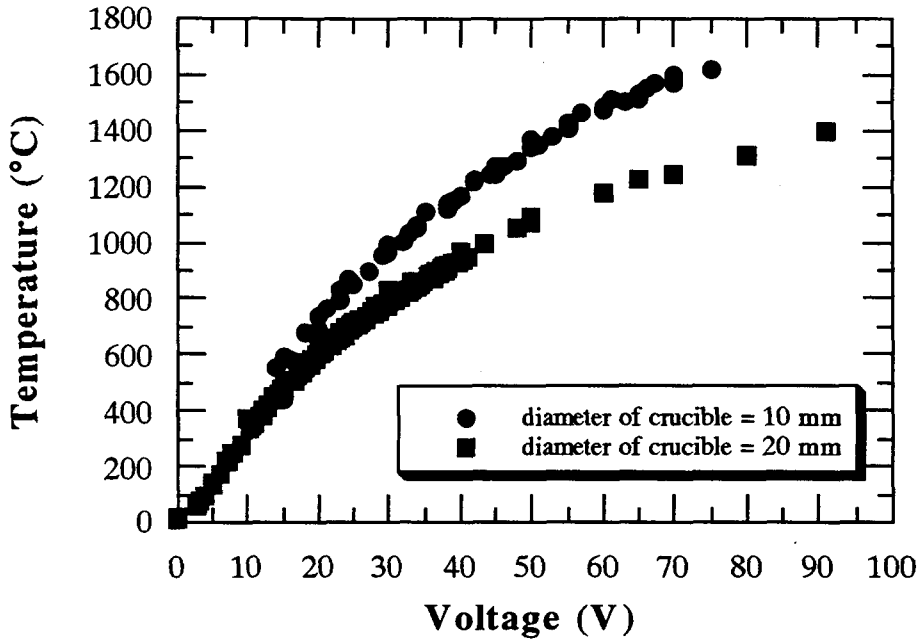

Figure A-4. The relation between the temperature and the applied voltage for the furnace. Circle symbols are a heater with small diameter of crucible (ϕ = 10 mm), and square symbols are a heater with large diameter of crucible (ϕ = 20 mm).

(b) Purification of Extracted Gases

Larger amounts of noble gases were extracted from samples during the gas extraction, because the samples were melted and exposed to noble gas mixture pressurized in pressure apparatus. Therefore, gas purification was performed in a single step in this line, although purification is very important part in the noble gas measurement. The other details of this operation are described in section of procedure with quadrupole mass spectrometer.

(c) Separation of Noble Gases

For at least one piece of individual samples, the extracted noble gases are separated into two fractions: helium and neon fraction and argon, krypton and xenon fraction after the purification. The details of separation procedure for noble gas were described in section of procedure with quadrupole mass spectrometer. Meanwhile, the other pieces of the samples were not separated into two fractions in order to save time as much as possible, because I had to analyze as many as ninety-two samples, and it generally takes very much time for noble gas analysis. I did not measure ^{20}Ne peak in this non-separated method to avoid the effect of interferences of double-charged ions of ^{40}Ar on ^{20}Ne peak. The ^{22}Ne peak was substituted for ^{20}Ne in the quantitative measurement of neon.

(d) Standard Gas Pipette System

One pipette is attached to the sample system and used to deliver the known aliquots of standard gases so as to calibrate instrument sensitivity. The pipette was fill with air whose amount was controlled. The amounts of ^{4}He, ^{20}Ne, ^{22}Ne, ^{40}Ar, ^{84}Kr and ^{132}Xe in the first pipette were 8.82×10^{-9}, 2.77×10^{-8}, 2.82×10^{-9} 1.57×10^{-5}, 1.09×10^{-9} and 3.93×10^{-11} (cm^3STP), respectively.

(e) Measurement

The ^{4}He, ^{20}Ne, ^{22}Ne, ^{40}Ar, ^{84}Kr and ^{132}Xe in cold blanks during the experiments of these systems ranged on $(4.4\text{-}460) \times 10^{-10}$, $(0.77\text{-}110) \times 10^{-10}$, $(4.5\text{-}13) \times 10^{-10}$, $(6.8\text{-}130) \times 10^{-9}$, $(1.6\text{-}4.8) \times 10^{-12}$ and $(4.2\text{-}12) \times 10^{-13}$ cm^3STP, respectively. Values of helium, neon and argon in cold blank fluctuate dramatically. I consider that this large fluctuation is due to the gases leaked from samples. However, except for He, the lost amounts of these gases in a high vacuum line do not influence amounts of noble gases dissolving in silicate melts.

The ^{4}He, ^{20}Ne, ^{22}Ne ^{40}Ar, ^{84}Kr and ^{132}Xe in hot blanks at 1250, 1400 and 1500 °C ranged on $(0.31\text{-}47) \times 10^{-8}$, $(0.21\text{-}90) \times 10^{-9}$, $(1.5\text{-}34) \times 10^{-9}$, $(0.75\text{-}230)$

x 10^{-7}, (0.18-420) x 10^{-10} and (0.47-130) x 10^{-10} cm^3STP, respectively. The amounts in hot blanks are usually less than 33%, 25%, 24%, 12%, 32% and 44% for the amounts of ^4He, ^{20}Ne, ^{22}Ne ^{40}Ar, ^{84}Kr and ^{132}Xe dissolving in silicate melts, respectively. For a few samples, however, the proportion of amounts in hot blanks to those in samples is up to 74% and 84% of ^{84}Kr and ^{132}Xe, respectively.

The production ratio of $^{40}Ar^{++}/^{40}Ar^{+}$ is about 25%. Meanwhile double-charged ions of $^{44}CO_2$ also influence on ^{22}Ne peak, when gases extracted from the samples were not separated into two fractions. Therefore $^{44}CO_2$ was also measured and the production ratio of $^{44}CO_2^{++}/^{44}CO_2^{+}$ was about 2.7%.

APPENDIX B

Redlich-Kwong Equation

One-component fluid

Redlich and Kwong [1949] proposed an equation of state that retains the form of the ideal-gas equation and that satisfactorily represents P-V-T properties of fluids at the metamorphic P-T conditions:

$$P = \frac{RT}{V-b} - \frac{a}{T^{0.5}\, V\, (V + b)} \qquad \text{(B-1)}$$

(See Table B-1 for all notation). The empirical coefficients, a and b, are calculated from the following universal function of P_c and T_c:

$$a = 0.4278\ R^2 T_c^{2.5}/P_c \qquad \text{(B-2)}$$

$$b = 0.0867\ RT_c/P_c\ . \qquad \text{(B-3)}$$

Table B-1. Notation.

P pressure (bars)

T absolute temperature (K)

V molar volume (cm^3 / mole)

R universal gas constant (8.314 x 10 cm^3/K mole)

X mole fraction

f fugacity (bars)

a empirical coefficient in Redlich-Kwong equation of state (bar cm^6 $K^{0.5}$ / $mole^2$)

b empirical coefficient in Redlich-Kwong equation of state (cm^3 / mole)

Subscript Notation.

i refers to component i

j refers to component j

m refers to fluid mixture

c refers to variable at critical point

Fluid Mixtures

Equation (B-1) applies to the fluid mixtures when the coefficients, a and b, are taken for the mixture (a_m and b_m). The term, b, in Equation (B-1) refers to the volume of fluid occupied by themselves. The mixing rule for b, therefore, traditionally is:

$$b_m = \sum_j X_j \; b_j \; , \qquad \text{(B-4)}$$

where b_j is b in an equation of state for fluid that is pure component j. The mixing rule for a is also given by

$$a_m = \sum_i \sum_j X_i \; X_j \; a_{ij} \; , \qquad \text{(B-5)}$$

where

$$a_{ij} = (a_i a_j)^{0.5} . \qquad \text{(B-6)}$$

We can rewrite Equation (B-1) in the form

$$V_m^3 - \frac{RT}{P} V_m^2 + \left(\frac{a_m}{T^{0.5} P} - \frac{RTb_m}{P} - b_m^2 \right) V_m - \frac{a_m b_m}{T^{0.5} P} = 0 . \qquad \text{(B-7)}$$

We can obtain fugacity from Equation (B-7) using chemical thermodynamics:

$$\ln (f_i)^{V,T} = \ln \left(\frac{V_m}{V_m - b_m} \right) + \frac{b_i}{V_m - b_m} - \frac{2 \sum_{j \neq i} X_j a_{ij}}{RT^{1.5} b_m} \ln \left(\frac{V_m + b_m}{V_m} \right) + \left(\frac{a_m b_i}{b_m^2 RT^{1.5}} \right) \left\{ \ln \left(\frac{V_m + b_m}{V_m} \right) - \frac{b_m}{b_m + V_m} \right\} - \ln \left(\frac{V_m}{RT} \right). \qquad \text{(B-8)}$$

Therefore, we can first calculate the molar volume of each component from Equation (B-7). Using the obtained the molar volume and Equation (B-8), we can obtain the fugacity of each component. The molar volumes and the fugacities were automatically calculated with a personal computer. The program list is written in Mathematica for Windows and is shown below.

The program list. The list is an example for the synthetic condition of the run G205.

```
Print[" G205 "]
(* parameter: pressure & temperature *)


(* ---------------------------------------- *)
```

```
(* 1: mixture of noble gases *)
(* fraction of noble gases *)
x1 =  0.01*0.501              ; (* He *)
x2 =  0.01*0.0944             ; (* Ne *)
x3 =  1-x1-x2-x4-x5           ; (* Ar *)
x4 =  0.01*0.0998             ; (* Kr *)
x5 =  0.01*0.0103             ; (* Xe *)

X1 =        {x1, x2, x3, x4, x5}     ; (* list *)
X2 =        {X1}                     ; (* list -> Matrix *)
X3 =        Transpose[X2]            ;

Print["noble gas mixture", X1]       ;

(* ---------------------------------------- *)
(* 2: calculation of Redlich-Kwong constants *)

(* I: Redlich-Kwong constants of noble gas *)

(* a = Qa R^2 Tc^2.5 / Pc,  b = Qb R Tc / Pc *)
R  =        8.20575 10^-2    ; (* dm^3 atm K^-1 mol^-1 *)
Qa =        0.427480         ;
Qb =        0.086640         ;

(* Critical Constants of He *)
P1 =  2.26                   ; (* atm *)
T1 =  5.2                    ; (* K *)

(* Critical Constants of Ne *)
P2 =  26.9                   ; (* atm *)
T2 =  44.4                   ; (* K *)

(* Critical Constants of Ar *)
P3 =  48.0                   ; (* atm *)
T3 =  150.7                  ; (* K *)

(* Critical Constants of Kr *)
P4 = 54.3                    ; (* atm *)
T4 = 209.4                   ; (* K *)

(* Critical Constants of Xe *)
P5 = 58.0                    ; (* atm *)
T5 = 289.8                   ; (* K *)
```

```
Pc =  {P1, P2, P3, P4, P5}    ;
Tc = {T1, T2, T3, T4, T5}     ;


(* calculation of a and b *)
a =    Qa R^2 Tc^2.5 / Pc      ; (* dm^6 atm^1 K^0.5 mol^-2 *)
b =    Qb R Tc / Pc            ; (* dm^3 mol^-1 *)

(* calculation "a" and "b" in mixture *)
A1 = {a ^ 0.5}                 ;
A2 = Transpose[A1]             ;
A3 = A2. A1                    ; (* dm^6 atm^1 K^0.5 mol^-2 *)

A4 = X1. A3. X3                ; (* dm^6 atm^1 K^0.5 mol^-2*)
A  =  A4[[1]]                  ; (* dm^6 atm^1 K^0.5 mol^-2*)
B1 = b. X3                     ; (* dm^3 mol^-1*)
B  =  B1[[1]]                  ; (* dm^3 mol^-1*)

(* ---------------------------------------- *)
(* 3: Calculation of molar volume *)
(* parameter *)

Do[
p  =  100 * i                  ; (* bar *)
P  =  p / 1.01325              ; (* bar -> atm *)

(* **************  temperature  ***************** *)
Tem  =1200                     ;
T  =  273 + Tem                ; (* K *)
Print["temperature ", Tem, " C"]    ;
(* **************  temperature  ***************** *)

(* factor *)
a1 =  - (T R)/P                ; (* dm^3 mol^-1 *)
a2 =  (A /(P (T^0.5)) -
      (R T B)/P - (B^2) )      ; (* dm^6 mol^-2 *)
a3 =  - (A B)/(P (T^0.5))      ; (* dm^9 mol^-3 *)

(* Calculation of molar volume mv *)
Print["Pressure ",
      p = 100 * i, " bars" ]   ;
y  =  x^3 + (a1 x^2) + (a2 x) + a3  ;
mv =        Solve[ y == 0, x]      ;
```

```
V1 = x /. mv[[1]]        ;
V2 = x /. mv[[2]]        ;
V3 = x /. mv[[3]]        ;

Print["partial molar volume of mixture gases "] ;
pmv=V3 / X1                          ;
pmv //MatrixForm//Print              ;
Print["(dm^3/mole)"]                 ;


(* ---------------------------------------- *)
(* 4: Calculation of fugacity coefficients *)

fc1 = Log[V3/(V3 + B)]               ;
fc2 = R T^1.5                        ;
fc3 = Log[V3 /(V3-B)-A /(fc2 (V3+B))]   ;

shi =  Log[V3/(V3 - B)]+ b/(V3-B) +
       2 X1.A3 fc1/(fc2 B) -
       A b/(fc2 B^2) (fc1 + B/(V3+B)) -
       fc3                           ;

fhi =  Exp[shi]                      ;


(* ---------------------------------------- *)
(* 5: Summary *)
Print["partial pressure (bars) of each noble gas "]      ;
pp  =        X1 * p                                      ;
pp //MatrixForm//Print                                   ;

Print["fugacity (bars) of each noble gas "];
pp1 =        pp * fhi     //MatrixForm//Print     ;

Print["********************"],

(* ***************  pressure  *************** *)
{i, 18.85, 18.85}
(* ***************  pressure  *************** *)
]
```

APPENDIX C

List of Publications

1) Shibata T., E. Takahashi, and M. Ozima, Noble gas partition between basaltic melt and olivine crystals at high pressure. *In Noble Gas Geochemistry and Cosmochemistry, ed. by J. Matsuda*, pp. 343-354, Terra Scientific Publishing Company, Tokyo, 1994.

2) Shibata T., E. Takahashi, and J. Matsuda, Noble gas solubility in binary CaO-SiO_2 system. *Geophys. Res. Letter*, 23, 3139-3142, 1996.

Noble Gas Geochemistry and Cosmochemistry, ed. by J. Matsuda, pp. 343–354.

Noble Gas Partition between Basaltic Melt and Olivine Crystals at High Pressures

Tomo SHIBATA[1], Eiichi TAKAHASHI[2], and Minoru OZIMA[1]

[1]*Department of Earth and Space Science, Osaka University, Toyonaka, Osaka 560, Japan*
[2]*Earth and Planetary Sciences, Tokyo Institute of Technology, 2-12-1, Ookayama, Meguro-ku, Tokyo 152, Japan*

Abstract. Noble gas solubilities for basaltic melt and olivine crystals were determined for temperatures of 1250°C, 1300°C, and 1600°C and pressures of 0.5 Kbars, 1 Kbar, and 2 Kbars.

Solubilities in basaltic melt increased with temperature, but were almost independent of pressure. The solubilities in olivine increased with temperature, and were smaller at higher pressures. Olivine-basalt distribution coefficients (D_i) of noble gases were as follows; $0.02 < D_{He} < 0.7$, $0.03 < D_{Ne} < 0.6$, $0.087 < D_{Ar} < 2.0$, $0.1 < D_{Kr} < 3.0$.

Surface tensions for basaltic melt calculated from the noble gas solubility data were almost independent of temperature and pressure up to 2 Kbars with value of 130 ± 10 dyne/cm.

1. Introduction

Noble gases are inert and rare in the Earth, so that they serve as an excellent tracer in resolving the Earth evolution processes such as magma generation and its transportation, mantle degassing, atmospheric evolution, and so on. The fundamental physical process controlling the noble gas behavior in the above processes is described by noble gas distribution between melt and crystal. So far, few attempts have been made to estimate distribution coefficients of noble gases between silicate melt and crystal in spite of their great importance. This may be due to a common feeling that noble gases are extremely incompatible elements and cannot be accommodated in any significant amount in a crystal structure. A preliminary attempt to estimate distribution coefficients of noble gases was made by BATIZA et al. (1979). They compared the noble gas content of volcanic rock matrix and its constituting minerals, and estimated distribution coefficients. They obtained values of about 0.1 for Ne. However, values for heavy noble gases ranged from 2 to 8. Since the results were unexpected, Batiza et al. concluded that noble gases had been lost from the samples, that crystals (minerals) and melt (volcanic rocks) were not kept in equilibrium with respect to the noble gas phase, and that the calculated distribution

coefficients were not real.

The first systematic approach of measuring crystal-melt distribution coefficients in a laboratory was made by HIYAGON and OZIMA (1982, 1986). They did the experiments by growing crystals in silicate melt. Two methods of crystal growth were used; one was to grow crystals under high pressure (1.5 GPa) using a piston-cylinder-type apparatus, and the other was to grow crystals under flowing Ar at atmospheric pressure. The separation of the crystals from the melt was done by hand under microscopic observation. The obtained distribution coefficients were 0.2–0.5 for Ar and Kr at high pressure and 0.08–0.18 for Ar at atmospheric pressure. The distribution coefficients obtained by HIYAGON and OZIMA (1982, 1986) were likely to be upper limits, since in their experiments there was a possibility that the separated crystals contained submicroscopic melt or fluid inclusions which contained noble gases.

To avoid glass contamination of crystal separates, BROADHURST et al. (1990, 1992) developed an alternative experimental technique. Silicate melts and natural minerals were held in separate platinum capsules in a 1 bar flowing noble gas atmosphere. The samples were then quenched, and the gas concentrations were measured with a mass spectrometer. The obtained distribution coefficients were surprisingly high; 0.013–0.37 for Ne, 0.15–0.84 for Ar, 0.31–2.4 for Kr, and 3.2–47 for Xe. These results suggest that noble gases are compatible in crystals and the solubility of the noble gases increases with increasing noble gas atomic number. BROADHURST et al. (1990, 1992) concluded that noble gas solubilities in crystals were controlled by point defect abundances.

The results by HIYAGON and OZIMA (1982, 1986) and by BROADHURST et al. (1990, 1992) are very important in interpreting mantle degassing processes, since the results are contrary to the common assumption that noble gases solve more easily into melt than into crystal. It is very important to re-examine this problem, and therefore we performed experiments to measure noble gas solubilities in basaltic melt and olivine crystals at high pressures.

Surface tension is one of the most important parameters in discussing magma generation. Magma is formed by partial melting of mantle materials. The partially molten material migrates through grain boundaries and forms magma. The flow of melt through grain boundaries is primarily controlled by the surface tension of the melt. The surface tensions of silicate melts at atmospheric pressure were measured by MURASE and MCBIRNEY (1973). They used two experimental methods to measure surface tension: the sessile-drop technique and the pin method. The estimated values of surface tensions were about 250–450 dyne/cm at 1000–1400°C. However, the estimated values were those at atmospheric pressure, but not at high pressures which are relevant to the condition in the Earth's interior. Surface tension data at high pressure are extremely scarce owing to experimental difficulty. We, therefore, attempted to estimate surface tension of basaltic melt at high pressure through the measurement of noble gas solubility.

2. Experimental Procedures

2.1 Starting samples

We used basalt powder and olivine crystals in the experiments. Chemical analyses and sample source data for the basalt powder and olivine crystals are given in Table 1. Olivine crystals were crushed, and washed in ethanol. They were ground to powders in several steps, and their final size was a few microns. In the case of basalt powder, its size was about 250 μ.

2.2 High pressure experiments

Basalt powder and olivine crystals were contained in platinum capsules (2 mm in diameter and 5 mm in depth). Since one end of the platinum capsule was only

Table 1. Composition of samples.

sample	basalt (%)*	olivine (%)**
SiO_2	53.20	39.64
TiO_2	1.19	0.00
Al_2O_3	14.67	0.03
Fe_2O_3	3.13	-
FeO	10.09	10.52
MnO	0.20	0.16
MgO	4.66	48.25
CaO	9.89	0.08
Na_2O	2.03	0.01
K_2O	0.42	0.00
P_2O_5	0.10	-
H_2O^+	0.31	-
H_2O^-	0.07	-
Cr_2O_5	-	0.01
NiO	-	0.39
Total	99.96	99.09

* : Tholeiitic basalt from O-shima volcano in Japan. Chemical analyses are after Ando et al. (1989).

** : Olivine from peridotite KLB-1 (Kilborne Hole crater in New Mexico). Chemical analyses are after Takahashi (1986).

loosely pinched, the noble gas mixture (^{4}He:^{20}Ne:^{36}Ar:^{84}Kr = 1:0.905:0.326:0.570) used as a pressure medium could freely enter into the capsule. The samples were then loaded in a pressure vessel, and kept for 1, 2, 5, and more than ten hours at 1250°C, 1300°C, and 1600°C and at 0.5, 1, and 2 Kbars pressures of the noble gas mixture. At these temperatures, the basalt was melted, but olivine did not melt. The samples were then quenched to 100°C in about 5 seconds. No visible alteration of the samples was noticed.

2.3 Gas analyses

Samples used for noble gas analyses were weighed, wrapped in clean Al foil, and preheated to 150°C for several hours in a high vacuum gas extraction line to remove adsorbed atmospheric gases. Gases were extracted from the samples in one step (at 1400°C for basalt, and 1800°C for olivine) heating. Active gases were removed by Ti-Zr getters. After removal of active gases, He and Ne were separated from Ar, Kr, and Xe by adsorption of the latter on a charcoal trap at liquid nitrogen boiling temperature. The Ar, Kr, and Xe fractions were later desorbed from the charcoal trap at 100°C.

A BALZERS QMG421 quadru-pole mass spectrometer (QMS) was used for quantitative analyses of noble gases. The QMS had a crossbeam ion source, where emission current was 1 mA, and was fitted with two collectors: a Faraday collector with on-axis and a 17-stage secondary electron multiplier with 90° off-axis. In the experiments we used the secondary electron multiplier (SEM) with an ion counting collector.

We calibrated the instrument before and after every two or three sample analyses, and the average values of the before and after calibrations were used for the analyses. The reproducibility of the calibrations was less than 5% for all noble gases. We tried to keep the pressures of the samples close to the pressures at which the sensitivity measurements were carried out, since sensitivity of the QMS might depend on sample pressure.

3. Results

3.1 Solubility equilibrium of noble gases

To confirm whether or not solubility equilibrium was attained, we measured the time variation of noble gas contents. In Fig. 1 we show concentrations of noble gases in basaltic melt and olivine crystal normalized to the concentrations obtained after 2 hours. For the basaltic melt (Fig. 1(a)), there was little change in the concentrations of noble gases after 2 hours. Therefore, we concluded that 2 hours were enough to attain solubility equilibrium of noble gases in the basaltic melt. In the case of olivine crystal (Fig. 1(b)), we needed at least 5 hours to attain solubility equilibrium.

3.2 Noble gases solubilities and distribution coefficients

The results of solubility measurements are listed in Table 2. We plotted noble gas solubilities measured at various pressure and temperature conditions in Fig. 2. The He solubilities obtained in these experiments should be discarded because of

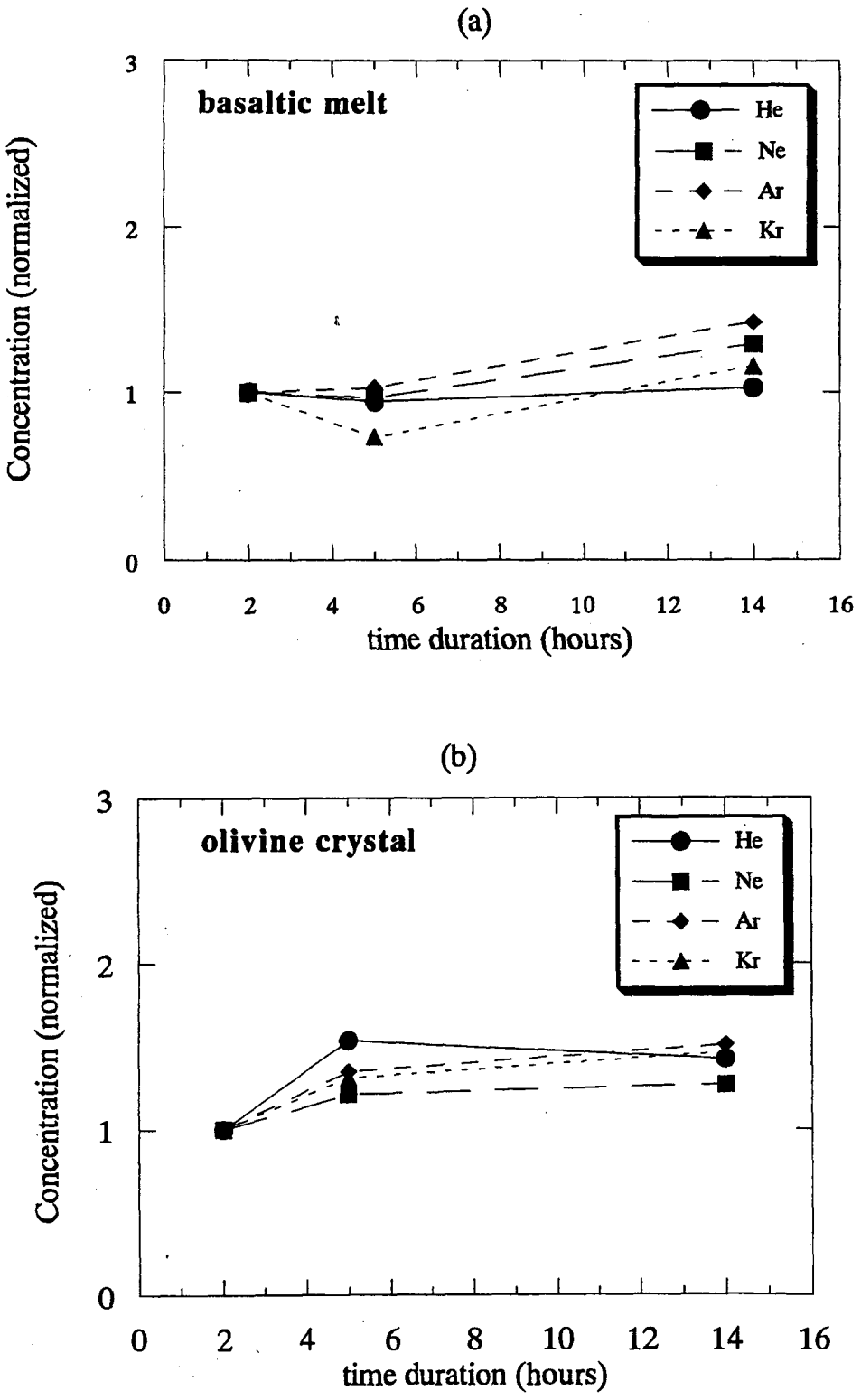

Fig. 1. (a) Noble gas concentration in basaltic melt is plotted against time duration during which basaltic melt samples were equilibrated with noble gases. The results show that there is little change in the concentration after 2 hours. Hence, we conclude that 2 hours are enough to attain solubility equilibrium. (b) Noble gas concentration in olivine is plotted against time duration during which the olivine crystal samples were equilibrated with noble gases. The results show that we need at least 5 hours to attain solubility equilibrium.

Table 2. Noble gas solubilities in basaltic melt and olivine crystal.

sample						
pressure	temperature	time duration	solubility			
(Kbars)	(°C)	(hours)	^{4}He	^{20}Ne	^{36}Ar	^{84}Kr
basaltic melt			(x 10^{-4} cm^3STP/g/bar)			
0.5	1300	13	(2.90)	3.53	1.47	1.04
			(±0.36)	(±0.43)	(±0.18)	(±0.19)
1	1300	12	(2.14)	3.65	1.77	1.09
			(±0.27)	(±0.45)	(±0.21)	(±0.21)
2	1300	14	(4.12)	3.76	1.58	1.16
			(±0.51)	(±0.45)	(±0.19)	(±0.21)
2	1250	10.5	(2.32)	2.55	0.896	0.421
			(±0.18)	(±0.20)	(±0.069)	(±0.033)
1	1600	1	(2.81)	5.00	2.34	1.64
			(±0.23)	(±0.42)	(±0.20)	(±0.14)
olivine crystal			(x 10^{-5} cm^3STP/g/bar)			
0.5	1300	13	(1.89)	2.54	3.93	3.57
			(±0.22)	(±0.22)	(±0.39)	(±0.28)
1	1300	12	(1.28)	1.67	2.25	2.32
			(±0.14)	(±0.14)	(±0.22)	(±0.18)
2	1300	14	(0.953)	1.02	1.39	1.41
			(±0.181)	(±0.21)	(±0.30)	(±0.28)
1	1600	1	(19.6)	30.4	47.1	50.5
			(±2.2)	(±2.6)	(±4.6)	(±3.9)

The solubilities of He in two materials can not be trusted because of possible He loss from the sample.

possible He loss from the samples. The possibility of He loss was inferred from hot blank of He that was much higher than usual. It seems that the higher hot blank of He was due to He leaked from samples. Therefore, the obtained solubility data of He could not be trusted. Noble gas solubilities in basaltic melts obtained in the present study are almost the same as other published values (LUX, 1987).

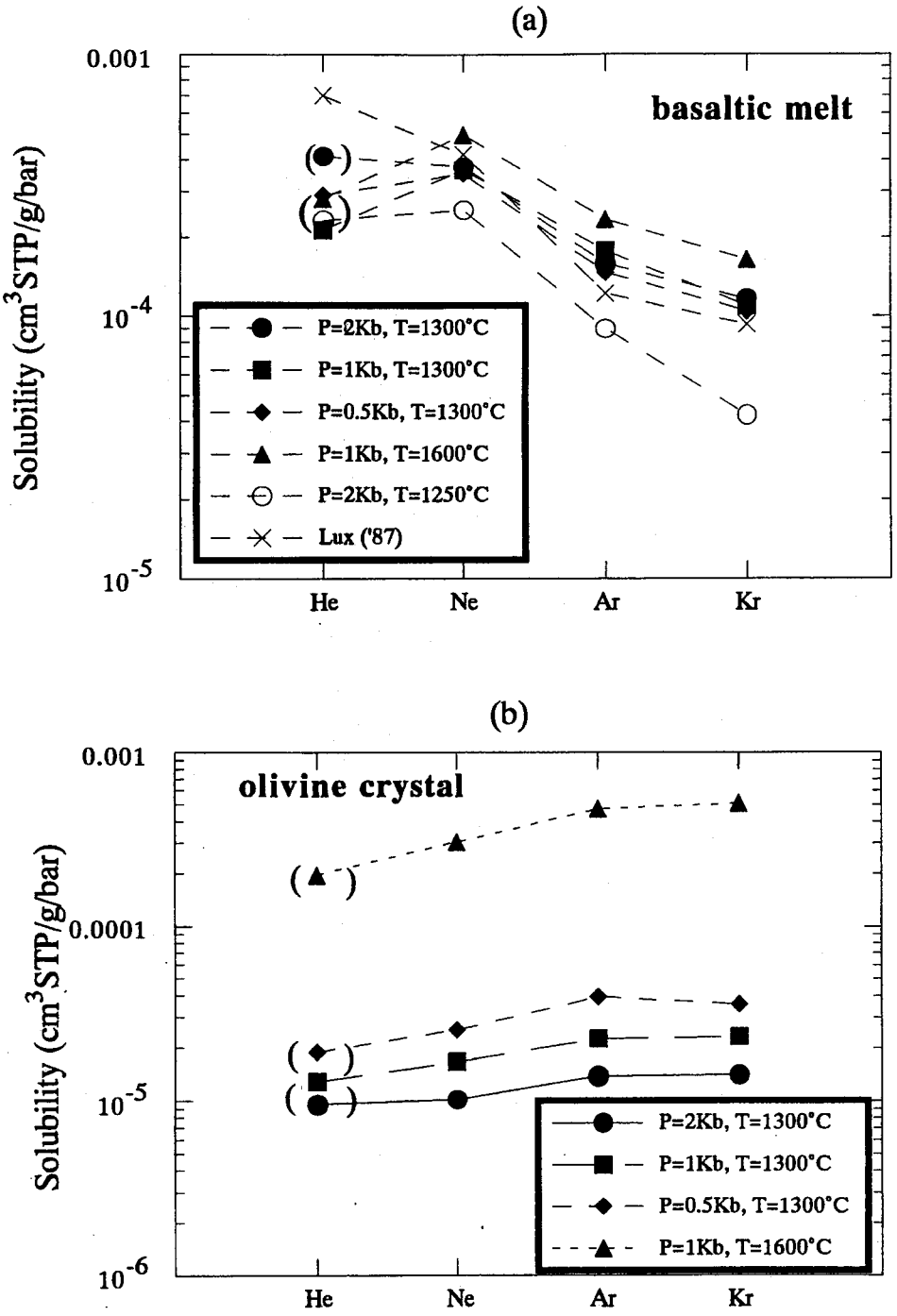

Fig. 2. (a) Noble gas solubilities in basaltic melts obtained by the present study and by LUX at 1350°C (1987): Helium data in the present study may not be trusted because of possible helium loss. (b) Noble gas solubilities in olivine: Helium data may not be trusted because of possible helium loss.

The results of distribution coefficients between basaltic melt and olivine crystal are shown in Fig. 3, that includes distribution coefficients obtained in a laboratory by HIYAGON and OZIMA (1982, 1986) and BROADHURST et al. (1990, 1992), and on natural samples by MARTY and LUSSIEZ (1993) and TRULL and KURT (1993). In Fig. 3, we see that our results agree with the laboratory experiments, but not with the

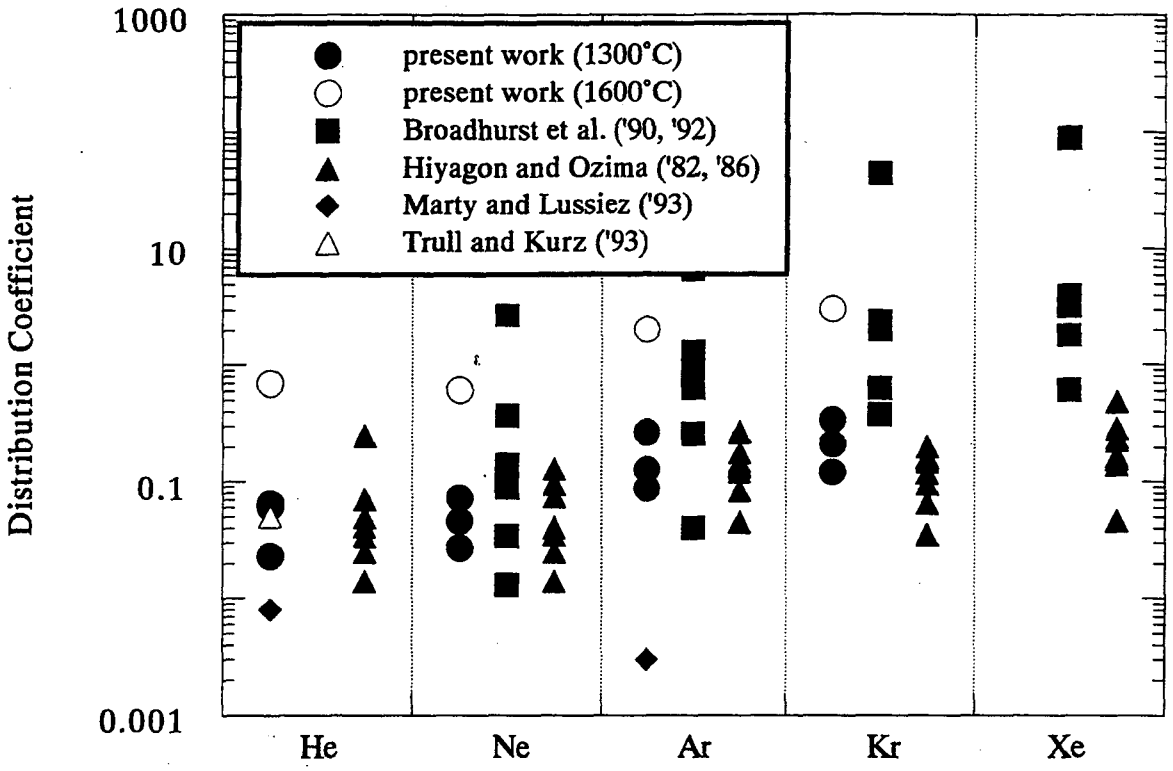

Fig. 3. Distribution coefficients of noble gases between crystal and melt (olivine/basalt).

natural sample result by Marty and Lussiez (see comments on Marty and Lussiez by HIYAGON (1994)).

4. Discussions

4.1 Equilibrium condition

We evaluated the equilibrium condition by comparing the typical diffusive length of a noble gas atom with the typical grain size of the basalt powder. We can write the equilibrium condition as

$$\sqrt{D_i t} > r,$$

where D_i is the diffusion coefficient for noble gas "i" in the basaltic melt, t is the time duration of the solubility experiment, and r is the radius of the basalt powder. We examined the equilibrium condition only for Kr, because it has the lowest diffusivity in the four noble gases (LUX, 1987). Taking value of 4.0×10^{-6} cm^2/s at 1350°C for Kr (LUX, 1987) for basaltic melt, we obtained a typical diffusive length of 1200 μ for one hour. This value is much larger than the typical grain size ($r \approx 250$ μ). Therefore, we believe that the equilibrium condition is safely satisfied for basaltic melt.

In principle we can apply the same method for an olivine crystal as applied for the basaltic melt. However, we examined the equilibrium condition of the olivine crystal for He, because diffusion coefficients of noble gases in olivine are scarce except for He. Therefore, we take a value of 1.97×10^{-8} cm^2/s at 1360°C for He (HART, 1984), and we obtain typical diffusive length of 84 μ for one hour. This value is far beyond the typical grain size ($r \approx 1$ μ). In the case of basaltic melt, the diffusion coefficient of Kr is 10 times smaller than that of He (LUX, 1987). If we assume that diffusion coefficients of the other noble gases are at most 10 times smaller than that of He, we obtain the typical diffusive length of 27 μ. This value is lower limit, but still larger than a typical grain size. Therefore, we believe that the equilibrium condition is also attained in the olivine crystal for the noble gases.

4.2 Solubilities and distribution coefficients

Noble gas solubilities in basaltic melt measured at various conditions are shown in Fig. 2(a). In Fig. 2(a), we can see that there is little change of the solubilities with pressure, but there is significant change of the solubilities with noble gas radius; the greater the noble gas radius, the smaller the solubilities. Also there is change of the solubilities with temperature between 1250°C and 1600°C; the higher the temperature, the larger the solubilities.

In the case of olivine crystal (Fig. 2(b)), the trend of solubility is different from the case in the basaltic melt. Figure 2(b) shows that the solubility slightly increases with increasing noble gas atomic number, and there is significant pressure and temperature dependences of the solubilities. As pressure increases, the solubility decreases, and the solubility is higher for higher temperature. These trends are contrary to what one would generally expect for solubility. Also, the observed values of the solubility are unexpectedly high. In accordance with the high solubility in olivine, the distribution coefficients between basaltic melt and olivine crystal are also high. Furthermore, the distribution coefficients are higher for heavier noble gases.

We examined carefully olivine crystals before and after the solubility experiments with a scanning electron microscope, and found that in the sample used for the solubility experiments, there developed submicroscopic crystals ranging from 1 μ to 10 μ. No such microscopic crystals were observed before the solubility experiments. Consequently, we cannot totally rule out a possibility that some fractions of the ambient noble gases used as a pressure medium might be trapped in the grain boundaries of the crystals to give the rather unexpected results such as the unusually high solubility values and the negative pressure coefficient of the solubility. However, we should also emphasize that the present experimental results are in accordance with the previous experimental results by HIYAGON and OZIMA (1982, 1986) and by BROADHURST et al. (1990, 1992), which were obtained with quite different experimental arrangements from the present one. We are currently working to answer the question whether the unexpected results truly represent solubility of olivine crystal or it is merely an artifact resulted from the trapped noble gas or from some other unknown causes.

5. Application for Estimation of Surface Tension

5.1 Thermodynamic theory

We follow FOWLER and GUGGENHEIM (1939) for a thermodynamic treatment of solution. A simple relation can be obtained from statistical thermodynamics:

$$\ln H = -\frac{\omega - \Lambda + kT \ln \frac{\upsilon}{kT}}{kT}, \tag{1}$$

where H is Henry's law constant, k is Boltzmann constant, T is absolute temperature, ω is the reversible work of adding a solute molecule to the solution, Λ is the molecular heat of evaporation, υ is free volume per molecule.

We then derive a relation between surface tension and solubility by using the assumption proposed by UHLIG (1937). Uhlig assumed that the reversible work of adding a solute molecule into a solution (ω) is done by producing a cavity of essentially the same size as the solute molecule in the solvent and therefore the reversible work is given by the increase in a surface area of the cavity multiplied by the surface tension of the solvent. Using above assumption, if the solute molecule is a spherical gas molecule of radius r, the reversible work is equal to $4\pi r^2\sigma$, where σ is the surface tension of the solvent. Since $\Lambda + kT\ln(\upsilon/kT)$ is only dependent on the solute molecule, it is set as E at the equilibrium condition. We can then rewrite Eq. (1) as

$$\ln H = -\frac{4\pi r^2\sigma - E}{kT}. \tag{2}$$

Hence, we have a relation between the surface tension of the solvent and the noble gas solubility.

5.2 Estimation of surface tension

If we know noble gas solubility, we can estimate surface tension from Eq. (2). It is easy to see from Eq. (2) that if we plot the logarithm of Henry's law constants against the square of noble gas radii, a straight line should be obtained. The slope of the line then should be proportional to surface tension. Therefore, we plotted the logarithm of the Henry's law constants in basaltic melts against the square of the noble gas radii in Fig. 4. For noble gas radii, we used Van der Waals radii (BONDI, 1964). As we can see in Fig. 4, the data lie nearly on straight lines for various conditions. From the slopes of the lines, we calculated the surface tensions between basaltic melt and noble gases. The surface tensions are almost independent of temperature and pressure with value of 130 ± 10 dyne/cm. The values are significantly smaller than the surface tensions (about 350 dyne/cm) at atmospheric pressure estimated between silicate melt and coexisting gas by MURASE and MCBIRNEY (1973) and by WALKER and MULLINS (1981). One of the possibilities for the differ-

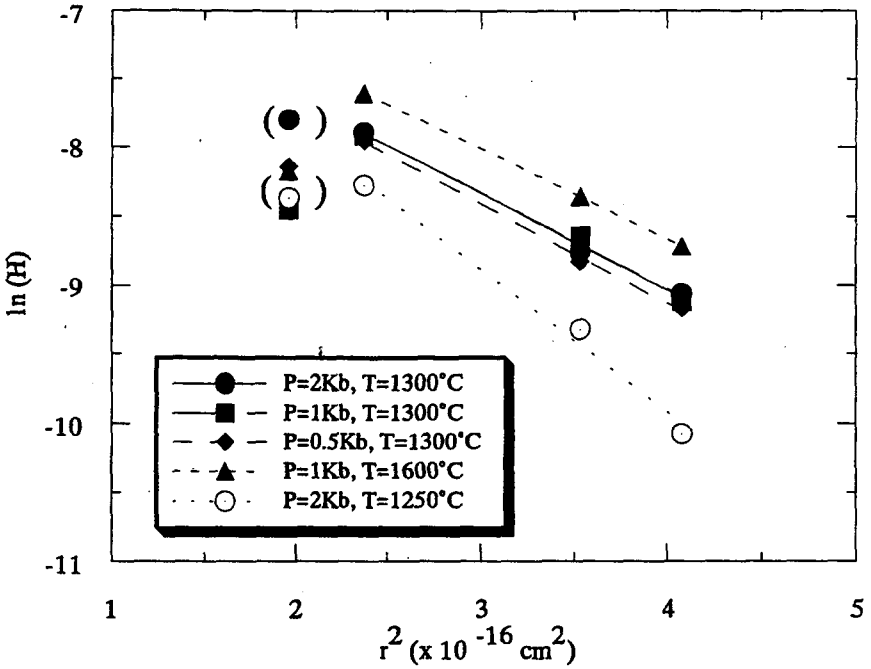

Fig. 4. Logarithm of Henry's law constants (ln(H)) is plotted against the square of noble gas atomic radii. Straight lines can be drawn through data. Surface tension is then determined from the slope of the lines.

ence is that the effective radius of noble gases in the liquid is different from that of Van der Waals. The crude approximation of Eq. (2) may also be suspected for the discrepancy. It is also possible that disagreement is due to the difference in the chemical composition of silicate melt between Murase and McBirney or Walker and Mullins and the present study. The present result must be considered to be preliminary, and more experimental and theoretical studies are needed. Nevertheless, we would like to emphasize that the proposed noble gas method is the first experimental approach for estimation of surface tension at high pressures, and its possibility should be exploited further.

6. Summary

(i) Solubilities of noble gases were determined for basaltic melt and olivine crystals for various temperature and pressure conditions, i.e., T= 1250°C, 1300°C, and 1600°C and P = 0.5 Kbars, 1 Kbar, and 2 Kbars.

(ii) Solubilities were dependent on temperature; the higher the temperature, the larger the solubility.

(iii) Solubilities in basaltic melt were independent of pressure up to 2 Kbars, but the solubilities in olivine were dependent on pressure; the higher the pressure become, the smaller the solubilities.

(iv) Distribution coefficients of noble gases between olivine crystals and basaltic melt were determined for four pairs of olivine crystals and basaltic melt at the same conditions as in (i). The distribution coefficients (D_i) of noble gases thus

obtained are $0.02 < D_{He} < 0.7$, $0.03 < D_{Ne} < 0.6$, $0.087 < D_{Ar} < 2.0$, $0.1 < D_{Kr} < 3.0$.

(v) The distribution coefficients were dependent on temperature and pressure; the distribution coefficients increased with increasing temperature. In contrast to the temperature dependence, the distribution coefficients decreased with increasing pressure.

(vi) Surface tensions were calculated from the noble gas solubilities. The surface tensions were approximately independent of temperature and of pressure up to 2 Kbars. The value is 130 ± 10 dyne/cm.

Acknowledgements. We would like to thank Professor Y. Akutsu of Osaka Univ. for many invaluable discussions and comments on noble gas solubility. We wish to thank Dr. J. Matsuda and Dr. K. Hashizume for their help in mass spectrometry, and Dr. A. Tsuchiyama for his help in scanning electron microscopy. We wish to thank Dr. T. W. Trull for very helpful comments.

REFERENCES

ANDO A., KAMIOKA H., TERASHIMA S., and ITOH S. (1989) 1988 values for GSJ rock reference samples, "Igneous rock series". *Geochemical J.* **23**, 143–148.

BATIZA R., BERNATOWICZ T. J., HOHENBERG C. M., and PODOSEK F. A. (1979) Relations of noble gas abundances to petrogenesis and magmatic evolution of some oceanic basalts and related differentiated volcanic rocks. *Contrib. Mineral. Petrol.* **69**, 301–313.

BONDI A. (1964) Van der Waals volumes and radii. *J. Phys. Chem.* **68**, 441–451.

BROADHURST C. L., DRAKE M. J., HAGEE B. E., and BERNATOWICZ T. J. (1990) Solubility and partitioning of Ar in anorthite, diopside, forstetite, spinel, and synthetic basaltic liquids. *Geochim. Cosmochim. Acta* **54**, 299–309.

BROADHURST C. L., DRAKE M. J., HAGEE B. E., and BERNATOWICZ T. J. (1992) Solubility and partition of Ne, Ar, Kr, and Xe in minerals and synthetic basalt melts. *Geochim. Cosmochim. Acta* **56**, 709–723.

FOWLER R. H. and GUGGENHEIM E. A. (1939) *Statistical Thermodynamics*, Chap. 8, pp. 319–376. Cambridge Univ. Press.

HART S. R. (1984) He diffusion in olivine. *Earth Planet. Sci. Lett.* **70**, 297–302.

HIYAGON H. (1994) Constraints on rare gas partition coefficients from analysis of olivine-glass from a picritic mid-ocean ridge basalt-Comments. *Chem. Geol.* **112**, 119–127.

HIYAGON H. and OZIMA M. (1982) Noble gas distribution between basalt melt and crystals. *Earth Planet. Sci. Lett.* **58**, 255–264.

HIYAGON H. and OZIMA M. (1986) Partition of noble gases between olivine and basalt melt. *Geochim. Cosmochim. Acta* **50**, 2045–2057.

LUX G. (1987) The behavior of noble gases in silicate liquids: Solution, diffusion, bubbles and surface effects, with applications to natural samples. *Geochim. Cosmochim. Acta* **51**, 1549–1560.

MARTY B. and LUSSIEZ P. (1993) Constraints on rare gas partition coefficients from analysis of olivine-glass from a picritic mid-ocean ridge basalt. *Chem. Geol.* **106**, 1–7.

MURASE T. and MCBIRNEY A. R. (1973) Properties of some common igneous rocks and their melts at high temperatures. *Geol. Soc. Am. Bull.* **84**, 3563–3592.

TAKAHASHI E. (1986) Melting of a dry peridotite KLB-1 up to 14 GPa: Implications on the origin of peridotitic upper mantle. *J. Geophys. Res.* **91**, 9367–9382.

TRULL T. W. and KURZ M. D. (1993) Experimental measurements of ^{3}He and ^{4}He mobility in olivine and clinopyroxene at magmatic temperatures. *Geochim. Cosmochim. Acta* **57**, 1313–1324.

UHLIG H. H. (1937) The solubilities of gases and surface tension. *J. Phys. Chem.* **41**, 1215–1225.

WALKER D. and MULLINS O., JR. (1981) Surface tension of natural silicate melts from 1200°C–1500°C and implications for melt structure. *Contrib. Mineral. Petrol.* **76**, 455–462.

GEOPHYSICAL RESEARCH LETTERS, VOL. 23, NO. 22, PAGES 3139-3142, NOVEMBER 1, 1996

Noble gas solubility in binary $CaO-SiO_2$ system

Tomo Shibata

Department of Earth and Space Science, Graduate School of Science, Osaka University, Toyonaka, Osaka, Japan

Eiichi Takahashi

Earth and Planetary Sciences, Faculty of Science, Tokyo Institute of Technology, Ookayama, Meguro-ku, Tokyo, Japan

Jun-ichi Matsuda

Department of Earth and Space Science, Graduate School of Science, Osaka University, Toyonaka, Osaka, Japan

Abstract. New noble gas solubility measurements in binary $CaO-SiO_2$ melts at 1100 bar and 1600 °C are presented. The range of estimated solubilities is He: 8.64-35.8, Ne: 6.54-27.6, Ar: 1.09-8.92, Kr: 0.524-5.67, and Xe: 0.181-2.48 (x 10^{-5} cm^3STP/g-bar). The solubility is greater for the lighter noble gases and is a strong function of melt composition; the solubility increases with increasing SiO_2 and decreasing CaO contents. It is generally known that CaO produces non-bridging oxygen by breaking the SiO_4 network, and thus the correlation between the solubility and SiO_2 content suggests that noble gases dissolve in the SiO_4 network. It is known that the network is formed by limited anionic structure units. In the case of $CaO-SiO_2$ melts, most noble gases would be accommodated by two anionic units; chain and three-dimension structural units. The equilibrium constants of He, Ne, Ar, Kr, and Xe for chain and three-dimension structure units are 26.9, 19.6, 3.49, 1.71, and 0.613 (x 10^{-4}) and 15.1, 11.3, 4.05, 2.68, and 1.23 (x 10^{-3}), respectively. It is concluded that noble gases dissolve in the three-dimension structure units more than in the chain units.

Introduction

Noble gases are inert and rare in the Earth, so they serve as an excellent tracer in resolving Earth evolution processes such as magma generation and its transportation, magma degassing and atmospheric evolution. The fundamental physical process controlling noble gas behavior in the above processes is described by noble gas solubility in silicate melt. Therefore, it is important to understand process of noble gas solution in the melt. Noble gas solubility in silicate glasses and melts has been the subject of considerable study in recent years. *Doremus* [1966] proposed a "free-volume" model which assumes that gas dissolves in fused silica containing a certain amount of accessible free volume. *Carroll and Stolper* [1991, 1993] have recently modified the free-volume model. They proposed that noble gases might dissolve in "holes" or "channels" in glass structure, and discussed the holes or voids and their size distributions in silicate melt and glass in terms of ionic porosity which is the difference between the bulk volume of a material and the calculated volume of constituent anion and cations. The ionic porosity is a kind of measure of integrated hole space in the melt and glass. They examined the relationship between the solubility and ionic porosity, and proposed that ionic porosity was a good indicator of noble gas solubility. However, this indicator was not useful for $CaO-MgO-Al_2O_3-SiO_2$ melts, since the noble gas solubilities in these melts [*White et al.*, 1989; *Broadhurst et al.*, 1992] were lower than those expected from ionic porosity. *Lux* [1987] indicated that noble gas solubilities in natural silicate melts decreased with increasing content of CaO or MgO and with decreasing content of SiO_2. It is obvious that both calcium and magnesium oxides in silicate melts reduce the amounts of noble gases dissolving in the melt, although the effect of the two oxides in silicate melt upon the noble gas solubility is not well understood. There are many chemical components in natural silicate melts, which make it complex and difficult to understand the process of noble gas solution. Therefore, we have started with a simple binary system ($CaO-SiO_2$) as the solvent for noble gas solution. Our objective is to examine the effect of CaO in silicate melts upon noble gas solubility. The structure of this binary system has been well investigated [e.g., *Virgo et al.*, 1980; *Mysen et al.*, 1980, 1982; *Furukawa et al.*, 1981], which aids in the interpretation of the noble gas solubility data.

Paper number 96GL03012.
0094-8534/96/96GL-03012$05.00

Materials

Three calcium silicate glasses were prepared from mixed reagent powders of SiO_2 and $CaCO_3$; the mixtures were decarbonated from 700°C to 1500°C for 6 hours, melted at 1500°C for 12 hours, quenched, and ground to produce powder with grain size less than 500 μm. Approximately 10-50 mg of this glass powder were introduced into a 3 mm diameter, 10-15 mm long Pt capsule whose top was loosely pinched. These capsules were loaded into an internally heated gas-medium high pressure apparatus with quenching device (KOBELCO SMC-2000). The three calcium melts in the unsealed Pt capsules were exposed to a pressurized noble gas mixture under 1100 bar and at 1600°C for 2 hours. The volume ratio of the noble gas mixture is 0.509, 1.03, 98.3, 0.102, and 0.0104 for He, Ne, Ar, Kr, and Xe, respectively, and isotope compositions of noble gases are the same as those of the atmosphere. The pressure was controlled to ± 2 bars and temperature to ± 2°C. Quench rate is over 200°C/sec. Detailed properties of this apparatus are described by *Takahashi and Tomiya* [1992], and the experimental methods are similar to those we used previously [*Shibata et al.*, 1994]. All the quenched glasses were transpar-

Table 1. Composition of sample (wt%)

sample	CA1	CA2	CA3
SiO_2	48.11	56.71	66.84
CaO	51.38	41.57	30.69
Al_2O_3	0.54	0.84	0.88
FeO	0.04	0.04	0.00
Na_2O	0.03	0.04	0.09
MgO	0.05	0.07	0.03
total	100.15	99.27	98.53

ent and no bubbles larger than 1 μm could be found with an optical microscope. Compositions of all the glasses after experiments were analyzed by electron microprobe (Table 1). The content of silicon oxide increases in the sequence of CA1 (48.11 wt%), CA2 (56.71 wt%) and CA3 (66.84 wt%).

Noble gas analysis

A quadrupole mass spectrometer (BALZERS QMG421) was used for the quantitative noble gas analyses. Each quenched glass was separated into several fractions and the amounts of noble gases in three fractions for each sample were measured. The glass was wrapped in clean aluminum foil, put into a crushing apparatus in a high vacuum gas extraction line, and preheated to 150°C for several hours to remove adsorbing atmospheric gases. The glass was slowly crushed by 300 kgf•cm in the high vacuum gas extraction line, and the amounts of noble gases extracted from the sample were measured. The small amounts of noble gases extracted from CA1 and CA2 during crushing experiment indicated that there were few bubbles in these glasses. Therefore, we measured noble gases in subsequent fractions of CA1 and CA2 by fusion at 1630°C without prior crushing. However, a large amount of noble gas was extracted from CA3 during the crushing experiment, indicating the presence of bubbles, so for this sample all three fractions were crushed, eliminating gas in occluded bubbles. The gases extracted during the crushing measurement are not counted as gases dissolving in specimens. These crushed glass samples were placed in the extraction line and again preheated to 150°C. The fractions were fused at 1630°C and the extracted noble gases were measured.

Results of noble gas solubility

Taking diffusion coefficient of 3 x 10^{-6} cm^2/s at 1350°C for Xe in tholeiite basalt [*Lux*, 1987] yields a typical diffusion length of 1000 μm for one hour; this is larger than the typical grain size (diameter ≤ 500 μm) in our experiment. Though the diffusion coefficient in basalt melt may not be equal to that in CaO-SiO_2 melt, we suppose that the values of diffusion coefficient among the silicate melts do not differ so much above liquidus temperature, and therefore believe that the equilibrium condition is safely satisfied.

Solubility can be approximated by Henry's law; i.e., $f_i = X_i H_i$, where X_i is the equilibrium concentration of gas "i" in solution (here reported in units of cm^3STP/g), H_i is the Henry's law constant of gas "i", and f_i is fugacity of gas phase "i". The fugacity during the dissolution experiment is calculated from a modified Redlich-Kwong equation of state [*Ferry and Baumgartner*, 1987]. The calculated Henry's law constants for all melts are listed in Table 2. The large variation in He solubility data suggests the possibility of He loss from samples

Table 2. Henry's law constant in CaO-SiO_2 melts under 1100 bar and 1600 °C

sample	weight (mg)	He	Ne	Ar	Kr	Xe
				(x 10^{-5} cm^3STP/g-bar)		
CA1						
#1*	6.20	0.0145	0.00399	0.000488	0.000210	0.0000927
#1**	6.20	11.3	6.98	1.13	0.532	0.180
#2	1.38	7.88	6.31	1.06	0.516	0.174
#3	1.10	6.65	6.32	1.09	0.524	0.188
mean		8.64(±2.41)	6.54(±0.37)	1.09(±0.03)	0.524(±0.007)	0.181(±0.006)
CA2						
#2*	2.08	0.00448	0.000399	0.000107	0.000154	0.000125
#1	1.46	15.3	14.4	3.17	1.77	0.676
#2**	2.08	13.4	11.8	2.63	1.44	0.541
#3	0.67	18.2	14.8	3.14	1.77	0.663
mean		15.6(±2.4)	13.7(±1.6)	2.98(±0.30)	1.66(±0.19)	0.626(±0.074)
CA3						
#1*	0.80	1.35	1.12	0.0302	0.0286	0.0259
#2*	1.49	6.86	8.35	1.60	1.57	1.39
#3*	3.79	7.94	15.8	2.78	2.71	2.51
#1**	0.80	37.5	29.6	8.76	5.61	2.44
#2**	1.49	41.0	29.7	9.32	6.02	2.58
#3**	3.79	28.7	23.5	8.68	5.36	2.41
mean		35.8(±6.3)	27.6(±3.5)	8.92(±0.35)	5.67(±0.33)	2.48(±0.09)

All values were estimated from gases extracted by fusion at 1630°C.
*: values estimated from released gases by crushing
**: extracted gases by fusion at 1630°C after crushing extraction.
Hot Blanks at 1630°C (cm^3STP); ^{4}He: (5.7-440) x 10^{-12}; ^{20}Ne: (1.1-8.2) x 10^{-11}; ^{40}Ar: (1.3-37) x 10^{-9}; ^{84}Kr: (1.7-12) x 10^{-11}; ^{132}Xe: (1.6-36) x 10^{-13}.

before analyses and therefore the He data could not be trusted. The values of the Henry's law constants are lower than those estimated from the ionic porosity model of *Carroll and Stolper* [1993]. For example, our obtained results for Ar are 2-7 times lower than those estimated by ionic porosity. The Henry's law constants of all five gases increase in the sequence CA1, CA2, CA3 (i.e., with increasing SiO_2). It is generally known that there are two kinds of "space (free volume)" in silicate glass and melt structure. One kind of space is formed by the SiO_4 network and the other is characterized by percolation channel of cations clustering [*Greaves*, 1985]. Judging from the relationship between SiO_2 or CaO and noble gas solubility, we conclude that noble gases dissolve in the network structure of silicate melt rather than free-volumes formed by cations.

Relation between melts structure and solubility

Raman spectroscopy studies indicate that only limited anionic structural units exist in silicate melts [e.g., *Virgo et al.*, 1980; *Mysen et al.*, 1980, 1982; *Furukawa et al.*, 1981]. These units are SiO_2 (three-dimensional network structure), $Si_2O_5^{2-}$ (sheets), $Si_2O_6^{4-}$ (chains), $Si_2O_7^{6-}$ (dimers), and SiO_4^{4-} (monomers). As *Mysen et al.* [1982] observed and estimated the proportion of these units in binary CaO-SiO_2 system, we use their data to model the noble gas solubility in relation to anion structure units. As seen in Figure 1, the Ar solubility increases continuously as the fraction of three-dimension structure units increases. The same trends are observed for other noble gases. If we assume that noble gas dissolved in silicate melt is accommodated by these limited structure units, it is possible to estimate the contribution of each unit to the noble gas solubility. If the noble gases in the units are in equilibrium with those in the gaseous phase and other units, the "bulk" equilibrium constant is given by;

$$K_i^{bulk} = A^{3D} \cdot K_i^{3D} + A^{she} \cdot K_i^{she} + A^{cha} \cdot K_i^{cha} + A^{mon} \cdot K_i^{mon} \quad (1)$$

where A is abundance fraction, K_i is the equilibrium constant of noble gas "i", and superscript "3D", "she", "cha" and "mon" represent three-dimension, sheet, chain and monomer units, respectively. Because monomer units (SiO_4^{4-}) can not accommodate gases in their interior, due to their simple structure, we neglect their contribution to gas solubility (See Figure 1). Hence, we can rewrite Equation 1 as follows,

$$K_i^{bulk}/A^{cha} = A^{3D}/A^{cha} \cdot K_i^{3D} + A^{she}/A^{cha} \cdot K_i^{she} + K_i^{cha} \quad (2)$$

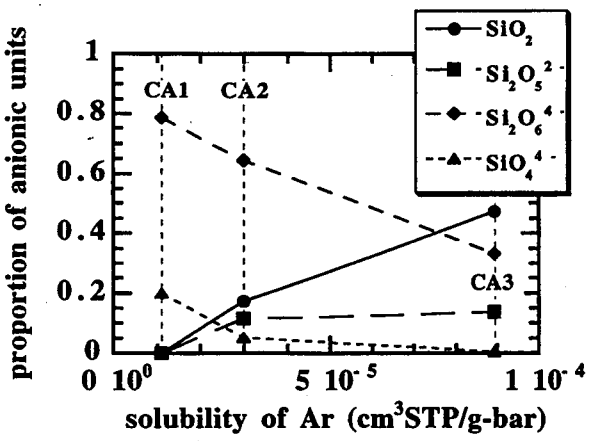

Figure 1. Abundance of structure units in binary CaO-SiO_2 melts as a function of Ar solubility. The content of SiO_2 increases in the sequence of CA1 (48.11 wt%), CA2 (56.71 wt%) and CA3 (66.84 wt%). Ar solubility is mainly related to SiO_2 (three-dimension structure) units. The same trends are observed for other noble gases.

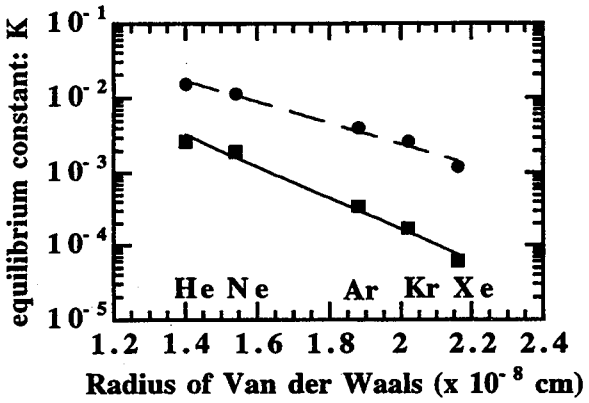

Figure 2. Equilibrium constants both three-dimension structure units (solid circle) and chain units (solid square) for all five noble gases are plotted against Van der Waals radius of the noble gases [*Bondi*, 1964]. The equilibrium constants are estimated after discarding sheet units.

Three sets of K_i^{bulk}/A^{cha}, A^{she}/A^{cha} and A^{3D}/A^{cha} are obtained from the data of our experiment and the estimated units by *Mysen et al.* [1982] for three binary CaO-SiO_2 melts (CA1, CA2 and CA3). From three sets of equations, three equilibrium constants can be calculated. This analysis yielded negative equilibrium constants for sheet units ($Si_2O_5^{2-}$) for all noble gases, which we take to indicate that $Si_2O_5^{2-}$ species can be neglected in modeling noble gas solubility. *Mysen et al.* [1982] also showed that sheet units played a less significant role in these melts. Therefore, after discarding the sheet units we estimated equilibrium constants, which are very close to those obtained without neglecting them. Figure 2 shows the estimated values of the equilibrium constants in chain and three-dimension units; most important are the observations that (a) the equilibrium constants in three-dimension units are much higher than those in chain units and (b) the equilibrium constants are greater for smaller gases. The variation in equilibrium constant with gas atom size in chain units is greater than that in three-dimension units. It is known that the three-dimension units are more polymerized units than chain units. We propose that noble gases dissolve in silicon oxide networks and the more polymerized units contain greater "holes" in the network. Noble gases accommodated in more polymerized units would interact less with surrounding atoms, yielding higher solubility and weaker size dependence. Therefore, noble gas solubility in silicate melts would be defined by degree of polymerization in silicate melt.

Noble gas solubility is related to network structure which is featured by coordination number of Si. *Xue et al.* [1991] observed the occurrence of five- and six-coordinated Si species in $Na_2Si_4O_9$ glass at high pressure (6 GPa) and that the abundance of the these species increased with pressure. Such highly coordinated Si species could contribute to the increase of melt density and decrease abundance of free-volume in silicon oxide network accommodating noble gases. Therefore, we can expect that noble gas solubility decreases below the transition zone in upper mantle.

Conclusions

New experimental results and consideration presented in this study allow a comprehensive characterization of noble gas solubility variation with melt composition for CaO-SiO$_2$ melts. We find a systematic relationship between gas atom radius, solubility and anion structure units in melts, allowing quantitative characterization of the solubility of noble gases as a function of melt composition. Our results and conclusions can be summarized as follows:

1) Noble gas solubilities in the CaO-SiO$_2$ system are sensitive to the fraction of calcium as well as differences in gas atom size, with the larger gas atoms being most sensitive to changes in the fraction of calcium. The solubilities are related to network structure in silicate melt, and are higher in more polymerized melt.

2) In the CaO-SiO$_2$ system noble gas solubility is not governed by cations induced holes or channels but is governed by the tetrahedral network structure. Specifically, the important network structure units are mainly three-dimension and chain units. Therefore, noble gas solubility in silicate melts will be defined by the degree of polymerization in silicate melt. In fact, reported Ar solubilities in albite and orthoclase (fully polymerized melts) are higher than those in less polymerized natural melts [*Carroll and Stolper*, 1993]. Dependence of solubility on gas atom size becomes more remarkable as structure units are less polymerized.

The proposed idea is very important for understanding the process of noble gas solution into silicate melt. The idea could predict the change of the noble gas solubility together with the change of coordination number of Si under high pressure.

Acknowledgments. This research was supported by the Grant-in-Aid for Scientific Research on JSPS Research Fellowships for Young Scientists from the Japanese Ministry of Education, Science and Culture. We thank Prof. K. Kawamura and Dr. K. Funakoshi in Tokyo Institute College for their advice of production of CaO-SiO$_2$ melts. Prof. S. Shimokawa at Hokkaido National Agricultural research Institute and Dr. H. Maekawa in Hokkaido University offered helpful comments regarding structure units in silicate melts. Dr. I. Miyagi and Dr. A. Tomiya in Tokyo Institute College provided kindly advice and valuable assistance with the operation of an internally heated gas medium high-pressure apparatus with quench device. We gratefully acknowledge anonymous reviewers and Prof. M. Ozima for critical comments and suggestions.

References

Bondi A. Van der Waals Volumes and Radii, *J. Phys. Chem., 68,* 441-451, 1964.

Broadhurst C. L., M. J. Drake, B. E. Hagee, and T. J. Bernatowicz, Solubility and partitioning of Ne, Ar, Kr, and Xe in minerals and synthetic basaltic liquids, *Geochim. Cosmochim. Acta , 56,* 709-723, 1992.

Carroll M. R. and E. M. Stolper, Argon solubility and diffusion in silica glass: Implications for the solution behavior of molecular gases, *Geochim. Cosmochim. Acta , 55,* 211-225, 1991.

Carroll M. R. and E. M. Stolper, Noble gas solubilities in silicate melts and glasses: New experimental results for argon and the relationship between solubility and ionic porosity, *Geochim. Cosmochim. Acta , 57,* 5039-5051, 1993.

Doremus R. H., Physical solubility of gases in fuse silica, *J. Amer. Ceram. Soc., 49,* 461-462, 1966.

Ferry J. M. and L. Baumgartner, Thermodynamic models of molecular fluids at the elevated pressures and temperatures of crustal metamorphism, *Mineralogical Society of America Review in Mineralogy , 17,* 323-365, 1987.

Furukawa T., K. E. Fox and W. B. White, Raman spectroscopic investigation of structure of silicate glasses, III. Raman intensities and structural units in sodium silicate glasses *J. Chem. Phys., 75,* 3226-3237, 1981.

Greaves G. N., EXAFS and the structure of glass, *J. Non-Crystal Solids, 71,* 203-217, 1985.

Lux G., The behavior of noble gases in silicate liquids: Solution, diffusion, bubbles, and surface effects, with applications to natural samples, *Geochim. Cosmochim. Acta, 51,* 1549-1560, 1987.

Mysen B. O., D. Virgo, and C. M. Scarfe, Relations between the anionic structure and viscosity of silicate melts- A Raman spectroscopic study, *Am. Mineral., 65,* 690-710, 1980.

Mysen B. O., D. Virgo, and F. A. Seifert The structure of silicate melts: Implications for chemical and physical properties of natural magma, *Reviews of Geophysics and Space Physics, 20,* 353-383, 1982.

Shibata T., E. Takahashi, and M. Ozima, Noble gas partition between basaltic melt and olivine crystals at high pressure, in *Noble Gas Geochemistry and Cosmochemistry,* edited by J. Matsuda, pp. 343-354, Terra Scientific Publishing Company, Tokyo, 1994.

Takahashi E. and A. Tomiya, An internally heated gas-medium high-pressure apparatus with quench device (SMC-2000) (abstract) *Program and abstracts the Volcanological Society of Japan, at Kyoto, 28,* D31-P83, 1992.

Virgo D., B. O. Mysen, and I. Kushiro, Anionic constitution of 1-atmosphere silicate melts: Implications for the structure of igneous melts, *Science, 208,* 1371-1373, 1980.

White B. S., M. Brearley, and A. Montana, Solubility of Argon in silicate liquids at high pressures, *Am. Mineral., 74,* 513-529, 1989.

Xue X., J. F. Stebbins, M. Kanzaki, P. F. McMillan, and B. Poe, Pressure-induced silicon coordination and tetrahedral structure changes in alkali oxide-silica melts up to 12 GPa: NMR, Raman, and infrared spectroscopy, *Am. Mineral., 76,* 8-26, 1991.

J. Matsuda, Department of Earth and Space Science, Faculty of Science, Osaka University, Toyonaka, Osaka 560, Japan (e-mail: matsuda@ess.sci.osaka-u.ac.jp)

T. Shibata, Department of Earth and Space Science, Graduate School of Science, Osaka University, Toyonaka, Osaka 560, Japan (e-mail: tomo@ess.sci.osaka-u.ac.jp)

E. Takahashi, Earth and Planetary Sciences, Faculty of Science, Tokyo Institute of Technology, 2-12-1, Ookayama, Meguro-ku, Tokyo 152, Japan (e-mail: etakahas@geo.titech.ac.jp)

(Received May 7, 1996: revised September 20, 1996;
accepted September 24, 1996)